
Towards autonomous DNA-based Nanodevices

Tim Liedl



München 2007

Towards autonomous DNA-based Nanodevices

Tim Liedl

**Dissertation an der Fakultät für Physik
der Ludwig-Maximilians-Universität
München**

**vorgelegt von
Tim Liedl
aus München**

München, den 4.4.2007

Erstgutachter: PD Dr. F. C. Simmel
Zweitgutachter: Prof. Dr. J. O. Rädler
Tag der mündlichen Prüfung: 23.5.2007

Contents

1	Introduction - DNA-based Nanodevices	1
1.1	DNA-based structures	2
1.2	DNA-based devices (Ref. [1])	3
1.3	Enzymatically driven DNA-based devices (Ref. [1])	4
2	Theoretical and Experimental Basics	7
2.1	Physical properties of DNA	7
2.2	Thermodynamics of DNA	9
2.3	Characterization of DNA-based nanodevices	11
2.3.1	Energy transfer between fluorophores	11
2.3.2	Energy transfer near metal surfaces	13
3	Determination of DNA Melting Temperatures	15
3.1	DNA melting temperature determination by thermal denaturation	15
3.2	DNA Melting temperature determination in chemical gradients (Ref. [2])	17
4	A DNA switch driven by a Chemical Oscillator	21
4.1	Non-equilibrium systems	22
4.2	Reaction diffusion processes	23
4.3	Oscillatory systems	26
4.4	pH-sensitive DNA devices	29
4.5	Switching the conformation of a DNA molecule with a chemical oscillator (Ref.[3])	30
4.6	A surface-bound DNA switch driven by a chemical oscillator (Ref.[4])	32
4.7	Conclusion	34
5	Controlled Trapping and Release of Quantum Dots	35
5.1	Reversible hydrogels	35
5.2	Fluorescent nanocrystals as colloidal probes in complex fluids (Ref. [5])	38
5.3	DNA-crosslinked gels as programmable drug delivery system (Ref. [6])	41
5.4	Conclusion	45
6	Glossary	47

Appendix	49
Determination of 1D diffusion constants	49
Reference [1]	53
Reference [2]	59
Reference [3]	71
Reference [4]	83
Reference [5]	93
Reference [6]	101
Bibliography	106

List of Figures

1.1	DNA cube	2
1.2	DNA tweezers	3
1.3	Enzymatically driven DNA device	5
2.1	DNA double helix	8
2.2	Förster resonance energy transfer	12
3.1	Melting behavior of DNA	16
3.2	Formamide lowers T_M	17
3.3	Multilayer microfluidics	18
3.4	DNA dissociation along a formamide gradient	19
3.5	Microfluidic for 2D gradients	20
4.1	Cell in non-equilibrium	21
4.2	Pattern formation	24
4.3	Activator-substrate reaction	26
4.4	Predator-prey model	27
4.5	Activator-substrate reaction without diffusion	28
4.6	Belousov-Zhabotinsky reaction	29
4.7	pH-dependent DNA devices	30
4.8	pH-Oscillator	32
4.9	DNA tethered to gold islands	33
5.1	Polyacrylamide network	37
5.2	Antigen responsive hydrogel	38
5.3	Fluorescent nanocrystals	39
5.4	Fluorescent correlation spectroscopy	40
5.5	Saturation of fluorophores	41
5.6	Acrydite	42
5.7	Gel crosslinking	43
5.8	Trapped quantum dots	44
5.9	Dissolution of a DNA crosslinked hydrogel	44
6.1	Particle displacement statistics	50

Abstract

Molecular recognition, programmability, self-assembling capabilities and biocompatibility are unique features of DNA. The basic approach of DNA nanotechnology is to exploit these properties in order to fabricate novel materials and structures on the nanometer scale. This cumulative dissertation deals with three aspects of this young research area: fast analysis, autonomous control of functional structures, and biocompatible autonomous delivery systems for nanoscale objects.

1. At low temperatures and under favorable buffer conditions, two complementary DNA strands will form a double-helical structure in which the bases of the two strands are paired according to the Watson-Crick rules: adenine bases bind with thymine bases, guanine bases with cytosine bases. The melting temperature T_M of a DNA duplex is defined as the temperature at which half of the double strands are separated into single strands. The melting temperature can be calculated for DNA strands of known sequences under standard conditions. However, it has to be determined experimentally for strands of unknown sequences and for applications under extreme buffer conditions. A method for fast and reliable determination of DNA melting temperatures has been developed. Stable gradients of the denaturing agent formamide were generated by means of diffusion in a microfluidic setup. Formamide lowers the melting temperature of DNA and a given formamide concentration can be mapped to a corresponding virtual temperature along the formamide gradient. Differences in the length of complementary sequences of only one nucleotide as well as a single nucleotide mismatch can be detected with this method, which is of great interest for the detection of sequence mutations or variations such as single nucleotide polymorphisms (SNPs).

2. Knowledge of the stability of DNA duplexes is also of great importance for the construction of DNA-based nanostructures and devices. Conformational changes occurring in artificially generated DNA structures can be used to produce motion on the nanometer scale. Usually, DNA devices are driven by the manual addition of fuel molecules or by the periodic variation of buffer conditions. One prominent example of such a conformational change is the formation of the so-called i-motif, which is a folded four-stranded DNA structure characterized by noncanonical hemiprotonated cytosine-cytosine base-pairs. In order to achieve controlled autonomous motion, the oscillating pH-value of a chemical oscillator has been employed to drive the i-motif periodically through its conformational states. The experiments were conducted with the DNA switch in solution and attached to a solid substrate and constitute the first example of DNA-based devices driven autonomously by a chemical non-equilibrium reaction.

3. Finally, a DNA-crosslinked and switchable polyacrylamide hydrogel is introduced, which is used to trap and release fluorescent colloidal quantum dots in response to externally applied programmable DNA signal strands. Trapping and release of the nanoparticles is demonstrated by studying their diffusion properties using single molecule fluorescence microscopy, single particle tracking and fluorescence correlation spectroscopy. Due to the biocompatibility of the polymerized acrylamide and the crosslinking DNA strands, such

gels could find application in the context of controlled drug delivery, where the autonomous release of a drug-carrying nanoparticle could be triggered by naturally occurring, potentially disease-related DNA or RNA strands.

Zusammenfassung

DNA, der Träger der Erbinformation, ist nicht nur ein langlebiger Informationsspeicher, sondern hat auch die Fähigkeit zur molekularen Erkennung und programmierbaren Selbstorganisation. Die DNA-Nanotechnologie bedient sich dieser einzigartigen Eigenschaften um neuartige Materialien und funktionale Strukturen zu erschaffen. Diese kumulative Dissertation beschäftigt sich mit drei verschiedenen Aspekten dieses jungen Forschungsgebietes: schnellen und zuverlässigen Analysetechniken, Wegen zur autonomen Kontrolle von funktionalen Nanostrukturen und biokompatiblen programmierbaren Transportsystemen.

1. Die Stabilität einer DNA-Doppelhelix hängt sowohl von der Sequenz der Basen als auch von Temperatur und Zusammensetzung des Lösungsmittels ab. Die Schmelztemperatur T_M einer DNA-Doppelhelix ist definiert als die Temperatur, bei der die Hälfte der Doppelstränge in Einzelstränge dissoziiert ist. Unter Standardbedingungen kann die Schmelztemperatur eines Doppelstrangs bekannter Basenfolge berechnet werden, jedoch muss sie für Stränge unbekannter Basenfolge sowie für Anwendungen unter extremen Pufferbedingungen experimentell bestimmt werden. In dieser Arbeit wurde ein Verfahren zur schnellen und zuverlässigen Bestimmung der Schmelztemperatur kurzer DNA-Stränge entwickelt. Dafür wurden in einem Mikrofluidikchip Diffusionsgradienten der denaturierenden Substanz Formamid erzeugt. Mit Hilfe des Chips konnten Schmelztemperaturen verschiedener DNA-Stränge so genau gemessen werden, dass Längenunterschiede von einem Basenpaar oder einzelne Basensubstitutionen detektiert werden konnten. Diese Methode könnte daher Anwendung in der Analyse von Einzelnukleotidpolymorphismen finden.

2. Für die Entwicklung von Nanostrukturen, die aus selbstorganisierenden DNA-Strängen bestehen, ist die Kenntnis des Dissoziationsverhaltens der in der Struktur enthaltenen DNA-Doppelstränge von großer Bedeutung. Bei einer Vielzahl DNA-basierter Strukturen kann durch eine Veränderung der Umgebungsbedingungen, z.B. durch eine Änderung des pH-Wertes des Lösungsmittels, eine Konformationsänderung ausgelöst werden. Auf diese Weise lassen sich kontrollierte Bewegungen auf der Nanometerskala erzwingen. In den meisten Fällen wird der momentane Zustand dieser dynamischen Strukturen durch einen externen Operator kontrolliert. Um autonome Bewegung zu erzeugen, wurden in diesem Projekt Konzepte der nicht-linearen Chemie genutzt. Es ließ sich zeigen, dass der pH-abhängige Übergang eines Cytosin-reichen DNA-Stranges von einer ungeordneten Konformation zum so genannten "i-Motiv" durch einen chemischen pH-Oszillator getrieben werden kann. Das i-Motiv konnte auf diese Weise sowohl in Lösung als auch an eine Oberfläche gebunden reversibel und periodisch geöffnet und geschlossen werden. Das System stellt die erste bewegliche DNA-basierte Struktur dar, die sich durch eine chemische Nichtgleichgewichtsreaktion autonom schalten lässt.

3. Abschließend wird ein schaltbares Polyacrylamidgel vorgestellt, das durch Zugabe von programmierbaren DNA-Strängen reversibel vernetzt werden kann. Ein derartiges Gel wurde genutzt, um fluoreszierende Nanokristalle einzuschließen und anschließend wieder freizugeben. Die sich ändernden Diffusionseigenschaften der Nanokristalle wurden mit Einzelfluoreszenzmikroskopie und Fluoreszenzkorrelationspektroskopie nachgewiesen.

Aufgrund der Biokompatibilität der polymerisierten Acrylamidstränge und der vernetzenden DNA könnten solche Gele als Transportsysteme für pharmazeutische Wirkstoffe angewendet werden. Krankheitsbedingt auftretende, zelleigene DNA- oder RNA-Stränge könnten hierbei die Freigabe der Wirkstoffe auslösen.

1 Introduction - DNA-based nanodevices (Ref. [1])

In science and industry nanotechnology is expected to provide novel materials, novel drugs, and novel functional systems engineered on the molecular level. Summarizing the diverse aspects of nano sciences it can be stated, that the scope of nanotechnology is the control of matter on the nanometer scale. For the achievement of this goal, generally two approaches are available.

On the one hand, a well established top-down approach is pursued, which has its origins in semiconductor technology. It applies large technical equipment like scanning probe microscopes or electron beam microscopes to image and manipulate features with dimensions of only a few nanometers. Although these elaborate techniques nowadays are indispensable in a modern nanotechnology lab they exhibit some intrinsic disadvantages such as high acquisition and maintenance costs and poor potential for process parallelization.

The bottom-up approach on the other hand makes use of the emergence of order by self-organization and cooperative actions on the molecular level. Inspired by biological systems this approach is exploiting molecular recognition and aspires large, complex systems built from small, programmable entities. Similar to the assembly of proteins, which are built up entirely from chains of amino acids and fold - sometimes assisted by enzymes - into a functional structure by themselves, the self-assembly of man-designed building blocks is endeavored. Some possible building blocks are shortly listed: (i) Colloidal nanocrystals are crystalline clusters of a variety of materials dispersed in a solvent. Nanocrystals of special interest are fluorescent semiconductor nanoparticles, also called quantum dots, magnetic nanoparticles and gold nanoparticles. Since these particles have a variety of unique properties, they are in the focus of scientific interest for several years now. (ii) Fullerenes are macromolecules consisting entirely of carbon atoms. Famous representatives of the fullerene family are the C₆₀ molecules, also called buckyballs, and carbon nanotubes (CNTs). CNTs consist of curved sheets of graphite forming cylinders with single or multiple walls. The cylinders have diameters of single nanometers, while they can reach an aspect ratio of 1:10 000. Single wall CNTs (SWNTs) form seamless cylinders and exhibit, depending on their structure, interesting electrical properties like metallic or semiconducting behavior. (iii) Block copolymers are polymer chains, which are built of blocks of different monomers. By using blocks of monomers with dissimilar polarity, it is hence possible to design polymer chains with hydrophobic and hydrophilic sections. Depending of the polarity of the

solute the representatives of one kind of these sections aggregate with themselves, thus building supramolecular vesicles, cylinders, laminar planes, and more complex structures. (iii) *Deoxyribonucleic acid*, in short DNA, the molecule of heritage and biological information storage. DNA is a robust, easy-to-handle, and versatile material. Its advantages and some of its realized and potential applications will be discussed in the next paragraphs.

1.1 DNA-based structures

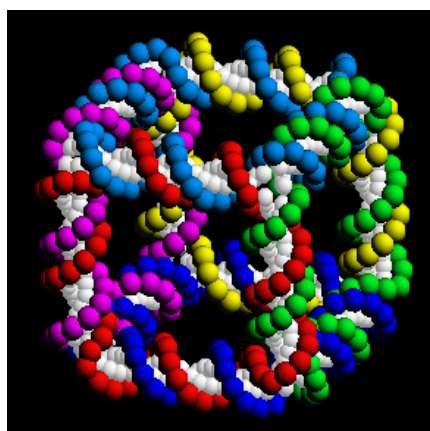


Figure 1.1: *Schematic illustration of a DNA cube. (Reprinted with kind permission from N. C. Seeman)*

DNA is commonly known as the carrier of hereditary information in every single- or multicellular organism. But the unique properties of DNA, such as molecular recognition, self-assembly, programmability, and biocompatibility, also predestine this biochemically stable material outside its biological context as a building block for highly structured materials with specific nanoscale features [7]. DNA has the capacity of recognizing complementary sequences according to the essential rule, that of the four bases *adenine*, *thymine*, *guanine*, and *cytosine* always two, namely *adenine* with *thymine* and *guanine* with *cytosine* form a base pair in the double helix (cf. chap. 2.1). The basic idea is to employ this base pairing property to generate structures and machines from artificially designed DNA strands, which self-assemble autonomously into the desired shape. Such a DNA-based supramolecular assembly has been presented by the group of Nadrian Seeman in the year 1991 [8]. They demonstrated a structure with the connectivity of a cube, which was built entirely from DNA (Fig. 1.1). DNA acts in such a structure as an intelligent glue that connects specifically the designated subunits.

By now, various stable 3D structures have been realized, for example an octahedron built from one 1.7-kilobase long, partly self-complementary DNA strand stabilized by a set of 40 base pair long connecting strands [9] and DNA tetrahedra, with a length of less than

10 nanometers on one side and composed of four short synthetic DNA oligonucleotides [10]. Rothemund [11] presented a study, where viral 7-kilobase DNA strands were folded with the help of hundreds of short synthetic “staple” strands into arbitrary shapes such as words, smilies, and even miniaturized maps of America.

1.2 DNA-based devices (Ref. [1])

Besides these stable and static structures, DNA has also been successfully employed to build functional devices and DNA nanomachines. DNA nanodevices can cyclically undergo large conformational changes in the presence of certain trigger molecules such as other DNA strands or small molecules and can thereby accomplish versatile motions like opening and closing of DNA tweezers [12] (Fig. 1.2) or motion along DNA tracks [13].

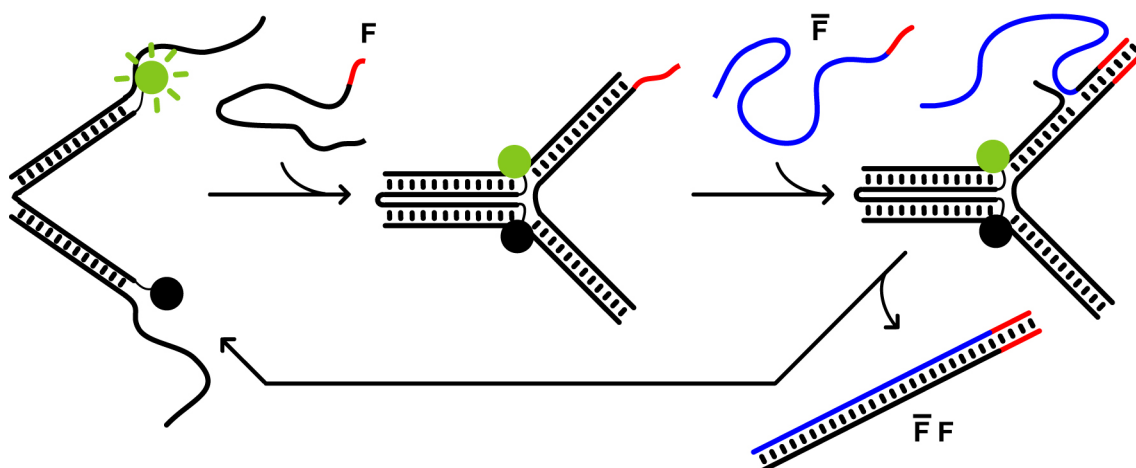


Figure 1.2: *DNA-based nanomachine (cf. text).*

Since the DNA tweezers by Yurke *et al.* constitute the first example of a DNA-fueled molecular machine, we will take a closer look at their working principle. In the open state (Fig. 1.2, left), the DNA tweezers are composed of two rigid double stranded regions, which are linked by a short single stranded hinge. On the opposite side of the hinge, each double stranded region exhibits a single stranded extension. Addition of a ‘fuel’ strand F which is complementary to both of these extensions induces the closing of the tweezers (Fig. 1.2, middle). The fuel strand, in turn, can be removed by an ‘anti-fuel’ strand \bar{F} (blue), which is fully complementary to the fuel strand F , by a process called ‘branch migration’ [14, 15]. The fuel strand possesses a short single stranded overhang, the so-called ‘toehold’ region (red), which facilitates the binding of the anti-fuel strand to the fuel strand and ensures the correct outcome of the branch migration process (Fig. 1.2, right). The intersection point, i.e. where the anti-fuel strand competes with the former single stranded extension for the binding to the fuel strand, performs a random walk along the strand. Since the

toehold region is a stable double strand, the intersection point will finally hit the opposite end, which results in the complete dissociation of the fuel strand from the device. Fuel strand and anti-fuel strand form a double stranded waste product $F\bar{F}$ and the tweezers return to their open state. The opening and closing of the tweezers can be monitored with fluorescence resonance energy transfer (FRET) measurements, a method that visualizes distance changes between two fluorophores or a fluorophore and a quencher with overlapping emission and absorption spectra (cf. chapter 2.3).

1.3 Enzymatically driven DNA-based devices (Ref. [1])

To achieve autonomous motion of DNA-based devices, most approaches involve the enzymatic activity of proteins or nucleic acids [16, 17, 18]. Here, a few enzymatically driven devices will be briefly introduced.

Chen *et al.* [16], for example, presented experiments involving a simple DNA machine (Fig.1.3) comprising two short double stranded regions connected on one end by a short ssDNA hinge and on the other end by an RNA-cleaving deoxyribozyme (blue strand), which is able to cut a single stranded DNA-RNA chimera (black and red strand). As long as chimeric fuel molecules are present, the machine is continuously opened through hybridization of the chimera to the RNA-cleaving element and closed back into a folded state after the chimera is cut apart by the enzyme. After cleavage, the remaining strands are too short to form stable double helices, dissociate from the enzyme and give room for a new chimera strand to hybridize to the enzyme and restart the cycle. As for the tweezers presented in the last chapter, the opening and closing of the device can be monitored with FRET measurements.

Bath *et al.* [17] demonstrated directed motion of a free-running DNA motor, which moves a DNA cargo in discrete steps along a DNA track and is powered by a nicking enzyme. Recently, Pei *et al.* [18] employed ribozymes to accomplish the independent motion of a spider-like, polycatalytic assembly, which moves through an oligonucleotide matrix, while cutting the sites where the “arms” of the assembly have rested.

Another step towards autonomous motion of DNA devices was taken by employing genetic mechanisms to actuate a DNA device [19]. The DNA sequence of the bacteriophage T7 encodes for an enzyme that is highly selective to its own promoter sequence and catalyzes the synthesis of nucleic acids on preexisting nucleic acid templates. This commercially available enzyme is called T7 RNA polymerase and transcribes *in vitro* under appropriate buffer conditions a synthetic DNA template starting with the T7 promoter sequence into an arbitrary mRNA strand. After encountering a stop-sequence along the template, the freshly transcribed RNA strand is released into solution, where it can fulfill the task it was designed for, for example the closing of a DNA tweezer (cf. chapter 1.2). On the base of the interaction between T7 RNA polymerase and its promoter sequence Kim *et*

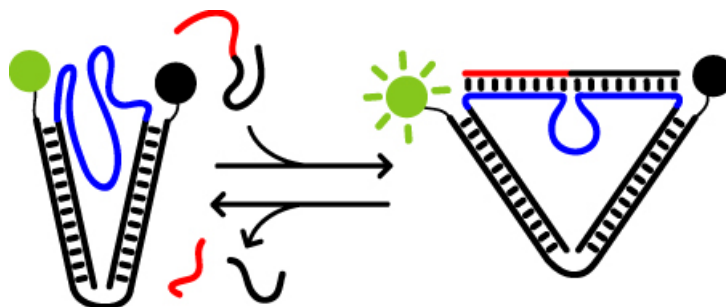


Figure 1.3: A DNA-based device driven by the enzymatic activity of an RNA-cleaving deoxyribozyme (cf. text).

al. [20] proposed artificial transcriptional circuits composed of mutually inhibiting and activating genes which could provide controlled amounts of various actuator RNA strands for networks of DNA. Recently, an *in vitro* bistable circuit from synthetic transcriptional switches was realized by the same group [21]. In still unpublished experiments Kim *et al.* demonstrated even *in vitro* oscillatory circuits, which provide alternating concentrations of different effector RNA strands. In a collaboration with our group, the periodic opening and closing of DNA tweezers has been achieved with this oscillatory system. The review article [1] introduces more DNA-based nanodevices, which perform nanoscale movements, fulfill sensory tasks or are controlled by genetic mechanisms. Further reviews can be found in [22, 23].

The scope of this dissertation is to introduce novel concepts of autonomous behavior of DNA-based nanodevices and materials. This includes on the one hand the application of oscillating chemical reactions, which have often been studied as model system for biological rhythms and oscillations, as chemical “pace-maker”. In future applications this approach may lead to temporal ordering in self-assembly and self-organization processes. On the other hand it will be demonstrated, how a DNA-crosslinked hydrogel can be programmed to release model drug carriers on demand. This might constitute a major step towards controlled drug release from an autonomously acting delivery system. Firstly, the physical and thermodynamic properties of DNA, experimental methods for the characterization of DNA-based devices, and a novel method for fast and reliable melting temperature determination of DNA will be introduced in the following two chapters.

2 Theoretical and experimental basics

The determination of the structure of the DNA double helix by Franklin and Wilkins and Watson and Crick [24] using X-ray diffraction in 1953 gave rise to a fast development of already existing and newly emerging disciplines in the life sciences. Few biologically relevant molecules have been studied in such a great detail as DNA. We are today in the situation to have a polymer at hand, which is not only excellently characterized but at the same time easy to obtain in a length from 5 up to 10^5 nucleotides and commercially available with numerous functionalizations. This chapter gives a short overview of the physical and thermodynamic properties of DNA and introduces experimental methods for the characterization of DNA-based nanodevices.

2.1 Physical properties of DNA

The four universal bases that build up the DNA of all known cellular organisms are *adenine* (A), *thymine* (T), *guanine* (G) and *cytosine* (C) (Fig. 2.1a). In RNA thymine is substituted by the base *uracil* (U). A *nucleoside* is made up of one of these bases linked to the 1' carbon atom of a monosaccharide desoxyribose (ribose in RNA). Together with a mono-, di- or triphosphate attached to the 5' carbon atom of the sugar ring the nucleosides are known as *nucleotides*. Single nucleotides with sometimes slightly modified sugars are employed by living cells as signaling elements and as energy storage entities. Any of the monophosphate nucleotides can be linked via one oxygen atom of the phosphate group to the 3' atom of the sugar ring of any other monophosphate nucleotide. Thus, long polymers of monophosphate nucleotides of arbitrary sequences can be built, so-called *polynucleotides* or single stranded DNA (ssDNA). Since the binding always occurs via the 5' and the 3' carbon atom of the sugar rings, the ssDNA or the ssRNA possesses directionality. Just like the reading direction is important to understand the meaning of a written text, the 5' end to 3' end directionality of polynucleotides is important for all enzymes involved in transcription and translation processes. In figure 2.1 (left), for example, the sequence of the left strand is 5' ACTG 3' and for the reverse complementary strand depicted on the right 5' CAGT 3'. Under a wide range of buffer conditions the bases undergo the canonical, hydrogen bond mediated base pairing (G with C and A with T, A with U in RNA). Two polynucleotides with reverse complementary base sequences can form the well-known double helix, where the two strands wind around each other with opposite directionality (Fig. 2.1, right). This process is called hybridization.

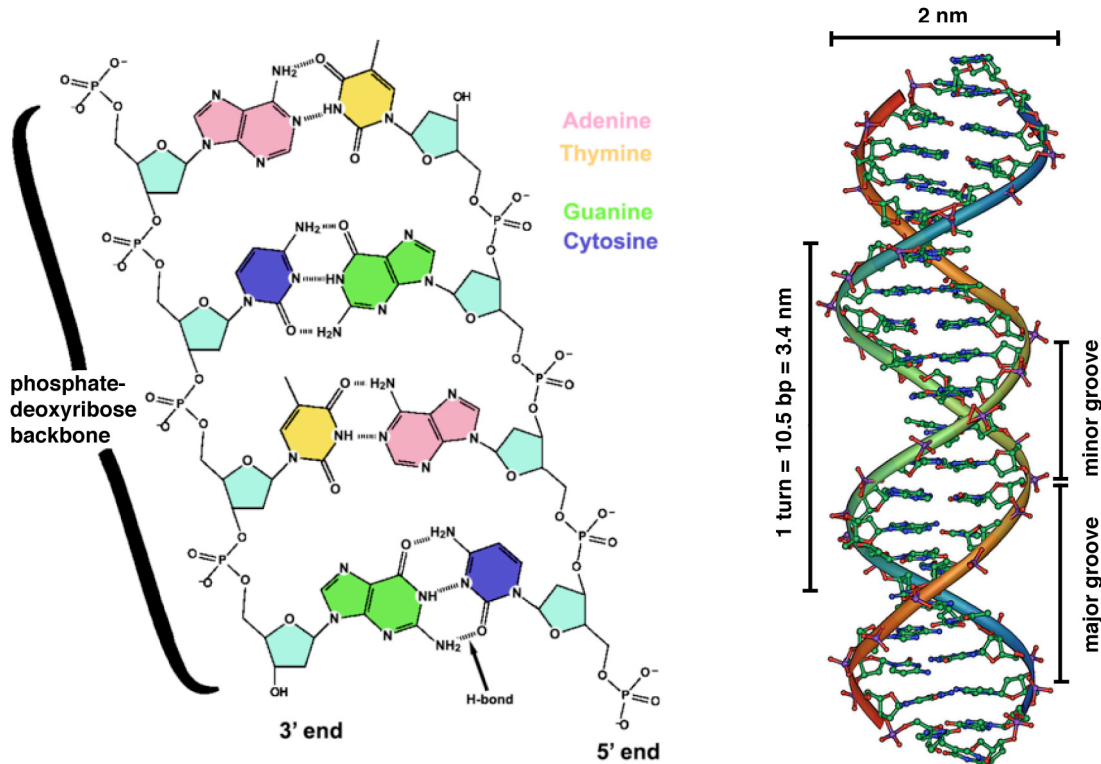


Figure 2.1: *DNA Double Helix*. (adopted from <http://en.wikipedia.org/wiki/Dna>)

Mediated by dipole interactions between the neighboring bases, the carbon rings of the bases align and water is expelled from the space between the base pairs. This so-called base stacking contributes significantly to the DNA binding free energy and stabilizes the Watson-Crick base pairing [25]. Under physiological conditions double stranded DNA (ds-DNA) adopts the right-handed 'B'-form, where the diameter of the helix is 2 nm and a full turn is completed by roughly 10.5 base pairs (bp). The vertical distance between two stacked bases in this conformation is 0.34 nm.

Each phosphate of the phosphate "backbone" is deprotonated at pH values > 1 and hence carries one negative charge at higher pH values. This makes DNA one of the most strongly charged polymers known. In the absence of salts like NaCl or KCl electrostatic repulsion of two complementary strands would be sufficient to prevent these strands from hybridization. The screening of the charges by dissociated, mobile salt ions can be described by the Debye-Hückel theory, which assumes a screening layer of relatively localized cations close to the DNA (Stern-layer) and a diffusive layer of cations and anions, loosely associated to the Stern-layer. The screening of the charges is not only relevant for interactions on the inter-molecular level, but also for the intra-molecular repulsion.

The mechanics of a fully screened single stranded oligonucleotide is well described by the freely jointed chain (FJC) model. This model assumes a chain of thin segments of uniform

length, where each segment can adopt all orientations in space with equal probability. The mean-squared end-to-end distance $\langle d^2 \rangle$ can then be expressed as $\langle d^2 \rangle = 2L_p Na$ where $2L_p$ is equals the Kuhn length, which is roughly 2 nm for ssDNA, N is the number of nucleotides, and $a = 0.43$ nm the distance between bases in ssDNA [26]. For the mechanical description of double stranded DNA, the Worm-Like Chain (WLC) model is employed. The main difference to the FJC model is the assumption of a continuous elastic medium, since dsDNA is a rather stiff molecule with a correlated orientation of its successive segments. The persistence length L_p is then a measure for the stiffness of the polymer and is defined as the distance at which the correlation between two tangential vectors \vec{t} along the polymer decreases to $1/e$:

$$\langle \vec{t}(s) \cdot \vec{t}(0) \rangle = e^{-s/L_p}$$

Here, s denotes the contour distance between two points of the polymer. For DNA, L_p depends on the concentrations of salts in the buffer. As a rule of thumb, the persistence length of dsDNA is approximately 50 nm or 150 bp. This makes dsDNA a fairly stiff polymer in comparison to synthetic polymers, like e.g., poly(ethylene glycol) (PEG), which has a persistence length of ~ 0.4 nm [27].

2.2 Thermodynamics of DNA

Whether two complementary strands adopt the stable double stranded helix conformation or the single stranded random coil conformation depends on buffer conditions, such as pH-value or salt concentrations, the concentration of the two strands, and critically on the buffer temperature. Since the transition from a rigid dsDNA helix to two flexible single strands is accompanied by a significant increase in entropy (ΔS), it is energetically more favorable for a given dsDNA to melt apart into two random coils above a certain temperature. The temperature at which half of the double strands have been separated into single strands is called the melting temperature T_M . Thus T_M is a measure of the stability of a DNA duplex and depends primarily on the length and on the base sequences of the DNA molecules.

Although the exact partitioning of the contributions to the stability of DNA - conformational entropy, stacking interactions, forming of hydrogen bonds, condensation of counterions around the backbone, and solvent effects - is not yet possible [25], there exist a variety of numerical methods to determine T_M [28]. As a simple approximation, the Wallace rule can be applied [29]:

$$T_M = 2^\circ\text{C} \cdot \#\text{AT} + 4^\circ\text{C} \cdot \#\text{GC} \quad (2.1)$$

$\#\text{AT}$ and $\#\text{GC}$ are the numbers of A-T and G-C base pairs in the double strand. The Wallace rule implies that due to the three hydrogen bonds between the bases G and C in the double helix this pair is stronger bound than the A-T pair, where only two hydrogen bonds are formed. It turns out that this model is too simple and is only roughly applicable for DNA sequences of a length of up to 18 bases. Marmur and Doty stated an expression,

where T_M is a linear function of the G-C content [30, 31]:

$$T_M = (69.3 + 0.41 \cdot (\%GC))^\circ\text{C} \quad (2.2)$$

Further extensions of the model of Marmur and Doty included the molarity of monovalent ions $[M+]$, the formamide content ($\%F$) [32], the total number of bases of the sequence n , and the number of mismatches D [33]. This allows for the approximation of T_M of DNA strands of more than 60 bp with the following expression:

$$T_M = (81.5 + 0.41 \cdot (\%GC) + 16.6 \cdot \log([M+] \frac{1}{M}) - \frac{500}{n} - f \cdot (\%F) - 1.2D)^\circ\text{C} \quad (2.3)$$

For f values between 0.60 and 0.71 have been stated (cf. chap. 3.2). The most accurate and complex method includes the thermodynamic interaction of all nearest-neighbor parameters in a DNA sequence [34, 35]. The 10 Watson-Crick nearest-neighbors and their interaction values are listed in table 2.1. The free energy ΔG^0 for each interaction in

Interaction	ΔH^0 ($\frac{kcal}{mol}$)	ΔS^0 ($\frac{cal}{molK}$)	$\Delta G_{37^\circ C}^0$ ($\frac{kcal}{mol}$)
AA/TT	-7.6	-21.3	-1.00
AT/TA	-7.2	-20.4	-0.88
TA/AT	-7.2	-21.3	-0.58
CA/GT	-8.5	-22.7	-1.45
GT/CA	-8.4	-22.4	-1.44
CT/GA	-7.8	-21.0	-1.28
GA/CT	-8.2	-22.2	-1.30
CG/GC	-10.6	-27.2	-2.17
GC/CG	-9.8	-24.4	-2.24
GG/CC	-8.0	-19.9	-1.84
Initiation	+0.2	-5.7	+1.96
Terminal AT penalty	+2.2	+6.9	+0.05
Symmetry correction	0.0	-1.4	+0.43

Table 2.1: Nearest-neighbour parameters for DNA Watson-Crick pairs in 1M NaCl, 37°C adopted from [35]. The slash of AA/TT indicates, that the sequences are given in antiparallel orientation. Terminal AT penalty applies for each end of the duplex that terminates with an AT bp. Symmetry correction applies to self-complementary duplexes.

this table is calculated at 37 °C. Since we can assume a constant heat capacity of DNA, ΔH^0 and ΔS^0 are temperature independent [36] and ΔG_T^0 can be determined at any other temperature with the standard thermodynamic relationship

$$\Delta G_T^0 = \Delta H^0 - T\Delta S^0. \quad (2.4)$$

Noticeable in table 2.1 are the comparatively large free energies of the three nearest-neighbors containing only C and G bases. This explains why T_M increases with increasing content of GC base pairs.

After calculating and summarizing the changes of enthalpy ΔH^0 and entropy ΔS^0 for each dimer of a given sequence, the melting temperature for non-self complementary duplexes is given by the equation [35]:

$$T_M = \frac{\Delta H^0 \cdot 1000}{\Delta S^0 + R \cdot \ln(C_T/4)} - 273.15 \text{ K} \quad (2.5)$$

ΔH^0 is in units of cal mol⁻¹ and ΔS^0 in units of cal K⁻¹ mol⁻¹, R is the gas constant 1.9872 cal K⁻¹ mol⁻¹ and C_T denotes the total molar concentration of the DNA strands in solution. Generally it has to be taken into account, that many duplexes have competing single stranded structures. In this case, the approximation of a two state transition is no longer justified, which leads to systematically lower values for T_M than calculated by this model.

2.3 Characterization of DNA-based nanodevices

Biochemistry and biophysics comprise a range of experimental techniques for the characterization of all sorts of biomolecules. A commonly applied technique for the characterization of DNA-based nanodevices that exhibit physical dimension of only a few nanometers is gel electrophoresis, which allows for the study of hybridization events and conformational changes of DNA-based nanodevices. However, the examination of dynamic processes with gel electrophoresis is hardly possible. Atomic force microscopes (AFM) have been used for the visualization of DNA assemblies [11], movements within DNA scaffolds [37], force measurements with single DNA strands [38, 39], and recently for force measurements with ensembles of DNA devices [40]. Due to the slow frame rates of standard AFM, fast conformational changes are hard to image, whereas force measurements have time resolutions of ~ 1 kHz.

An elegant optical method to visualize distance changes between two fluorophores with overlapping emission and absorption spectra relies on Förster resonance energy transfer or fluorescence resonance energy transfer (FRET). Since synthetic DNA strands can be labeled with a variety of fluorophores, FRET experiments can be employed to obtain insight into conformational changes of DNA-based devices, which are labeled with appropriate FRET pairs at designated points. The following sections will briefly discuss the basic principles of FRET and comment on the influence of metallic surfaces on the fluorescence properties of a fluorophores.

2.3.1 Energy transfer between fluorophores

FRET is a non-radiative transfer of energy from a fluorophore initially in its excited state (donor) to another fluorophore initially in its ground state (acceptor) and is based on dipole-dipole interactions between the two fluorophores [41, 42]. A Jablonski diagram of a model FRET system is shown in figure 2.2. The transitions between the different states are depicted as vertical lines. After the absorption of a photon, a fluorophore (donor)

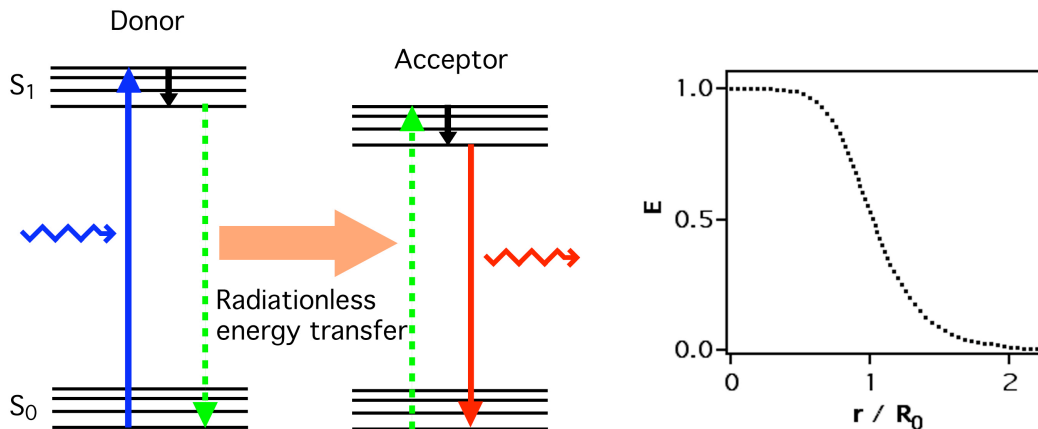


Figure 2.2: Förster resonance energy transfer. Left: Jablonski diagram of FRET between two fluorophores with overlapping emission and absorption spectra (cf. text). Right: $\frac{R_0^6}{R_0^6 + r^6}$ dependence of the FRET efficiency E .

is usually excited from the ground state S_0 to some higher vibrational level of S_1 if the energy of the photon matches the energy difference between the two states (blue arrow). The molecule relaxes in a process called internal conversion into the lowest vibrational level of S_1 (black arrow). This process is very fast and happens on a time-scale of picoseconds. Since fluorescence life-times of fluorophores usually are on the order of nanoseconds, the internal conversion is completed before the relaxation of the fluorophore to the ground state takes place. The relaxation to one of the vibrational states of the ground state is normally accompanied by the emission of a photon of the according energy. If a second fluorophore (acceptor) with an absorption spectrum that overlaps with the emission spectrum of the excited fluorophore resides in close proximity, the energy can be transferred radiationless, i.e. the first fluorophore relaxes without the emission of a photon and is thereby exciting the second fluorophore (green dashed arrows and orange horizontal arrow). The second fluorophore emits after internal conversion a red-shifted photon. The acceptor does not necessarily need to be a fluorophore itself, but can also be a dark quencher that dissipates the transferred energy non-radiatively.

The transfer efficiency between the donor and the acceptor E near the Förster radius R_0 strongly depends on their actual distance r :

$$E(r) = \frac{R_0^6}{R_0^6 + r^6} \quad (2.6)$$

Commonly used FRET pairs have Förster radii R_0 between 5 nm and 10 nm. The Förster radius depends on the quantum yield of the donor Q_D , the relative orientation in space κ , the refractive index of the medium n , and on the overlap integral $J(\lambda)$, which is a measure for the spectral overlap of the emission spectrum of the donor with the absorption spectrum

of the acceptor:

$$R_0^6 = \frac{9000(\ln 10)\kappa^2 Q_D}{128\pi^5 N_A n^4} J(\lambda) \quad (2.7)$$

N_A denotes the Avogadro constant and the overlap integral $J(\lambda)$ can be written as

$$J(\lambda) = \int_0^\infty F_D(\lambda)\epsilon_A(\lambda)\lambda^4 d\lambda \quad (2.8)$$

where $F_D(\lambda)$ is the normalized fluorescence intensity of the donor in the wavelength range λ to $\lambda + \Delta\lambda$ and $\epsilon_A(\lambda)$ is the extinction coefficient of the acceptor at the wavelength λ .

2.3.2 Energy transfer near metal surfaces

The energy transfer between a metallic surface and a fluorophore is dependent on the roughness of the surface material, the media in which the transfer takes place and on the distance between the metal and the fluorophore. Some of the distance-dependent effects will be briefly discussed in the following.

At distances in the range of the emission wavelength of the fluorophore, i.e. usually hundreds of nanometers, the excited state lifetime of a fluorescent molecule shows distance dependent oscillatory behavior, which can be explained by a simple interference model, which accounts for the superimposed electromagnetic field of the emitter and the field reflected from a flat metallic surface [43, 44]. For the short distance regime, i.e. between $\sim 1 - 10$ nm, theoretical studies that assumed the fluorescent molecule as a point dipole predicted nonradiative energy transfer from the excited fluorophore to the metal surface [45]. In this picture, the distance dependence of the energy transfer rate is coupled to the dimensionality of the metal surface, since the rate must be integrated over the volume of the mirror point dipoles. The $1/r^6$ distance dependence for a zero dimensional mirror dipole is reduced to $1/r^3$ for 3D solid metal, to $1/r^4$ for a 2D metallic film, and to $1/r^5$ for a 1D metallic line. A study by Gueroui and Libchaber [46] found good agreement for the $1/r^6$ dependence of the quenching efficiency between a CdSe quantum dot and a 1.4 nm gold nanoparticle separated by dsDNA. As a function of dsDNA length, the observed transfer satisfied a Förster process with a Förster radius of 7.5 nm. Yun *et al.* investigated in a similar study the quenching efficiency between the organic dye fluorescein (FAM) and 1.4 nm gold nanoparticles [47]. This group found a distance dependence of $1/r^4$ and suggested, that the donor dipole would interact with a virtual plane of dipoles, which can be associated with the gold nanoparticle. Dulkeith *et al.* attribute the fluorescence quenching of gold nanoparticles to an increased nonradiative decay rate and a decrease in the radiative decay rate of the fluorophore.

Besides the long distance effects and the short-range quenching influence of metal surfaces, also short-range fluorescence enhancement has been observed indirectly for organic dyes near silver particles [48] and on a single emitter level for quantum dots adsorbed on rough metallic surfaces [49].

In conclusion it has to be stated that the findings for the fluorescence behavior of fluorophores near metal surfaces are diverse and not always consistent. Experiments involving metal-mediated quenching of fluorophores need to be interpreted carefully and should always involve systematic control experiments.

3 Determination of DNA Melting Temperatures in Diffusion-Generated Chemical Gradients (Ref. [2])

Although the melting temperature can be calculated quite reliably under standard conditions, the calculations fail under non-standard conditions. Such non-standard conditions could be extreme pH-values or salt concentrations or the utilization of DNA strands, which display mismatching regions or extensive secondary structures. In these cases T_M has to be determined experimentally.

3.1 DNA melting temperature determination by thermal denaturation

The melting temperature of polynucleotides can be determined by measuring the optical absorbance of the sample dissolved in buffer, while slowly sweeping the temperature. The optical absorbance A is defined as $A(\lambda) = -(\ln[I_d(\lambda)/I_0(\lambda)]/d$, where $I_0(\lambda)$ is the intensity of light of the wavelength λ before and $I_d(\lambda)$ after passing the optical pathway d . The optical pathway generally is normalized to 1 cm. DNA and RNA in solution have a characteristic absorption peak at 260 nm, which originates from excitable in-plane transitions of the π electrons of the nucleotides. The dipole interactions between nucleotides and their surroundings influence these transitions and causes the absorbance of a solution containing double stranded polynucleotides to be lower than the absorbance of a solution of the same polynucleotides in single stranded conformation. This effect is called hypochromism and is usually employed for measurements of the melting temperature of a polynucleotide. A plot of the normalized absorbance at 260 nm over temperature is depicted in Fig. 3.1 (left). For reliable measurements, the temperature is typically changed at 1° C every five to ten minutes to allow thermal equilibration of the whole sample volume. The sample volume in an experiment depends on the size of the cuvette employed and ranges from 75 μ l to 1 ml.

Alternative to absorbance measurements, it is sometimes more favorable to measure T_M by monitoring the Förster Resonance Energy Transfer (FRET, cf. chapter 2.3) efficiency of a FRET pair attached to the DNA strands of interest. For this purpose, generally two methods are conceivable: (i) The FRET pair is attached to the two ends of the same

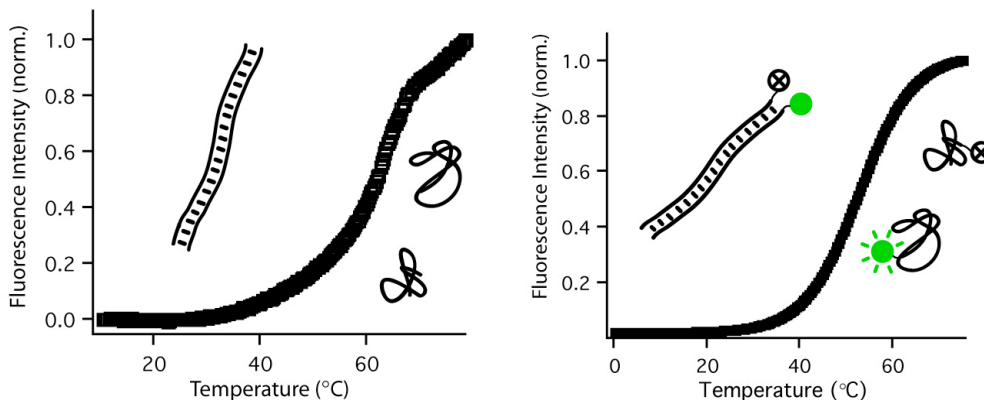


Figure 3.1: *Melting of dsDNA. At lower temperatures two complementary strands form a stable double helix and melt apart at higher temperatures. Left: The absorbance at 260 nm in the double stranded conformation is relatively small (cf. text) and increases at higher temperatures when the single strands adopt a random coil conformation. Right: The recorded fluorescence intensity of a solution containing complementary, labeled DNA strands changes while the temperature is swept and the strands dissociate (cf. text).*

ssDNA. In the random coil conformation, the end-to-end distance can be estimated with $d = \sqrt{2L_pNa}$ (cf. chapter 2.1) and is much shorter than the end-to-end distance of the stiff double helix. E.g. the end-to-end distance for an approximately rod-like 30 bp helix is ~ 10 nm, while a 30 bases long single strand has an end-to-end distance of only ~ 5 nm. This change in distance can be easily monitored, since Förster radii of available FRET-pairs are in the range between 5 nm and 10 nm. This labeling method finds its limitation in the fact, that for long strands the random coil end-to-end distance is already much larger than the available Förster radii. (ii) The donor of the FRET pair is attached to the 3' or 5' end of one strand and the acceptor is attached to the 5' or 3' end of the complementary strand in such a manner that in the duplex conformation, the donor and the quencher are in close proximity. The distance between the donor and the acceptor linked to the dissociated strands depends mainly on the concentration of the strands in the solution but it will certainly be much larger than in the duplex conformation (Fig. 3.1, right). In principle, this method is suited for all lengths of polynucleotides, although possible stepwise dissociation of parts of the duplex far away from the FRET pair remains undetectable. In both methods, the fluorescence labeling is not necessarily restricted to the ends of the oligonucleotides. Since synthetic oligonucleotides can also be labeled at certain bases along the sequence, the melting behavior of a long DNA sequence could be investigated in detail, by positioning the labels at various regions of interest.

3.2 DNA Melting temperature determination in Chemical gradients (Ref. [2])

The common methods to determine T_M described above exhibit two major drawbacks: the high sample consumption and the long measurement times. In reference [2] a method is proposed to determine T_M in a fast and efficient way. The basic idea is to determine the melting temperature along a diffusively generated gradient of a denaturing agent in a microfluidic setup. As already indicated in equation 2.3, the melting temperature of a DNA duplex is lowered by the molecule formamide (CH_3NO), which is able to form hydrogen bonds with the bases and therefore competes with the Watson-Crick pairing (Fig. 3.2).

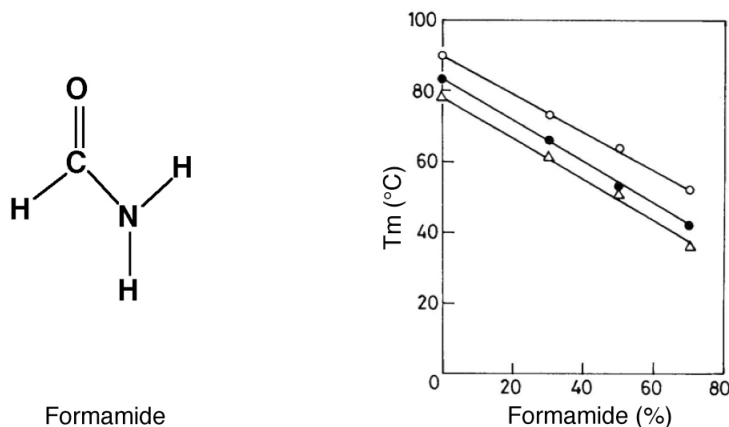


Figure 3.2: *Left: Chemical structure of formamide. Right: Melting temperatures of DNA samples from three different organisms at varying formamide concentrations. Linear fits reveal a slope of $-0.6\text{ }^\circ\text{C} / \%$ formamide in solution (from [50], with kind permission of the Journal of Bioscience).*

The first study examining the correlation between DNA melting temperature and formamide concentration in solution by McConaughy *et al.* [51] claimed for DNA duplexes a T_M dependence of $-0.72\text{ }^\circ\text{C} / \%$ formamide in solution. Later Casey *et al.* [52] determined a slope of $-0.63\text{ }^\circ\text{C} / \%$ formamide. Both studies presumed a G-C content dependence of the slope. A later study [50] found a dependence of $-0.60\text{ }^\circ\text{C} / \%$ and no influence of the sequence composition between 38% and 66% G-C content. The latest study by Blake *et al.* [53] revealed an almost linear dependence of the denaturing behavior of formamide from the G-C content between $-0.60\text{ }^\circ\text{C} / \%$ for 0% G-C content and $-0.72\text{ }^\circ\text{C} / \%$ for 100% G-C. Since our data could be described best with a value of $-0.64\text{ }^\circ\text{C} / \%$ formamide, we chose this value for evaluation.

To generate a stable chemical gradient, a multilayer polydimethylsiloxane (PDMS) mi-

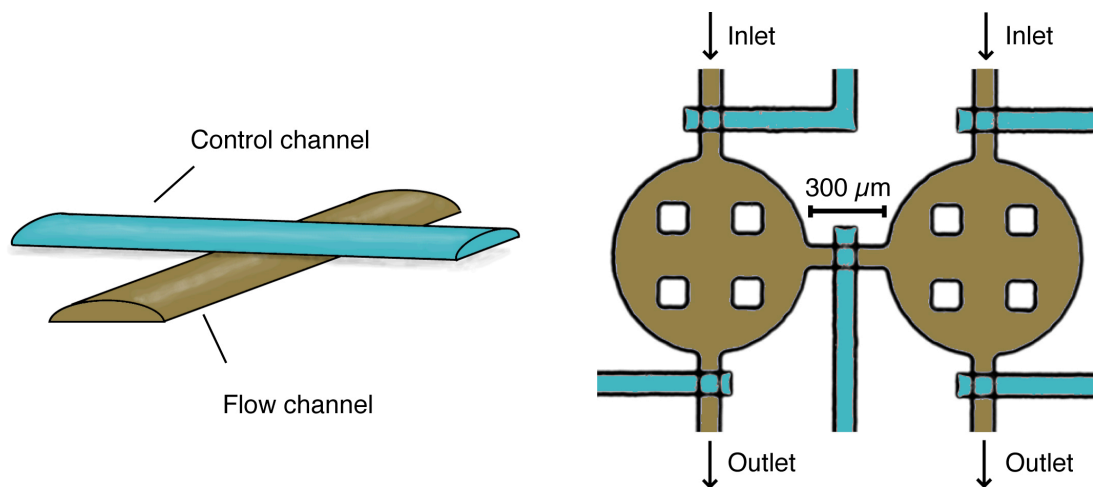


Figure 3.3: *Multilayer microfluidics. Left: At intersecting points of flow and control channels the two volumes are separated by a thin PDMS membrane. If a high enough pressure is applied in the control channel, the membrane is pushed down and closes the tunnel-shaped flow channel. Right: Color enhanced top view of the microfluidic setup. The control channels can be addressed individually, which allows the independent filling of the two circular reservoirs. The eight squares are supporting columns, which prevent the reservoirs from collapsing.*

crofluidic chip with built-in monolithic valves was fabricated with soft lithography methods [54, 55]. The core element of the lower layer - or flow layer - of the chip consists of two reservoirs ($\varnothing = 750 \mu\text{m}$, height = $20 \mu\text{m}$), which can be filled with the liquids of interest (Fig. 3.3). The reservoirs are connected by a narrow channel ($300 \mu\text{m} \times 100 \mu\text{m}$). At designated points the channels of the top layer - or control layer - cross the flow channels. At these points the two layers are only separated by a thin membrane ($\sim 20 \mu\text{m}$) of PDMS. If pressure is applied to a control channel, the membrane acts as valve as it is pushed down and thereby closes the underlying flow channel. If the connecting channel is closed by such a valve each reservoir can be filled with a different solution. After completed filling, the intersecting valve is opened and the two liquids mix in the connecting channel by means of diffusion thus building up a stable, linear gradient of each differing compound of the two solutions.

In a simplified model, the connecting channel can be considered as a one-dimensional tube of length L , containing molecules or particles with a constant diffusion coefficient D and fixed concentrations $c(x = 0, t) = 0$ and $c(x = L, t) = c_0$ at its ends. With these boundary conditions the solution to the 1D diffusion equation

$$\frac{\partial c(x, t)}{\partial t} = D \frac{\partial^2 c(x, t)}{\partial x^2} \quad (3.1)$$

is time independent and reads

$$c(x) = c_0 \cdot \frac{x}{L} \quad \text{for } 0 \leq x \leq L. \quad (3.2)$$

Hence, we expect a linear gradient along the connecting channel. Finite element simulations for the described setup yield a linear gradient of solutions along the connecting channel if we assume that the concentrations in the reservoirs remain constant during the measurements (cf. Fig. 2 in Ref. [2])

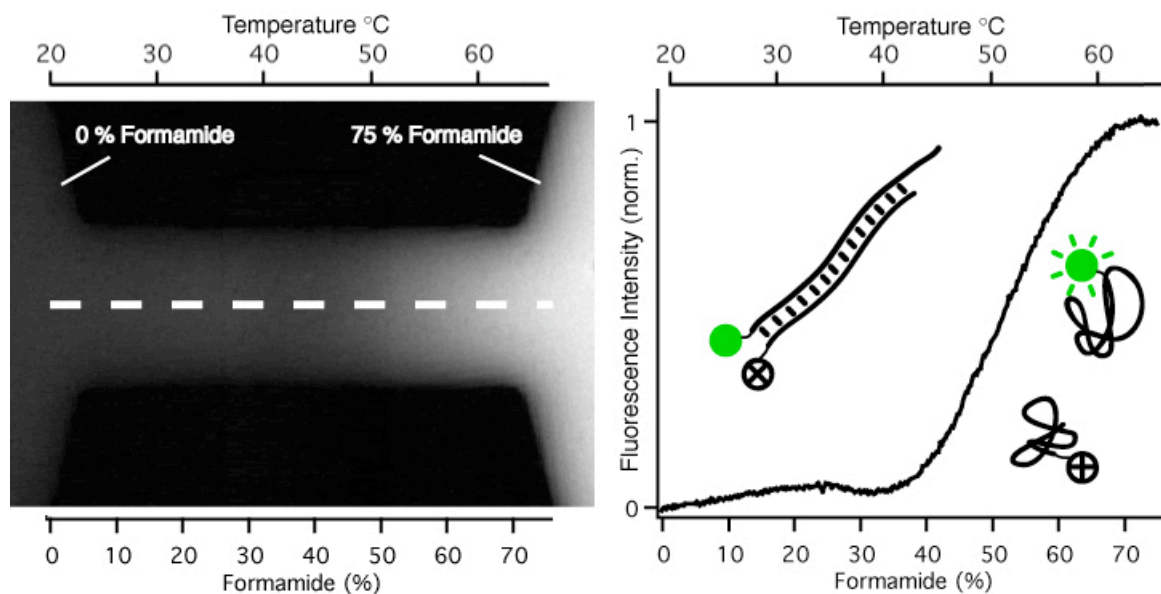


Figure 3.4: *DNA dissociation along a formamide gradient. Left: Fluorescence micrograph of the connecting channel between the two reservoirs (cf. Fig. 3.3) one minute after opening the intersecting valve. Both reservoirs were filled initially with PBS buffer containing two DNA strands with 14 bp complementary sequence. One strand was labeled with a dye on the 5' end, the other strand with a quencher on the 3' end. The left buffer contained 0 %, the right buffer 75 % formamide. Right: Normalized fluorescence intensity along the dashed line of the left image. The linear formamide gradient along the channel can be mapped to a corresponding virtual temperature.*

In Ref. [2] the melting temperatures of five pairs of partly complementary DNA strands were measured. To determine T_M of one DNA pair the reservoirs were separately filled with two buffers of which both contained the same amount of DNA while one buffer contained 0 % and the other 75 % formamide. Shortly after opening the intersecting valve a stable formamide gradient established between the reservoirs. Above a certain formamide concentration in the solution the DNA duplexes dissociated into single strands, which was monitored by measuring the FRET efficiency of a donor and acceptor pair tethered to the

ends of the DNA strands (cf. Fig 3.4).

Comparison of the gradient measurements with conventional temperature sweeps (cf. chapter 3.1) yielded very good agreement. The study demonstrated the possible application of diffusion generated formamide gradients to determine melting temperatures at single base pair resolution. In contrast to time-consuming temperature sweeps of ten or more hours, each measurement in the microfluidic setup took only a few minutes while consuming only a few microliters of sample volume. Although PDMS has a considerable absorption in the ultra violet, the setup could be adjusted to enable 260 nm absorption measurements. This is desirable, since labeling of DNA strands with fluorescent dyes is cost intensive. In figure 4 of [2], the detection of a single nucleotide mismatch in a 14 bp strand is demonstrated. Thus, the method presented here could find application in Single Nucleotide Polymorphism (SNP) detection. The microfluidic chip is reusable and could be applied to generate solution gradients of all kinds of chemical agents. Furthermore, this principle is not restricted to the generation of 1D gradients of only two solutes. In figure 3.5 a possible design for a microfluidic chamber with four reservoirs and an area for diffusive mixing of up to four components is depicted.

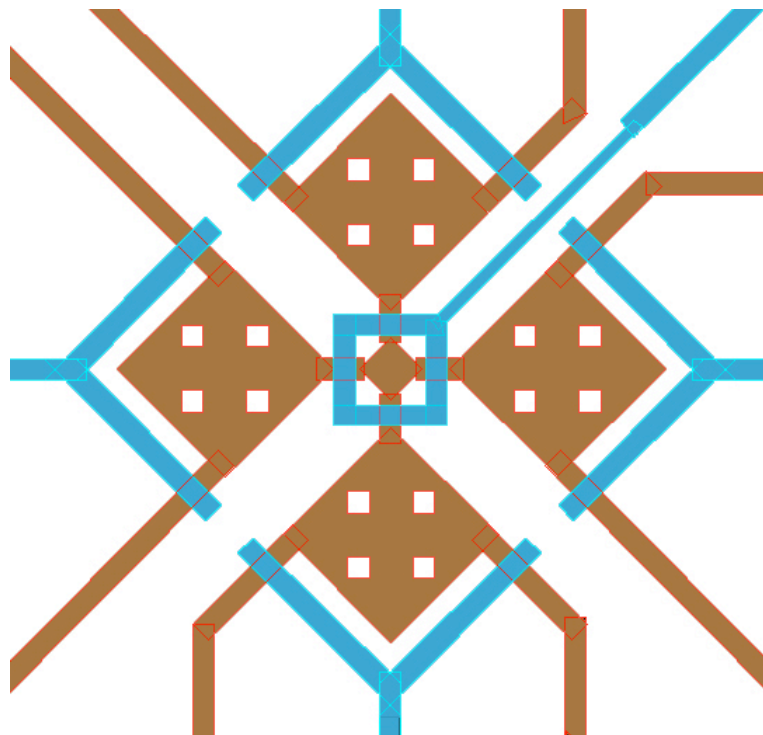


Figure 3.5: *Design for the creation of 2D gradients of four different solutes. Four reservoirs surround the quadratic measurement region in the middle.*

4 A DNA switch driven by a Chemical Oscillator (Ref.[3] and[4])

In living cells directed movements on the micrometer scale are accomplished by a large variety of molecular motors, such as myosin or kinesin. These biological motors convert chemical energy during the breakdown of ATP to ADP and inorganic phosphate. This breakdown introduces an irreversible chemical step into the operation cycle of these motors which gives rise to the directionality of their movement. In a closed system, these motors would stop running after all the ATP has been consumed. However, biological systems are open systems and high ATP levels are sustained by metabolic processes such as oxidative phosphorylation. In that sense a cell provides a specific sort of chemical energy that is converted into motion under permanent consumption of energy offered by the organism (Fig. 4.1). As long as the cell and its surrounding organism is living, this state of non-equilibrium is maintained. After death, an organism decays towards a state of thermodynamic equilibrium.

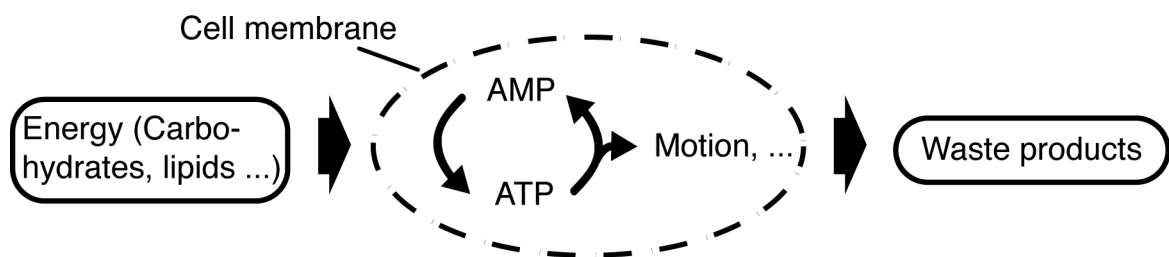


Figure 4.1: *A living cell constantly provides its internal molecular motors with specific molecules, e.g. adenosinetriphosphate (ATP), whose stored energy can be converted by the motors into motion. The cell itself is in a situation of non-equilibrium and breaks down nutrition (e.g. carbohydrates and lipids) into disposal forms of energy and waste products.*

So far, operation mechanisms for artificially constructed DNA-based molecular devices - as the DNA tweezers presented in the introduction - were not availing these aspects. Usually, a conformational change in these devices was enforced by the addition of DNA “fuel” strands – leading to the stiffening of a previously flexible single stranded part of the device or the connection of previously distant sections of it [12, 56]. Other DNA machines were

driven by a change of buffer conditions which was accompanied by conformational changes of the devices [57, 58, 59]. To return to the original state – and enable cyclical operation – fuel strands had to be removed by “anti-fuel” strands or the original buffer conditions had to be restored. Continuous operation of these devices requires keeping track of the state of the devices and the external initiation of transitions at the right moment. Under closed conditions, waste products accumulate and soon become the dominant chemical species in the system and impair proper function of the devices. In this chapter a novel concept for autonomous movements of DNA devices will be introduced. In particular, two publications of our group (cf. ref. [3] and ref. [4]) demonstrate how the conformational transition of a single-stranded DNA switch can be driven autonomously and continuously by an oscillating chemical reaction, keeping it under non-equilibrium conditions all the time. From a conceptual perspective, by this means the situation of molecular motion in a living cell is mimicked, where motion occurs in a situation of permanent non-equilibrium.

4.1 Non-equilibrium systems

Before we address non-equilibrium systems, let us first recall the basics of the formation of ordered structure in thermodynamic equilibrium. An example for such a process is the formation of a monocrystal in a saturated solution. Structures in equilibrium form in closed systems¹ if the system’s loss of entropy S is over-compensated by the binding energy U . Finally, the free energy $F = U - T \cdot S$ reaches a minimum at a certain temperature T . Thus, every fluctuation away from the minimum causes a restoring force that drives the system back to equilibrium.

Structures in non-equilibrium - or dissipative structures - form in open systems under constant supply of energy and/or mass transfer from the surrounding, which may result from diffusion, convection or chemical reactions. The system’s entropy has two contributions and is changing over time:

$$\frac{dS}{dt} = \frac{dS_{int}}{dt} + \frac{dS_{ext}}{dt}. \quad (4.1)$$

$\frac{dS_{int}}{dt}$ describes the internal production of entropy (we assume irreversible processes inside the system) and $\frac{dS_{ext}}{dt}$ is the change of entropy due to energy and mass exchange with the environment. In general, $\frac{dS}{dt} > 0$ and in the special case of a steady state $\frac{dS}{dt} = 0$ or

$$-\frac{dS_{ext}}{dt} = \frac{dS_{int}}{dt} > 0. \quad (4.2)$$

It can be stated, that a steady state - or the formation of a pattern under non-equilibrium conditions - occurs due to constant supply of negative entropy from the environment [60]. If we define entropy as a quantification of disorder, then this flux of negative entropy can be understood as the cause for the emergence of order in dissipative systems.

¹Here, a closed system may exchange only energy with its surrounding.

In nature, only a comparatively small number of systems can be described as equilibrated systems. An example of a dynamic system that is sustained in permanent non-equilibrium is the sand dune. Such a structure emerges although the wind dislocates the single sand grains fast and over huge distances. The growth of a dune can be initiated by a small fluctuation, e.g. a rock in the sand. The accumulation of sand in the slipstream behind the rock leads to growth of the dune, which causes a larger slipstream and further accumulation of sand. This is a short ranged positive feedback mechanism. On the other hand, a long-range mechanism of suppression is necessary to obtain a single dune within a certain area. Here, this mechanism is the accumulation of sand in the slipstream, which is responsible for the depletion of sand in the air and suppresses the formation of a second dune in the adjacencies [61].

In this example, we have already seen two basic elements of pattern formation in dynamic systems: a local positive feedback on a so-called activator that leads to further amplification of a fluctuation of the activator concentration and a far-ranging antagonistic reaction, which suppresses the unhindered amplification. For the development of a dynamic system, the temporal evolution of these two reactions is crucial. E.g., the concentration bursts of a species in an oscillatory system - such systems will be discussed in chapter 4.3 - can be caused by slow reacting antagonistic feedback. In such a case, the increase of the activator concentration is not down-regulated instantaneously, which causes the concentration burst. The burst lasts until the antagonistic system - this can be the rising concentration of an inhibiting species - reacts or the substrate is exhausted. Usually, the burst is followed by a refractory period where either the excessive concentration of inhibitor is degraded or the substrate is regenerated to the point where a new activation is possible.

4.2 Reaction diffusion processes

The interest in reaction diffusion (RD) processes was particularly driven by the wish to understand spatiotemporal ordering in biological surroundings. RD systems rely on the competition between two classes of processes: i) reaction processes, which are responsible for the production or consumption of chemical species, where the species can autocatalyze or inhibit their own production. Furthermore, one chemical species can activate or inhibit the production of other species. ii) diffusive processes driven by concentration gradients of the reacting species. In a biological context, the chemical species are called *morphogens*. Some examples for biological spatiotemporal ordering are fur patterns of mammals, pigmented patterns on sea shells, and the embryonal development of *drosophila melanogaster* (fruit fly) [62] (Fig. 4.2). The underlying interactions between inhibiting and promoting genes, which are expressed during early development stages of a *drosophila* embryo emerged from numerous experiments [63, 64].

RD systems² can be described mathematically by a set of partial differential equations of

²A detailed review on pattern formation in non-equilibrium can be found in [65]

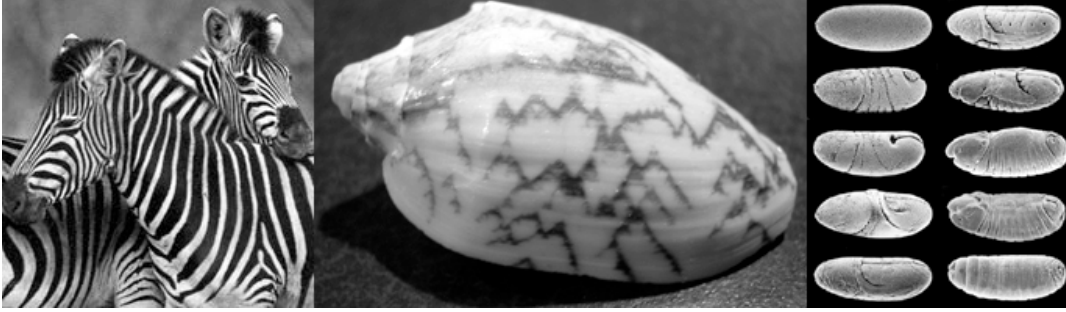


Figure 4.2: The basic assumptions for the pattern formation depicted in these images are: (i) Activating and inhibiting molecules, so-called morphogens, are responsive for the local or temporal emergence of a color or a feature; (ii) The activation or inhibiting processes are coupled in a non-linear fashion; (iii) The activating and inhibiting morphogens have different diffusion properties. Left: Zebra with striped patterns. Middle: Shell with a triangular pattern. Right: During the different stages of development the drosophila embryo converts from a unrippled ellipsoid (called cellular blastoderm) to a striped larva. ©FHCRC

the following form:

$$\frac{\partial c_i}{\partial t} = \nabla \cdot (D_i \nabla c_i) + R_i(\{c_j\}, r, t) \quad (4.3)$$

where c_i denotes the concentration of species i , D_i its diffusion coefficient and R_i is the reaction term, which is potentially dependent on the location, time and the concentrations of other species j . With such a set of equations, the formation of pigmented patterns of animals (Fig. 4.2, left and middle) can be described if we assume that pigmentation only occurs in regions with high enough concentration of an activator A . As stated earlier, the basic requirement for the spontaneous establishment of a pattern is the local self-amplification of the activator coupled with a far-ranging antagonistic response. For the example of the dune in chapter 4.1 we have already seen that an antagonistic effect can rely on the depletion of a substrate, which is needed for the production of the autocatalytic activator. Another possible reason for an antagonistic effect can be the inhibition of the autocatalytic process by an inhibitor B . Both models are briefly discussed in the following. An activator-inhibition mechanism can be described by the following equations [61]:

$$\begin{aligned} \frac{\partial c_A}{\partial t} &= D_A \frac{\partial^2 c_A}{\partial x^2} + d \left(\frac{c_A^2}{c_B} + b_A \right) - r_{ACA} \\ \frac{\partial c_B}{\partial t} &= D_B \frac{\partial^2 c_B}{\partial x^2} + b_B + d c_A^2 - r_{BCB} \end{aligned} \quad (4.4)$$

c_A is always the concentration of the activator A and c_B denotes the concentration of the inhibitor B . d is a measure of the density of the pigment producing cells, r_A and r_B the constant degradation rates of both species, and b_A and b_B the basic production rates of the activator and the inhibitor. The activator has a non-linear autocatalytic influence ($d \cdot c_A^2$) and its production is inhibited by the Inhibitor (d/c_B). The degradation of a species depends

on its own concentration (r_{AC_A} and r_{BC_B}) but a concentration-independent production of the activator (b_A) is necessary for initiation and regeneration processes. For the formation of a stable pattern an inhibitor that diffuses much faster than the activator is crucial, i.e. $D_B \gg D_A$.

A model that relies on the consumption of a substrate S by the activator A can be given:

$$\begin{aligned} \frac{\partial c_A}{\partial t} &= D_A \frac{\partial^2 c_A}{\partial x^2} + d \cdot c_S \left(\frac{c_A^2}{1 + s_A c_A^2} + b_A \right) - r_{AC_A} \\ \frac{\partial c_S}{\partial t} &= D_S \frac{\partial^2 c_S}{\partial x^2} + b_S - d \cdot c_S \left(\frac{c_A^2}{1 + s_A c_A^2} + b_A \right) - r_{SC_S} \end{aligned} \quad (4.5)$$

In this model, c_S denotes the concentration of the substrate S . Here the autocatalytic production of the activator A depends directly on the concentration of the substrate ($d \cdot c_S c_A^2$) and the degradation of the substrate depends likewise on the production of the activator. The saturation term s_A reduces the number of activated cells to a fraction of the whole ensemble and helps to prevent the simulation from numerical instabilities.

For the establishment of a stable pattern, the substrate needs to be produced at a high enough rate (i.e. $b_S > r_A$) to avoid the emergence of oscillatory behavior over time (cf. chapter 4.3). Also in this model, the range of the antagonist must be much larger than the range of the activator (i.e. $D_S \gg D_A$).

Although Turing proposed already in 1952 a model for RD systems relying on autocatalytic morphogens [66] and seminal work on dissipative systems was provided by Prigogine *et al.*³ [67, 60] in the 1960's, the application of the underlying chemical and physical framework to the field of nanotechnology and materials science is only just beginning.

In recent experiments the group of B. A. Grzybowski demonstrated how reaction diffusion processes can be employed to structure material with sub-micrometer features. They developed a 'wet stamping' technique for patterning hexacyanoferrate ($K_4Fe(CN)_6$) doped gelatine gels by bringing an agarose stamp inked with an inorganic salt (typically iron(III) chloride, cobalt(II) chloride, or copper(II) chloride) in contact with the gel [68, 69]. While the salt cations, which are constantly delivered from the stamp, precipitate all hexacyanoferrate they encounter, they establish a sharp concentration gradient of hexacyanoferrate at the reaction front. The unreacted hexacyanoferrate diffuses in direction of that gradient leaving a depleted region behind. If two of these traveling waves encounter each other, a narrow region containing no hexacyanoferrate - and thus no precipitating material - remains between the reaction fronts. These regions are only 300 nm wide, while the features of the stamp are separated 50 μm .

³Prigogine and Lefever introduced the term 'dissipative structure'. The fact that the work was conducted at the Université Libre de Bruxelles bestowed the introduced mathematical models the name 'Brüsselator'.

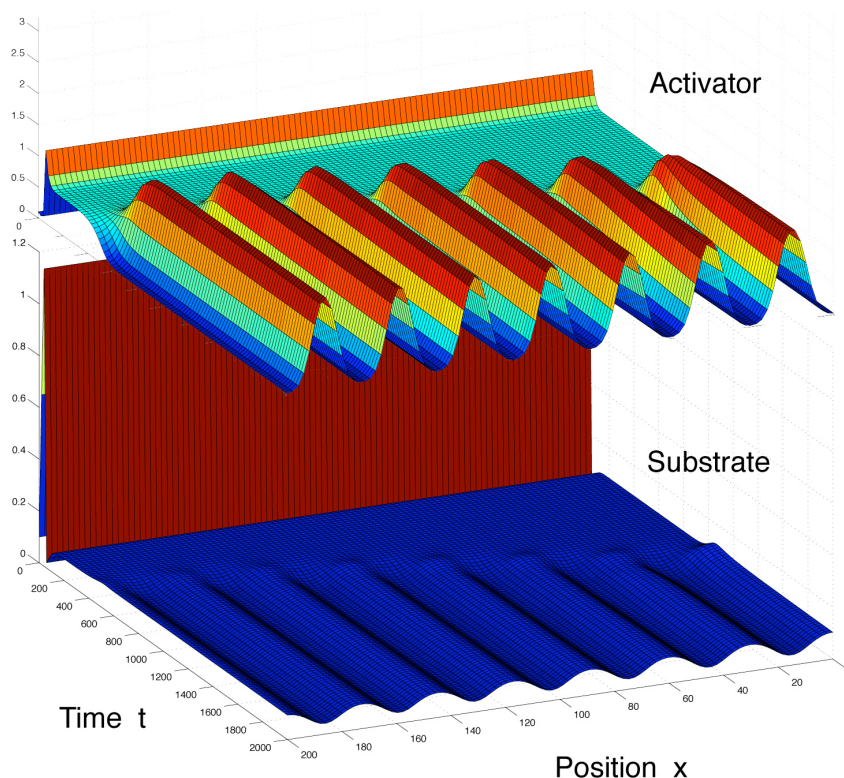


Figure 4.3: *Pattern formation with the activator-substrate mechanism (Eq. 4.5). A slightly increased initial activator concentration on the left induced the formation of an activator maximum. The maximum grows under consumption of the substrate, which initiates the formation of further maxima and at the same time inhibits the formation of secondary maxima in close proximity. The simulations were conducted with MATLAB.*

4.3 Oscillatory systems

Besides stationary pattern formation, also oscillatory reactions play an important role in nature. Almost a century ago Alfred J. Lotka proposed a simple set of non-linear differential equations, with which the population oscillations of predator-prey systems could be described⁴[70]:

$$\begin{aligned}\frac{\partial H}{\partial t} &= h_r H - h_d H L \\ \frac{\partial L}{\partial t} &= -l_d L + l_r H L\end{aligned}\tag{4.6}$$

⁴Vito Volterra developed independently the same set of equations. The equations are therefore named ‘Lotka-Volterra equations’.

A set of data which could be captured with this equations was provided by the Hudson Bay Company. It consisted of the records of hunted lynx - the predator - and hunted snowshoe hares - the almost exclusive prey of the lynx - between the years 1850 and 1930. In the equations 4.6 H and L are then measures for the populations of hares and lynx, h_r and l_r are the constant reproduction rates of the species, and h_d and l_d their constant death rates. It can be shown, that near the fixed point of this system ($H = l_d/l_r$ and $L = h_r/h_d$), the trajectory in the H, L space is described by an equation of an ellipse, which means that near the stationary point the system acts like a harmonic oscillator [71].

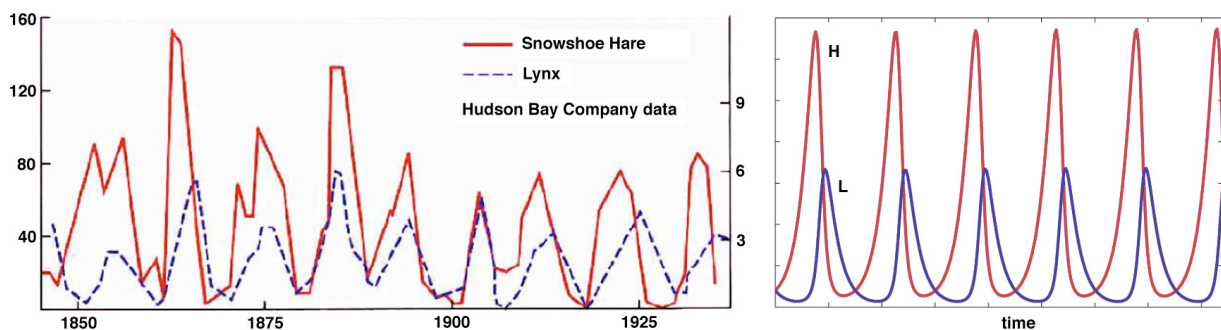


Figure 4.4: *Predator Prey Model. Left: Data on hunted furs provided by the Hudson Bay Company. Right: The simple equations 4.6 describe the data qualitatively well. Note, that in the real data and in the simulation the number of the predators always lags behind the number of the prey.*

Other examples of naturally occurring oscillations are circadian clocks [72, 73], calcium oscillations in cells [74], glycolytic oscillations [75], and oscillating concentration of cyclic adenosine monophosphate (cAMP) during the aggregation of slime molds [76, 77]. In recent years, the design of artificial oscillatory systems in biological surroundings has been aspired. Elowitz and Leibler constructed an oscillatory network of three mutually repressing transcriptional systems in *Escherichia coli* and termed it ‘Repressilator’ [78]. An oscillatory transcriptional network of Kim *et al.* (cf. chapter 1.3) is based on inhibiting and activating genes, operates *in vitro*, and can provide DNA-based machines with ‘fuel’ RNA ([20, 21] and unpublished results).

Chemical oscillatory reactions are artificial systems, which represent a situation of permanent non-equilibrium and exhibit overall oscillating concentrations of chemical species in a stirred open or closed reactor. The first chemical oscillator that was described in detail is the Belousov-Zhabotinsky reaction [79]. While studying the Krebs cycle in the 50’s, Boris Belousov discovered periodic color changes in a mixture of citric acid, bromate, and cerium catalyst in a sulfuric acid solution. The changes in color indicated the cyclic formation and depletion of cerium in different oxidation states. However, Belousov’s attempts to publish his work failed. The common picture of a chemical oscillation at that time was a damped

pendulum passing with each oscillation through its thermodynamic equilibrium position. This indeed would be impossible, since moving away from equilibrium would require an increase of Gibbs free energy. Today we know that a chemical oscillatory system - exactly like a mechanical system - does not reach its equilibrium until the end of its oscillations. In 1961 A. M. Zhabotinsky reproduced Belousov's results and was able to modify the reaction by using malic or malonic acids as reductants. The reaction could be described mathematically ten years later by Field, Koros, and Noyes (FKN)⁵ [80].

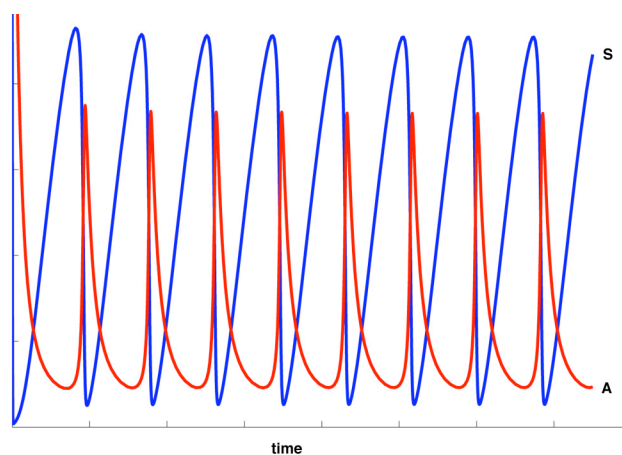


Figure 4.5: *Activator-substrate reaction without diffusion. Without the diffusion term the equation 4.5 describes oscillatory behavior of an activator A (red) and a substrate S (blue) if the basic production of the substrate b_S is too low to permit a steady production of the activator, i.e. the condition $b_S < r_A$ is fulfilled.*

Without the continuous stirring, the Belousov-Zhabotinsky reactions display spatio-temporal pattern development, which relies on local, propagating concentration changes. Figure 4.6 depicts such propagating waves in a petri dish generated by the Belousov-Zhabotinsky reaction.

Besides the well-known Belousov-Zhabotinsky reaction, there are numerous other examples of reactions in which chemical concentrations oscillate in time or travel in space as chemical waves [81, 82].

The motivation for the studies on oscillatory reactions presented in chapter 4.5 and 4.6 was to apply the concepts of non-equilibrium dynamics to actuate a DNA-based nanomachine. In this context, a special group among the oscillatory reactions captured our interest: the group of the pH-oscillators. During these reactions, the concentration of H^+ -ions varies over time. This is of particular relevance, since various DNA-based devices can be switched

⁵Following the nomenclature of the Brüsselator of Prigogine *et al.*, a simplification of the FKN model was referred to as the ‘Oregonator’, since the studies were conducted at the University of Oregon.



Figure 4.6: *The Belousov-Zhabotinsky reaction: In an unstirred mix of sodium bromate, ferroin, malonic acid and sulfuric acid in a petri-dish, changes of the concentrations of ferroin (red-orange) and ferrin (colorless-blue) ions are propagating in spiral-like waves.*

between their conformational states by changing the pH-value of the solution.

4.4 pH-sensitive DNA devices

Under certain conditions, DNA can adopt conformations quite different from the canonical double helix introduced in chapter 2.1. In particular, cytosines become protonated at low pH-values - the pK value for cytosine is approximately 4.2 - which allows for the formation of cytosine-protonated cytosine base pairs ($C-C^+$). At low pH-values DNA strands containing tracts of cytosines have the ability to adopt a conformation known as the “i-motif”, a tetrad structure of four anti-parallel DNA strands sustained by the non-canonical interaction of intercalating protonated and unprotonated cytosine residues [83]. Liu *et al.* [57] took advantage of this effect and designed a pH-dependent DNA machine based on the transition between a canonical DNA duplex and the i-motif. In the particular case of the device used here, a DNA strand containing four triples of cytosines is able to form six intramolecular $C-C^+$ base-pairs at pH values below 6.2. This leads to the folded DNA structure depicted in Fig. 4.7 (left). At higher pH values, the cytosines are deprotonated and the strand containing the i-motif sequence is able to hybridize to a complementary ssDNA, which is present during the whole experiment. The two strands thus form a stiff double helix. The transition between the i-motif and the double helix conformation can be visualized with Förster Resonance Energy Transfer (FRET) experiments (cf. chap. 2.3). To this purpose, Liu *et al.* labeled one end of the DNA strand with the sequence 5' - CCC ATT CCC ATTT CCC ATT CCC - 3' with a pH-insensitive dye, the other end with a fluorescence quencher. At low pH values the i-motif forms, which brings the labeled ends in close proximity. In this conformation the fluorescence is quenched due to radiationless energy transfer between the dye and the quencher. At pH-values above 6.2 the strand hybridizes to its complementary counterpart. Now both ends of the stretched double helix are far apart and no or only little quenching occurs. This leads to a strong change of the

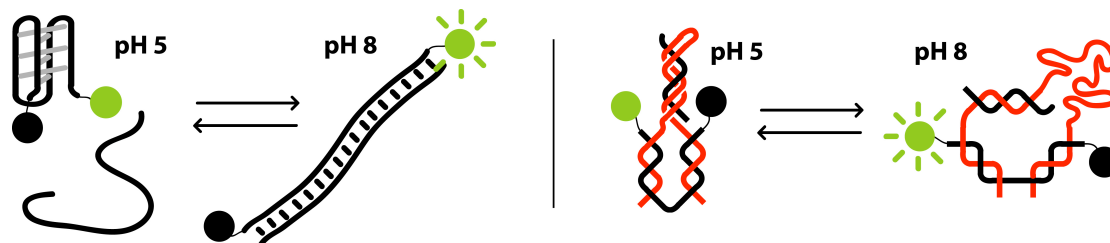


Figure 4.7: *Two pH-dependent DNA devices. Both devices are labeled with a pH insensitive FRET pair. The dye (green circle) is attached to the 5' ends and the quencher is attached to the 3' end (black circle) of a ssDNA. The conformational changes of the devices can be observed by monitoring the FRET efficiency of pH independent FRET pairs. Left: Transition between the i-motif conformation at pH 5 and a double stranded helix at pH 8. The intercalating C^+ -C pairs in the i-motif are indicated as grey lines (cf. text). Right: At pH 5 a segment of this DNA devices forms a DNA triplex structure with the double helix of the neighboring segment under the formation of C^+ G-C and TA-T triplets. At pH 8 the same segment adopts a random coil conformation.*

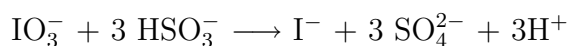
fluorescence intensity during the transition between the two conformations.

C^+ bases are also involved in the formation of DNA triplexes, where a third DNA strand binds along the major groove of a regular 'B'-form double helix by 'Hoogsteen' bonding, a base-pairing mode alternative to the Watson-Crick scheme [84, 85]. Making use of 'Hoogsteen' bonding, Chen *et al.* [58] designed a pH-dependent device based on the duplex-triplex transition (Fig. 4.7, right).

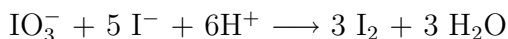
4.5 Switching the conformation of a DNA molecule with a chemical oscillator (Ref.[3])

In Ref. [3] a novel approach to achieve autonomous motion of a nanoscale device is presented. In contrast to the methods introduced in the beginning of this chapter, where motion is triggered by an external operator, it is demonstrated here, how a proton-fuelled DNA conformational switch can be driven by pH variations generated by a non-equilibrium oscillatory chemical reaction. An oscillatory variant of the Landolt reaction is adopted to periodically change the pH value in a continuously fed chemical reactor [86, 87, 88].

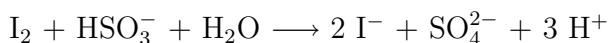
The classical, non-oscillatory Landolt reaction is based on the oxidation of sulfite (SO_3^-) by iodate (IO_3^-). In a first reaction step iodide (I^-) is generated:



This is the rate determining step. In a fast reaction, the iodide is oxidized by the iodate under the formation of iodine (I_2):



The liberated iodine is instantaneously retransformed by sulfite to iodide:



This is a very fast reaction, which effectively leads to the situation, that despite permanent iodine production, iodine never reaches appreciable concentrations as long as sulfite is retransforming it instantaneously to iodide. Only after the consumption of all of the sulfite, the reduction of iodine is stopped and the iodine can react with starch, which is present in the solution for visualization purposes, forming a deep blue iodine-starch complex. In the presence of thiosulfate ($\text{S}_2\text{O}_3^{2-}$) the system starts to oscillate, where one of the oscillating species in this system is the concentration of hydrogen ions. The full set of reaction equations and a set of differential equations modeling the chemical reactions mathematically is given in the supplementary information of [3] and [4].

For the experiments a solution of thiosulfate, sulfite, and sulfuric acid was slowly and constantly fed into a semibatch reactor⁶ already containing a solution of iodate and a ssDNA strand “M”. The M-strand comprised the base sequence of the i-motif (cf. chapter 4.4) and was labeled on the 5’ end with the dye Alexa Fluor 488 and on the 3’ end with the quencher BHQ-1. The fluorescence of the solution was excited with an argon ion laser and collected with a Si photodiode at an angle of 90°. After a pre-oscillatory phase the pH value of the solution started to oscillate between pH 5 and 6.5. During the oxidation of the sulfite some of the produced hydrogen ions protonated half of the cytosines of the strand M and the i-motif was formed. During the oxidation of the thiosulfite the cytosines got deprotonated and the strand adopted a random conformation again. This fully reversible process was monitored by observing the FRET-induced changes of the fluorescence intensity of the dye (cf. chapter 2.3) while simultaneously measuring the pH-value of the solution. In figure 3 in [3] the synchronous oscillation of the fluorescence intensity and the pH-value is displayed, which demonstrates the functionality of the system. It has to be noted, that addition of ssDNA M’ complementary to M did not change the fluorescence intensity traces. This indicates that hybridization of the two strands M and M’ did not occur during the ongoing oscillations. Also attempts to drive the pH-dependent machine of Chen *et al.* (Fig. 4.7, right) failed, which strengthens the hypothesis that no hybridization of complementary strands occurs under oscillatory conditions. Further experiments involving DNA strands and chemical oscillators will have to focus, among other issues, on the optimization of the reaction conditions to achieve canonical Watson-Crick pairing during the oscillations.

We also attempted to induce the switching of the i-motif with an oscillator based on the hydrogen peroxide (H_2O_2) mediated oxidation of thiosulfate ions in the presence of catalytic amounts of copper [88]. Although we achieved oscillatory behavior in the semibatch

⁶A semibatch reactor is an open reaction volume, which is constantly fed with reactants but has no outlet

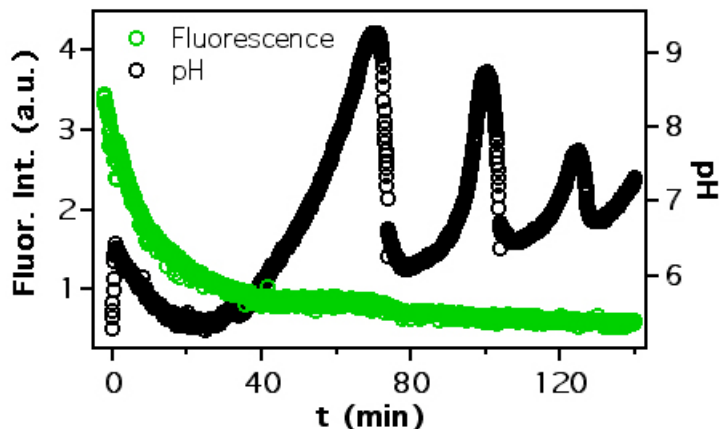


Figure 4.8: *pH-Oscillations* (black circles) were achieved by flowing a solution of 0.05 M $\text{Na}_2\text{S}_2\text{O}_3$ containing 0.07 M NaOH at 0.159 ml/min into 300 mL of a constantly stirred solution containing 0.1 M H_2O_2 and 8.83 μM CuSO_4 . Under this conditions, no response of the fluorescence (green circles) indicating opening and closing of the DNA switch could be observed.

configuration, periodic switching of the fluorophore labeled i-motif added to the reaction solution could not be observed (Fig. 4.8). We attributed this to the unfavorable conditions in the reaction solution (copper ions, hydrogen peroxide), which probably caused harm to the DNA or the fluorescent dye.

4.6 A surface-bound DNA switch driven by a chemical oscillator (Ref.[4])

The approach presented above suffers from the following drawbacks: (i) There is no control over the device, except that the current state of the ensemble of the device- predominantly folded i-motif or predominantly random coil - is known; (ii) Due to accumulation of waste products and the lack of supply of fresh iodate, the pH oscillations are damped and die out after only a few periods. Removal of waste products from the reactor and constant supply with fresh iodate would at the same time result in the eventual elution of the device strands from the reactor. Both of these problems are solved by tethering the DNA device to a solid substrate.

In reference [4] the 3' end of the strand M was no longer modified with a quencher, but with a thiol group. This enabled covalent coupling of the DNA device strands to gold, which also acts as a fluorescence quencher [89, 90] (cf. chapter 2.3). As supporting substrate for the surface bound DNA device a glass slide bearing gold islands much smaller than the optical diffraction limit was fabricated according to the supporting information of Ref. [4] (Fig. 4.9). The fluorescence intensity recorded with a fluorescence microscope

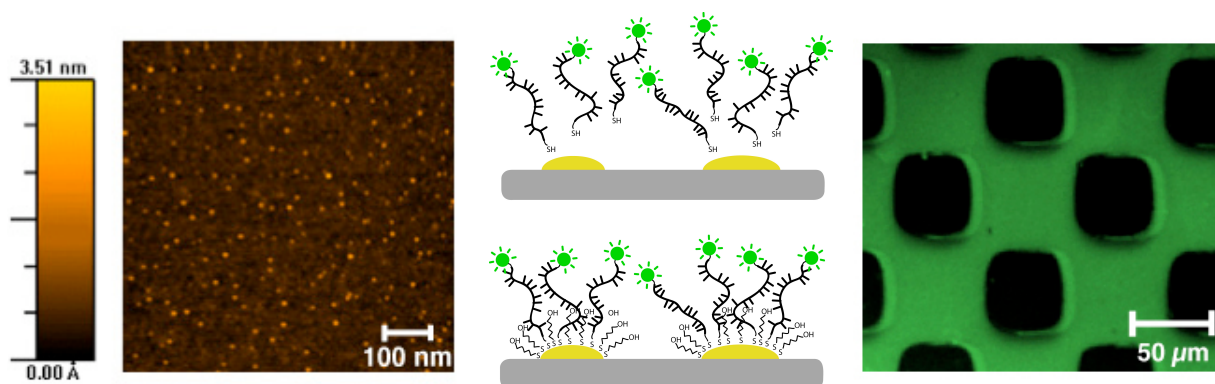


Figure 4.9: *Left: Atomic Force Microscope (AFM) image of gold islands on a Si-substrate, which was fabricated according to [4], supplementary information. The islands have a diameter of 10 - 20 nm. Middle: Schematic view of DNA strands modified at the 5' end with a dye (green circle) and at the 3' end with a thiol group (-SH) able to couple covalently to small islands of gold on a substrate. To prevent the DNA from non-specific binding to the surface, the gold was saturated with Mercaptohexanol. Right: A chessboard pattern of areas of gold islands was applied to a glass slide. Dye-labeled, thiol-modified DNA attached specifically to the gold modified areas, which results in a chessboard patterned fluorescence microscope image.*

(Olympus IX 71, 20× objective) from such a surface patterned with fluorescently labeled DNA exhibited a signal-to-background ratio⁷ of 2.5 : 1 and a signal-to-noise ratio⁸ of 40 : 1. Using the same microscope setup and the same fluorophore labeled DNA tethered to a 100 nm thick layer of gold a signal-to-background ratio of 1.3 : 1 and a signal-to-noise ratio of 20 : 1 was achievable. The considerably lower signal-to-background ratio can be explained by the fact, that the fluorescence emitted from the fluorophores has to compete with reflected excitation light that is not cut out by the filters⁹. The fraction of the reflected light will be the higher the thicker the gold layer is and will be lowest for the case of a transparent glass slide supporting only residual gold. If illumination and detection is carried out on the backside of the sample - as it has been the case during our experiments - the reflectivity of the supporting material has an effect on the amount of the emitted and the collected photons. Since the incident light has to pass through the gold layer before it excites the fluorophores and the emitted photons have to pass the same layer again before they can be collected, the number of detectable photons will decrease

⁷The signal-to-background ratio is here defined as the ratio of the mean pixel value of an area displaying a signal to the mean pixel value of area displaying no signal.

⁸The signal-to-noise ratio of an image is defined as the ratio of the mean pixel value of a certain area to the standard deviation of the pixel values of the same area.

⁹It has to be noted, that only the introduction of an infrared filter (HM-07, UQG Optics, Cambridge, UK) into the optical pathway before the CCD-camera allowed for the detection of any signal in the latter experiments.

with rising reflectivity of the supporting material. A further contribution to the different signal intensities could originate from the different quenching properties of gold layers and gold islands (cf. chapter 2.3.2).

The fluorescence changes accompanying the opening and closing of the i-motif during the oscillations were monitored with a customized fluorescence spectrometer. To this end, the gold-modified glass slide with the tethered DNA devices was glued to the inside of a Continuously Stirred Tank Reactor (CSTR), which has two inlets and one outlet in contrast to only one inlet in the semibatch case. The two incoming tubes supply the reactor with (i) thiosulfate, sulfite, and sulfuric acid and (ii) iodate. Through the outlet tube, the excess solution is pumped out of the reactor. Using the CSTR configuration, undamped pH-oscillations with a periodicity of ~ 15 min were achievable (cf. Fig. 3 in [4]), which drove the DNA device through its conformational states for more than three hours.

4.7 Conclusion

Recently, Shu *et al.* [40] demonstrated, that bound to the top of a cantilever arm, the i-motif can even generate a measurable force. From this point of view the system presented in [3] and [4] is close to an autonomously and periodically working motor, which could generate forces under the consumption of fuel-protons produced during a chemical reaction. In case of the surface-bound device, the motion can in principle continue as long as the pumps provide the fresh chemicals and remove the excess volume.

The system constitutes the first example of a DNA nanoswitch permanently maintained in a non-equilibrium situation and opens up a novel range of applications for oscillating and pattern-generating chemical reactions. The approach to apply well studied chemical oscillations in the nanosciences could be used to operate DNA nanodevices within spatiotemporal chemical patterns or oscillations. This could open up the way to novel designs of molecular machines, which assist in nanoassembly tasks or which are able to transport nanocomponents along supramolecular tracks. A ratchet design of the track in combination with a chemical oscillator, which switches a chemical potential on and off, could allow for autonomous directed motion of a conceivable pH-dependent DNA walker. pH oscillations should be readily applicable to existing pH-dependent DNA machines such as devices based on the duplex-triplex transition [58, 91]. However, the approach is not restricted to DNA-based systems. It should also be possible to drive other pH-dependent molecular machines like the recently demonstrated rotaxane-based supramolecular “elevator” [92, 93] with a pH oscillator. Neither a restriction to the application of oscillations in pH is necessary. Kurin-Csorgei *et al.* [82] recently demonstrated concentration oscillations of calcium, aluminum and fluoride ions by linking a core oscillator to a complexation or precipitation equilibrium. This may lead to experiments where nanodevices could probe or be coupled to concentration oscillations of chemical species which are ubiquitous in living systems.

5 Controlled Trapping and Release of Quantum Dots in a DNA-linked Hydrogel (Ref. [5] and [6])

In popular science, science fiction literature, and visionary framework programs for research one of the expectations from biomolecular nanoscience is the miniscule intelligent agent patrolling inside the human body always alert for early detection of diseases or tumor emergence. In case of a detection event, the agent would either report the event or directly take the necessary measures to prevent the affected organism from illness. A realistic intelligent agent system comprises drugs, which are suited to fight, e.g., certain bacteria or viruses, and a vehicle to transport the drugs to the affected region of the body. Since most drugs also have negative side effects on healthy cells, a controlled release of the active component at the site of interest can reduce the absolute amount of administered drug and keep the adverse reaction at a minimum. Besides location or disease dependent release of the drug, also time controlled release is often desirable. To this end, active agents are often embedded in porous matrixes, which release the drug to the body in a slow and controllable manner.

New strategies to achieve such intelligent drug delivery systems require interdisciplinary efforts in biochemistry, biophysics, polymer science, pharmaceuticals, and molecular biology. A new class of drugs has already been introduced by combining pharmaceutically active agents with polymers or colloidal nanocrystals. For further progress, the development of new stimuli-sensitive carrier systems with programmable structure and properties needs to be aspired. The biocompatibility and its exceeding versatility as structural material predestine DNA as a building block for such sophisticated carrier systems. This chapter presents a concept for the controlled release of active substances and discusses the potential of DNA crosslinked hydrogels as biocompatible and programmable drug delivery system.

5.1 Reversible Hydrogels

Hydrogels, which consist of 3D networks of crosslinked polymer chains dispersed in water are intensively studied as novel drug delivery systems [94, 95]. Other promising carrier systems include micelle forming block copolymers, nano and microspheres, liposomes and dendrimers [95]. In addition to drug delivery, hydrogels have been employed amongst oth-

ers as surgical suture materials, soft tissue prostheses, body implants, and soft contact lenses and have thereby proven their biocompatibility [96].

For the purpose of drug delivery, hydrogel systems which undergo a reversible sol-gel phase¹ transition in response to a change of the ambient conditions are of particular interest. Since many different methods are available for the fabrication of hydrogels, response to external stimuli - like pH or temperature changes - has been implemented successfully in a variety of hydrogel systems [97, 98, 99]. Yoshida *et al.* [100], for example, vastly accelerated the deswelling of the temperature sensitive hydrogel Poly(*N*-isopropylacrylamide) (pNIPAm), by the incorporation of unlinked side chains into the polymer network. The pNIPAm chains are soluble in aqueous media below 32°C but turn hydrophobic above this lower critical solution temperature (LCST). The hydrophobic pNIPAm chains dehydrate and cause the expulsion of water from the polymer network, which in turn induces the collapse of the hydrogel. In the experiments of Yoshida *et al.*, the grafted side chains formed hydrophobic nuclei above the critical temperature, which enhanced the aggregation of the crosslinked chains and sped up the expulsion of water from the hydrogel more than 1000-fold in comparison to a standard pNIPAm gel without additional side chains.

Besides the numerous examples for pH and temperature sensitive hydrogels, only few hydrogels have been presented which respond to the presence of biologically relevant molecules. Various studies introduced glucose sensitive phase reversible hydrogels [101, 102, 103], which is of special interest for controlled insulin release as a function of the glucose concentration in the environment.

In the following, we will restrict ourselves to a closer examination of polyacrylamide (PAAm) hydrogels, which are widely used in the life sciences. Polyacrylamide gel electrophoresis (PAGE) is a commonly used technique to characterize large charged biomolecules like DNA, RNA, and proteins. During polymerization acrylamide monomers form long chains which get crosslinked and build up a 3D polymer network upon the addition of the crosslinker molecule *N,N'*-methylene-bis(acrylamide) (Fig. 5.1). The polymerization process creates covalent bonds between carbon atoms of the bis(acrylamide) and carbon atoms of the acrylamide chains, thus rendering the process effectively irreversible. By altering the total concentration of the acrylamide (T) and the concentration of the crosslinker with respect to the monomer (C), the average pore size of PAAm gels can be controlled. Different methods were applied to measure the average pore size of PAAm gels for varying monomer and crosslinker concentrations [104, 105, 106, 107]. Holmes and Stellwagen [105, 106] deduced from Ferguson plots pore diameters of 140 nm ($T=10.5\%$) to 260 nm ($T=3.5\%$). These values are an order of magnitude larger than the values presented in a later study by Pluen *et al.* [107], who obtained pore diameters between 13 nm ($T=8\%$) and 19 nm ($T=4\%$) using fluorescence recovery after photobleaching (FRAP) and electric birefringence measurements. These smaller diameters seem to be more consistent, since they are in good agreement with theoretical values based on the reptation model and with electron microscope measurements that revealed a pore diameter of 9 nm for $T=5\%$ [104]. The concentration dependence suggested by the studies follows a power law T^γ with

¹The sol phase is defined as a flowing fluid, while the gel phase is solid on the experimental timescale.

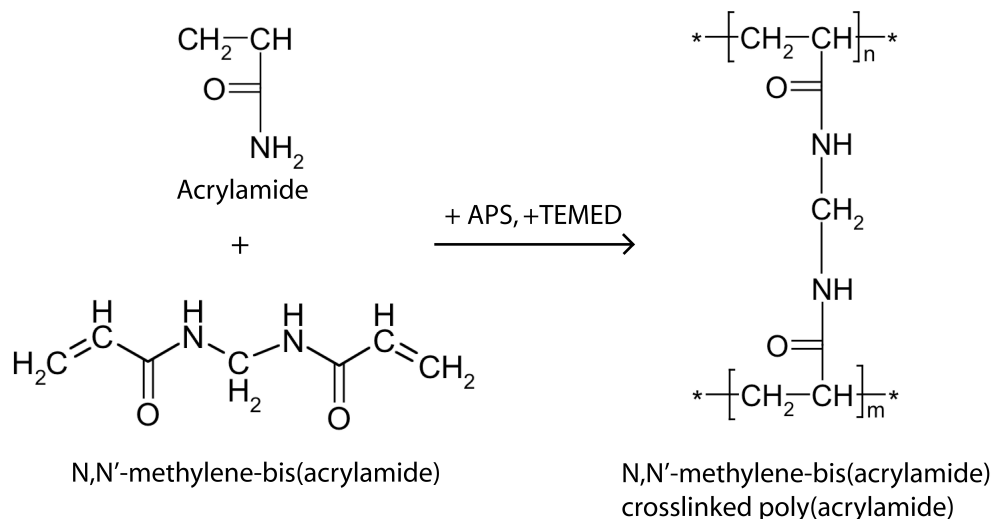


Figure 5.1: *Acrylamide mixed at a certain ratio with N,N'-methylene-bis(acrylamide) and buffer polymerizes after addition of ammonium persulfate (APS) and N,N,N',N'-Tetramethylethylenediamine (TEMED). In the presence of the crosslinking molecule N,N'-methylene-bis(acrylamide) a 3D network of crosslinked poly(acrylamide) chains is formed.*

$$-0.75 \leq \gamma \leq -0.5.$$

Other chemical agents than bis(acrylamide) have been proven to be suitable crosslinkers with some of them even forming reversible crosslinks, e.g. N,N'-Dihydroxyethylene-bis(acrylamide) [108].

Miyata *et al.* [109] demonstrated a biomolecule-crosslinked PAAm gel by employing the reversible binding between the antigen rabbit immunoglobulin (rabbit IgG) and the antibody goat anti-rabbit IgG (GAR IgG) as crosslinking mechanism. For the synthesis of such a gel, two batches of modified PAAm chains were prepared, where in one batch rabbit IgG and in the other batch GAR IgG was grafted on the PAAm chains (Fig. 5.2). Mixing of the two batches resulted in an antigen-responsive hydrogel, whose gel swelling ratio² increased upon the addition of free antigens since the free antigen molecules competed with the crosslinking antibody-antigen bindings. This effectively led to an opening of the crosslinking sites.

Recently, Lin *et al.* [110] employed synthesized DNA oligonucleotides as a reversible crosslinking agent for PAAm gels. The study presented in chapter 5.3 gives insights into the nanoscopic properties of such a gel and describes how the trapping and release of fluorescent nanocrystals as model drug carrier system was controlled by the addition of synthetic DNA effector strands. Beforehand, a publication dealing with the benefits and drawbacks of colloidal nanocrystals as fluorescent probes in single molecule experiments will be presented.

²The swelling ratio denotes the mass ratio of the incorporated water and the dry polymer

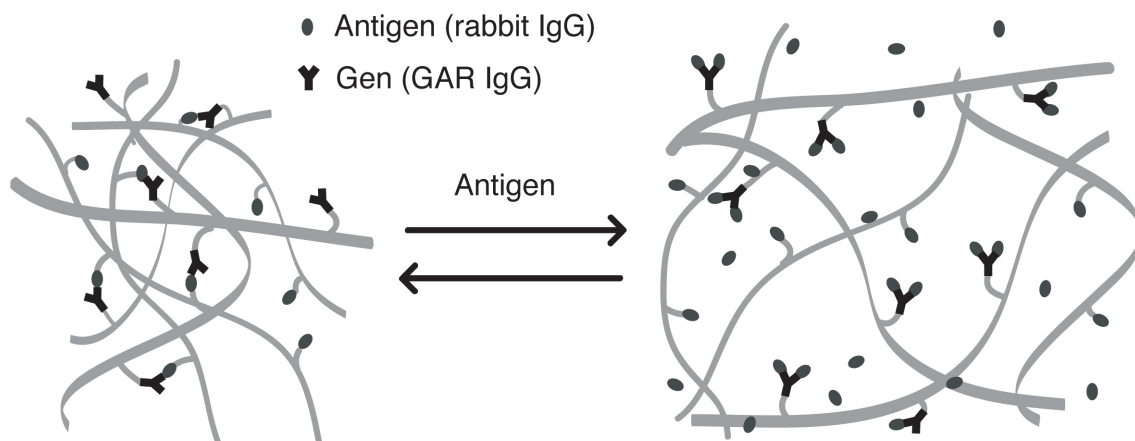


Figure 5.2: A PAAm hydrogel can be prepared by grafting an antigene and the corresponding antibody to the polymer network. The reversible binding between the antigen and the antibody can be used to trigger a change in the gel volume upon addition of free antigenes, which bind competitively to the antibodies.

5.2 Fluorescent Nanocrystals as Colloidal Probes in Complex Fluids (Ref. [5])

Colloidal nanocrystals are crystalline clusters ranging in size from a few hundred to a few thousand atoms, which are chemically synthesized and dispersed in a solvent. Nanoparticles have already been employed as nanosized vehicles for biomolecules [111], for cancer targeting [112, 113], or as active elements in medical applications, e.g. in the destruction of tumor tissue by generating heat with magnetic nanoparticles exposed to an alternating electromagnetic field [114, 115]. Colloidal fluorescent semiconductor nanoparticles, also called quantum dots (QDs) are of particular interest for fluorescence experiments, since they possess several favorable features [116, 117]: In comparison to organic fluorophores they exhibit high photostability, a broad absorption and a narrow, symmetrical emission spectrum. Due to quantum confinement of electrons and holes within the nanocrystal core material, the color of fluorescence can be tuned by the size of the nanocrystals. The available emission spectra of QDs range from blue to near infrared. Their size of 5 - 20 nm, the large number of already commercially available coatings and their tolerable biocompatibility [118] render these novel fluorophores highly suited for single molecule experiments like Fluorescence Correlation Spectroscopy (FCS) in biologically relevant environments.

In FCS, intensity fluctuations from fluorophores inside the fixed focal volume of a confocal microscope are recorded. The temporal autocorrelation function of these fluctuations is related to the diffusion properties of the fluorophores. The technique is introduced briefly

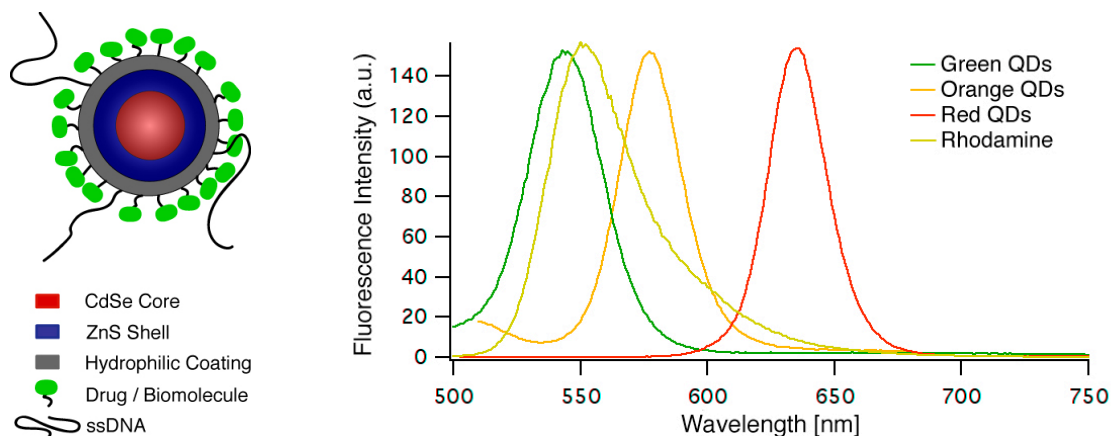


Figure 5.3: *Left: Scheme of a functionalized semiconductor nanocrystal. The CdSe core (red) is embedded in a ZnS shell (blue), which provides efficient confinement of electron and hole wave functions inside the nanocrystal as well as high photochemical stability. The ZnS shell effectively enhances the quantum yield to over 50 %. A hydrophilic coating (grey) renders the nanocrystal water soluble. Finally, the particle can be functionalized with biological relevant molecules like streptavidin or DNA. Right: Emission spectra of nanocrystals of different colors and of the organic dye Rhodamine Green. Notable are the symmetric and narrow emission spectra of the fluorescent nanoparticles.*

in [5] and described in detail in various review articles [119, 120].

In reference [5] CdSe nanocrystals dispersed in organic solvent were characterized with FCS before and after coating with a fluorescence yield increasing ZnS shell. The nanocrystals used in this study had a hydrophobic surface due to the process used for particle synthesis. To obtain water soluble particles for FCS measurements in aqueous surrounding, the surface was rendered hydrophilic. To this end, CdSe/ZnS nanocrystals of the same production batch were modified separately with three different hydrophilic coatings: (i) Mercaptopropionic acid (MPA) molecules; (ii) crosslinked amphiphilic polymers; and (iii) a layer of crosslinked silane. The characterization of the hydrophilic particles with FCS yielded noticeable differences of the hydrodynamic radii of the different particles and additionally showed, that the silane coated particles had the lowest tendency to agglomeration.

In further experiments, these particles were used to study illumination saturation effects on FCS measurements with colloidal nanocrystals. Experimental data revealed a drastic impact of the illuminating laser intensity on the two basic measured parameters: diffusion time τ and number of particles N . Both parameters were overestimated as soon as saturation effects came into play. This can be understood in the following way. A fluorophore can “process” - i.e. absorb and reemit - only a certain number of photons in a given time interval. Once this limit is reached, further incoming photons will not be able to cause yet more emission, the fluorophore is saturated. We simulated this behavior with a fluorophore performing a random walk through an excitation volume with a varying

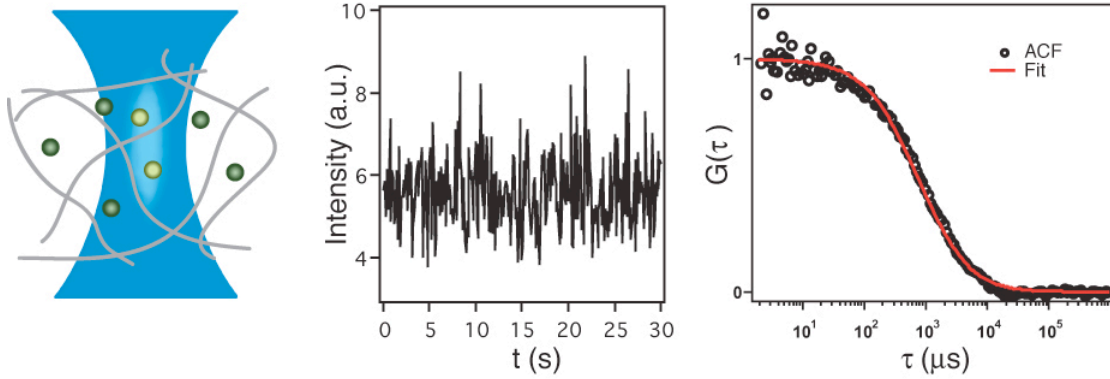


Figure 5.4: *Left: Scheme of fluorescent nanocrystals diffusing in an actin polymer solution observed with fluorescence correlation spectroscopy. The intensity fluctuation caused by the quantum dots are recorded. Right: The temporal autocorrelation function (ACF) of the intensity fluctuations of the diffusing quantum dots can be fitted with an analytically derived expression (cf. [5]), yielding the parameters diffusion time τ through and average number of particles N in the focal volume.*

shape. The fluorescence of an unsaturated fluorophore is proportional to the intensity of the excitation. In the case of a focussed laser beam, we expect an intensity distribution of a 3D gaussian volume:

$$I(x, y, z) = I_0 \exp\left(-\frac{2(x^2 + y^2)}{w_{xy}^2} - \frac{2z^2}{w_z^2}\right). \quad (5.1)$$

Here z is the direction of the incoming laser beam, w_{xy} the radius in x - y -plane and w_z the z -extension of the focal volume. For the simulations we restricted the calculations to one dimension and cut the gaussian above 1 (the normalized value for maximum excitability) to account for the saturation effects (Fig. 5.5):

$$\begin{aligned} I(x) &= I_0 \exp\left(-\frac{2x^2}{w_x^2}\right) & \text{for } I_0 \exp\left(-\frac{2x^2}{w_x^2}\right) < 1 \\ I(x) &= 1 & \text{for } I_0 \exp\left(-\frac{2x^2}{w_x^2}\right) \geq 1. \end{aligned} \quad (5.2)$$

The numerical simulation with these constraints reproduced the experimental data satisfactorily (cf. Fig 4 in [5]).

With that knowledge, the diffusive behavior of the silane coated particles was investigated in a polymerized actin network. An increase of the viscosity of the fluid could be observed with rising actin polymer concentrations. The slope of the fitted straight line to a plot displaying the normalized diffusion constants of the particles over the actin concentration in figure 6 of [5] revealed an intrinsic viscosity [121] of the polymerized actin

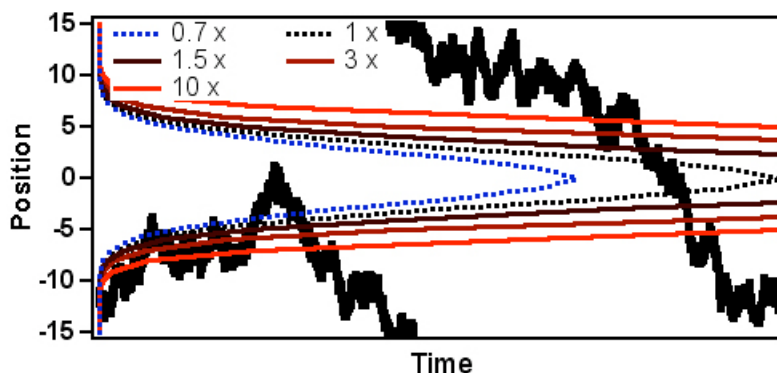


Figure 5.5: Simulation of a fluorophore performing a random walk (thick black line) through gaussian and cut-off gaussian excitation profiles. Depending on the degree of saturation (normalized to maximum excitability) the particles pass through different excitation profiles.

solution of $\eta_{int} = 0.12 \pm 0.02 \text{ ml mg}^{-1}$, in accordance with literature values [122]. In addition, the recorded data was tested for signatures of anomalous diffusion, which can be caused by immobilized inert obstacles that obstruct molecular motion by an excluded volume interaction. The mean-square-displacement of an anomalous diffusing particle is not simply proportional to time, but scales as $\langle x^2 \rangle \propto t^\beta$, with $\beta \neq 1$. Since the particle diameter in our experiments was far smaller than the average meshsize of the actin network at the highest achievable actin concentrations, no anomalous diffusion could be observed. These experiments, which proved the suitability of nanocrystals as colloidal probes in viscous fluids, motivated the examination of the nanoscopic properties of a DNA-crosslinked hydrogel with colloidal nanoparticles. The results of that study are discussed in the following chapter.

5.3 DNA-crosslinked Gels as Programmable Drug Delivery System (Ref. [6])

In reference [6] the controlled trapping and release of quantum dots in a DNA-linked hydrogel is described and a novel approach to intelligent drug delivery in which nanoparticle-based drug-carriers can be trapped and released from a gel matrix in response to a DNA or RNA signal molecule is suggested. The hydrogel system is a DNA-switchable structure based on a concept introduced by Lin *et al.* [110], where AcryditeTM-modified oligonucleotides act as crosslinker anchorage molecules. The acrylamide part of the AcryditeTM-molecule (Fig. 5.1 and 5.6) can be incorporated into polyacrylamide chains if co-polymerized with acrylamide monomers.

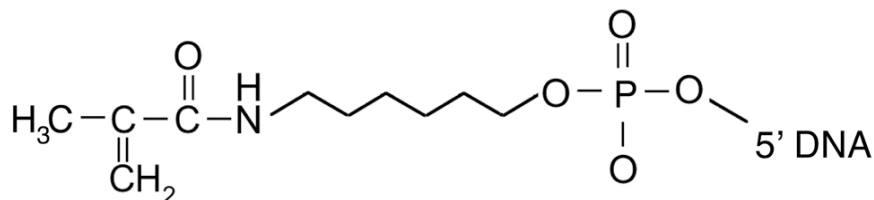


Figure 5.6: *AcryditeTM*. The acrylamide part on the left co-polymerizes with acrylamide monomers. Hence, polymer chains with addressable DNA handles can be formed.

To obtain a reversibly crosslinked hydrogel, two batches of non-complementary AcryditeTM-functionalized oligonucleotides are separately incorporated into acrylamide polymer chains. Mixing of the two resulting polymer solutions yields a viscous, but still fluid matrix which transforms into a solid gel after addition of a DNA crosslinker oligonucleotide. The crosslinker DNA comprises two sequence sections of which each is complementary to one of the two AcryditeTM-modified strands and a third “toehold” section, which later acts as a handle to facilitate the binding of the release DNA. To reverse the crosslinking, a release strand fully complementary to the crosslinker strand is added. The release strands hybridize to the toehold region and strip the crosslinker strands off the anchorage DNA via branch migration (Fig. 5.7). As a macroscopic result, the gel converts into a fluid again. Lin *et al.* characterized the mechanical properties of this reversibly crosslinked hydrogel.

Several outstanding properties predestine the DNA-PAAm gel as a versatile material for nanoscale applications in biological environment: i) The variable length of the DNA oligonucleotides allows for the adjustment of the physical properties of the crosslinked gel. ii) Due to the sequence and length dependent melting behavior of dsDNA, the sol gel transition of the gel can be chosen in a wide range of temperatures. iii) Due to the chemical inertness of the polymerized PAAm and the biocompatibility of DNA the system should be applicable in cell culture and other biologically relevant surroundings. iv) The programmable sequence of the crosslinking DNA strands enables the gel to respond to disease related external RNA or DNA stimuli.

In reference [6] fluorescent nanocrystals, which have proven to be suitable biomarkers and colloidal probes (cf. chapter 5.2) were utilized as model drug delivery system. Trapping and release of the nanoparticles is demonstrated by studying their diffusion properties using single molecule fluorescence microscopy and fluorescence correlation spectroscopy.

For video microscopy, movies of single particles dispersed in the unlinked matrix and in the crosslinked gel were recorded with a CCD-camera with single photon sensitivity. One of the applied methods to obtain information about the particle diffusion in 2D is to analyze the videos with particle tracking software. Besides this elaborate method, a simple and intuitive method is introduced in reference [6]: In figure 5.8 trajectories of free (left), trapped (middle) and released (right) nanocrystals are displayed. These images are

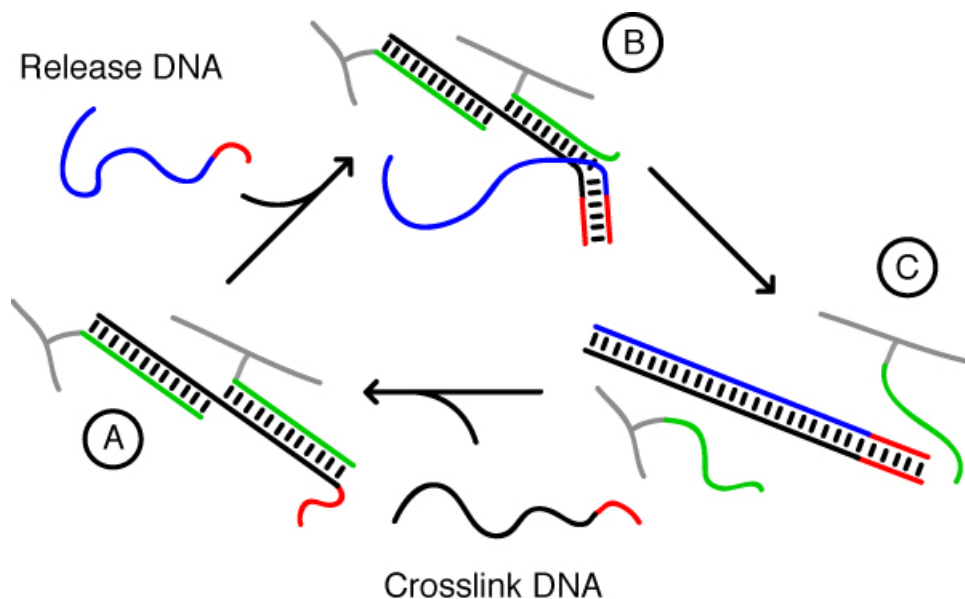


Figure 5.7: *DNA-mediated reversible crosslinking of a hydrogel. (A) AcryditeTM-modified DNA (green), incorporated into polyacrylamide chains (grey), is crosslinked by a fraction-wise complementary DNA strand (black) exhibiting a short ‘toehold’ section (red). (B) A release strand (blue) with a section complementary to the toehold section (red) will hybridize to the toehold of the crosslinking strand, compete with the AcryditeTM-modified strands for the binding to the crosslinking strand and finally remove the crosslinking strand entirely (C). The replacement process is called ‘branch migration’ (cf. chapter 1.2), since the intersection point of the competing DNA branches migrates along the crosslinking strand until it hits the opposite end of the end with the toehold section. As a result, the shorter strands are completely released. The system can be returned to the state (A) through further addition of the crosslinking strand.*

generated in the following way: The single images of a movie of nanoparticles diffusing in the focal x - y plane of a fluorescence microscope are stacked and then the whole image stack is tilted around the y -axis by 90° . The abscissa then corresponds to the time axis, while the ordinate displays the projection of the former x -axis. The 1D diffusion constant can be calculated by measuring the y -displacement for many particles from the moment they enter until they leave the focus (Fig. 6.1). A detailed description of this procedure can be found in Appendix A.

Additionally, the diffusion behavior of the nanoparticles was characterized with FCS (cf. chap. 5.2). The diffusion constants of the particles in the unlinked matrix and of the released particles obtained by the three different methods agreed well. Since the trapped quantum dots did not move and unmovable quantum dots do not - except for the well-known blinking - contribute to intensity fluctuations inside the focal volume of a FCS setup, FCS was inept to account for the trapped particles. On the other hand, FCS revealed an

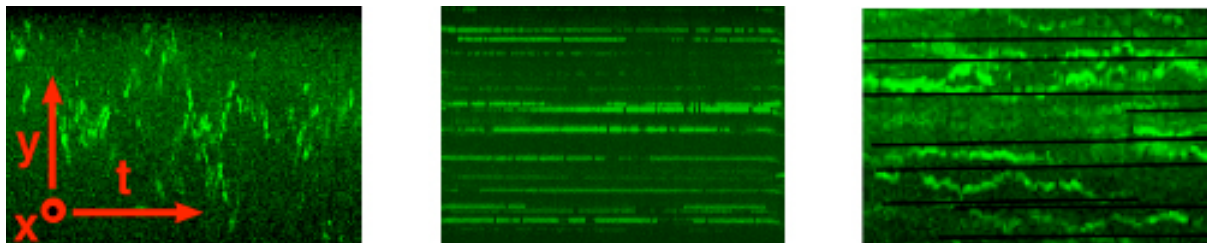


Figure 5.8: *Left: Fluorescence traces (cf. text) of quantum dots diffusing in the unlinked gel matrix. Each image represents a time interval of ~ 10 seconds (left to right) and $20 \mu\text{m}$ from top to bottom. Middle: Nanocrystals trapped in the DNA crosslinked hydrogel. On-off-blinking of the nanocrystals is observable, which indicates the trapping of single particles. Right: After addition of release DNA, the trapped particles start to move again. However, for some particles the motion appears restricted to a confined volume, indicated by the black lines.*

increasing contribution of anomalous diffusion during the ongoing crosslinking process as well as a high contribution of anomalous diffusion for the released particles.

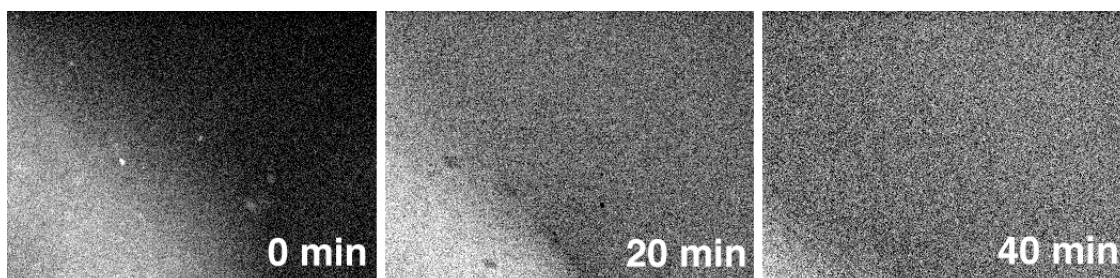


Figure 5.9: *Dissolution of a DNA crosslinked hydrogel. Each image displays the same area ($500 \mu\text{m} \times 500 \mu\text{m}$) of a coverslide supporting a quantum dot loaded gel, of which roughly one quarter is visible (down left corner). Fluorescence images were taken at 0 minutes (left), 20 minutes (middle) and 40 minutes after the addition of release DNA. The gel is slowly dissolved while the particles are released in the solution, which significantly lowers the contrast.*

Supplementary bulk experiments were performed. Therefore, the fluorescent nanocrystals were released from a small sample of DNA crosslinked gel ($\sim 5 \mu\text{l}$) into a large buffer volume ($300 \mu\text{l}$). The fluorescence increase of the solution after the addition of the release DNA was monitored with a fluorescence spectrometer (cf. Fig. 4 in [6]). In a further experiment the DNA-mediated dissolving of the crosslinked gel was demonstrated with fluorescence video microscopy (Fig. 5.9).

5.4 Conclusion

The experiments described above prove the suitability of a DNA crosslinked hydrogel as a carrier system, which releases nanoscale objects on demand. Due to the biocompatibility of the polymerized polyacrylamide and the crosslinking DNA strands, such gels could find application in the context of controlled drug delivery, where the release of a drug-carrying nanoparticle could be triggered by naturally occurring, potentially disease-related DNA or RNA strands. It may therefore be used to respond to the (over)expression of certain disease-related genes. Application of catalytic activity of hybridization catalysts³ [123, 124] or ribozymes [18] (cf. chapter 1.3) would be a possibility to enhance the sensitivity to external stimuli. Through incorporation of aptazymes⁴ or similar functional nucleic acids [125, 126, 127], gel may even be made responsive to more general disease indicators. For *in vivo* applications, the permeation of the hydrogel into cells would be desirable, which could be achieved by the utilization of gel microbeads produced by emulsion polymerization.

³Hybridization catalysts are short DNA strands that catalyze the relaxation of kinetically trapped metastable DNA strands and are able to act as signal amplifiers. Incoming signals could be naturally occurring DNA or RNA strands.

⁴Aptazymes are strands of nucleic acids whose enzymatic activity, like ribozyme-mediated self-cleavage, is triggered by the recognition of specific effector molecules. Reported effector molecules are, among others, cobalt, cyclic adenosine monophosphate (cAMP), and theophylline. This can be

6 Glossary

DNA: Deoxyribonucleic Acid. The structure of DNA is explained in chapter 2.1.

dsDNA: Double stranded DNA adopts under physiological conditions a double helical confirmation.

Enzyme: Enzymes are biomolecules, that catalyze biochemical reactions. Besides proteins also RNA and DNA can show enzymatic activity.

FCS: Fluorescence Correlation Spectroscopy can be employed to determine diffusion properties of dissolved fluorophores or fluorescently labeled molecules at a single molecule level.

FRET: Förster Resonance Energy Transfer or Fluorescence Resonance Energy Transfer is a strongly distance-dependent energy transfer process between fluorophores or between fluorophores and fluorescence quenchers, that can be employed to visualize distance changes on the nanometer scale.

i-motif: The i-motif is a tetrameric DNA structure formed of four intercalated, antiparallel DNA strands that are held together by hemiprotonated cytosines. The i-motif is formed below pH 6.2.

NIPAAm: Poly(*N*-isopropylacrylamide) is a hydrogel, which is soluble in aqueous media below 32°C and collapses at higher temperatures.

PAAm: Poly-Acrylamide (poly(C₃H₅NO)) is a biocompatible polymer (unpolymerized acrylamide is neurotoxic), which forms a hydrogel if co-polymerized with a crosslinker like N,N'-Methylene bis(acrylamide) (C₇H₁₀N₂O₂).

PAGE: In Poly-Acrylamide Gel Electrophoresis a DC voltage is applied on two opposite sides of a polyacrylamidegel. which is loaded with samples of molecules like DNA, RNA or proteins. Different molecule species can be separated by this technique, since the traveling speed of a molecule in the gel is influenced by the molecules size and electrical charge.

PDMS: Poly-Dimethylsiloxane is a optical transparent, two-component elastomer. After mixing of the unlinked polymer chains (first component) and a crosslinking agent (second component) the elastomer is still liquid and hardens slowly with time. Heating speeds up this curing process.

RNA: Ribonucleic Acid.

ssDNA: Single stranded DNA

QDs: With Quantum Dots we refer to colloidal fluorescent semiconductor nanocrystals.

6 Appendix

Determination of 1D diffusion constants

Particles diffusing in one dimension, let us say in y -direction, have a zero mean displacement

$$\langle y \rangle = 0 \quad (6.1)$$

and a mean-square displacement that is proportional to time t

$$\langle y^2 \rangle = 2Dt. \quad (6.2)$$

If we assume statistically independent motion in x -, y -, and z -direction for particles diffusing in 3D, the amount of time a particle spends in the focal plane and consequently the length of the trajectory will be random¹ (cf. Fig. 1 in [6]). To extract the diffusion constant from this set of trajectories of different length, we adopt the following procedure (Fig. 6.1): The probability of finding a particle between y and $y + dy$ after a time t is:

$$P(y)dy = \frac{1}{\sqrt{4\pi Dt}} \exp\left(-\frac{y^2}{4Dt}\right)dy. \quad (6.3)$$

The rescaled variable $Y = y/\sqrt{t}$ is distributed according to the time independent Gauss distribution:

$$P(Y)dY = \frac{1}{\sqrt{4\pi D}} \exp\left(-\frac{Y^2}{4D}\right)dY. \quad (6.4)$$

Since each trajectory constitutes one sample from $P(Y)$, we can estimate the second moment of $P(Y)$, and hence the diffusion constant D to

$$\frac{1}{N} \sum_i \frac{y_i^2}{\Delta t_i} \simeq \left\langle \frac{y^2}{t} \right\rangle = \langle Y^2 \rangle = 2D. \quad (6.5)$$

One could also choose a fixed time interval and analyze the corresponding y -displacements and would obtain the same result. Since for very short fixed intervals the error in each measurement would be large and for long intervals not all trajectories could be taken into account, we used variable time intervals for the analysis of the data.

¹Also blinking of the quantum dots is statistically independent from the motion of the particle and alters the length of the trajectories only randomly.

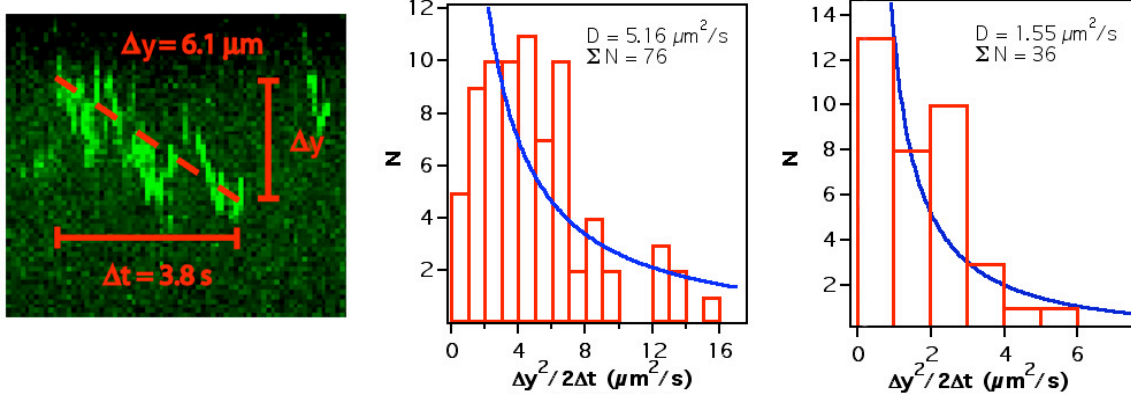


Figure 6.1: *Left: Fluorescence trace of a quantum dot diffusing in the unlinked gel matrix. By measuring the y -displacement and the corresponding Δt for a trajectory, one can calculate the particles square displacements over time y^2/t . By averaging over many particles and traces the obtained value matches the 1D diffusion constant $D = \langle y^2 \rangle / 2 \cdot t$. Middle: The value $D = 5.16$ for nanocrystals diffusing in the unlinked gel matrix is obtained by averaging over 76 traces. The fit with equation 6.9 (blue line) yields a value of $D = 6.2$. Right: The value $D = 1.55$ for released nanocrystals diffusing in the re-opened gel 60 minutes after addition of the release strand was obtained by averaging over 36 traces. The fit with equation 6.9 yields a value of $D = 1.3$*

For statistical analysis of $\Delta y^2 / 2\Delta t$ some more calculations were necessary. After the substitution $z = Y^2$ and the following considerations

$$\int_{z_0=Y_0^2}^{z_1=Y_1^2} dz P(z) = \int_{Y_0}^{Y_1} dY P(Y) \quad (6.6)$$

$$\begin{aligned} &\text{with } dz = 2Y dY \Rightarrow \\ &\int_{z_0}^{z_1} 2Y dY P(z) = \int_{Y_0}^{Y_1} dY P(Y) \\ &\Rightarrow P(z) = \frac{1}{2Y} P(Y) \end{aligned} \quad (6.7)$$

the probability distribution of $P(Y^2)$ could after normalization be written as

$$P(Y^2) = \frac{1}{2\sqrt{\pi D}} \frac{1}{2Y} \exp\left(-\frac{Y^2}{4D}\right) \quad (6.8)$$

or

$$P(z) = \frac{1}{2\sqrt{\pi D}} \frac{1}{\sqrt{z}} \exp\left(-\frac{z}{4D}\right). \quad (6.9)$$

Fitting the distributions in figure 6.1 with this equation yields good agreement of the value D with the values obtained from averaging according to equation 6.5 and with the values obtained by FCS and particle tracking measurements. However, the number of particles

with zero displacement is obviously too low. This can be explained by the fact, that the y -displacement measurements were carried out with an accuracy of $\sim 1 \mu\text{m}$, which makes the measurement of zero displacement improbable.



DNA-based nanodevices

DNA is not only in the focus of modern molecular biology, but also plays an increasingly important role as a building block for nanoscale materials and devices. In recent years, many researchers in nanoscience have used the unique, programmable molecular recognition properties of DNA to build nanostructures by self-assembly and to realize artificial, machine-like devices. We here give a brief survey of this field and discuss the possible applications of DNA-based nanodevices either as nanoscale motors and actuators, or as novel biosensors with built-in information-processing capability.

Tim Liedl, Thomas L. Sobey, and Friedrich C. Simmel*

Department of Physics and Center for NanoScience, LMU Munich, Geschwister-Scholl-Platz 1, 80539 Munich, Germany

**E-mail: simmel@physik.uni-muenchen.de*

Current research on molecular devices and machines is extremely diverse¹. Biophysicists and biochemists gain increasing insight into the nanomechanical principles of operation of the many machine-like macromolecular complexes found in living cells. There is a huge amount of research on the 'obvious candidates' such as the myosin² family or kinesin³ – molecules that have the function of molecular motors⁴. However, it has become clear in recent years that many other protein complexes display intimate coupling of nanomechanical switching and, for example, enzymatic function⁵. On the other end of the complexity scale, organic chemists are trying to synthesize machine-like devices 'from scratch' using the enormous recent progress in supramolecular chemistry.

As a comparatively new 'class' of molecular devices, DNA-based nanodevices⁶ assume an intermediate position between the biological and synthetic worlds. On the one hand, DNA nanodevices use the highly specific molecular recognition properties of DNA bases, which

are at the heart of DNA's biological role as an information storage molecule. On the other hand, DNA devices are 'designed' and synthesized chemically. Usually, there is no biological counterpart of these artificially constructed DNA-based nanodevices, although in some cases they bear a remarkable resemblance to naturally occurring RNA structures such as ribozymes or riboswitches⁷. In the following, a short survey is given of the basic principles of DNA nanodevices and the methods used for their experimental characterization. Two of the major research directions in the field are discussed: (i) progress towards realization of artificial molecular motors based on DNA; and (ii) the use of DNA-based nanodevices as novel biosensors and their coupling to biological phenomena.

Coupling information processing and mechanical action with DNA

What makes DNA so attractive for molecular self-assembly and the realization of molecular nanodevices is the intimate relationship

between DNA sequence and structure. Two DNA strands bind together in a double helix when their sequences are complementary. However, if there is a large fraction of base mismatches between the two strands, they will not bind but remain single stranded. As double-stranded DNA (dsDNA) is much more rigid than single-stranded DNA (ssDNA), control of the degree of hybridization allows the 'programming' of molecular structures composed of rigid and flexible elements. DNA sequences can also be regarded as molecular 'addresses' – the number of distinct sequences of length N is 4^N (there are four different DNA bases), and becomes extremely large for large N . Conformational changes induced by DNA duplex formation can therefore be designed in such a fashion that they are brought about by a specific input sequence. This allows, for example, the specific addressing of one type of device in a pool containing several species of DNA-based nanodevices. It also allows coupling of the action of DNA-based nanodevices to naturally occurring nucleic acids, e.g. mRNA, or to the output of artificial DNA-based information processing cascades as found in DNA computing.

Experimental methods for the characterization of DNA-based nanodevices

Experimental methods applied to the study of DNA-based nanodevices are, not surprisingly, very similar to the characterization methods of naturally occurring molecular structures and machines used in biochemistry and biophysics. One of the most commonly applied biochemical techniques to study DNA hybridization is gel electrophoresis. This technique is also extensively used to study hybridization events that induce conformational changes in DNA-based nanodevices. However, electrophoretic studies do not allow for more detailed biophysical and structural studies of the operation cycles of devices. Here, fluorescence resonance energy transfer (FRET) experiments have become the method of choice. FRET uses the nonradiative transfer of excitation energy between two fluorophores with overlapping emission and excitation spectra, which occurs via dipole-dipole coupling of the dyes. Energy transfer is distance dependent and efficiently occurs for dye-to-dye separations below 10 nm. FRET is therefore well suited to the characterization of conformational changes occurring in this range. As one turn of a DNA double helix is constructed from approximately ten base-pairs, corresponding to a length of approximately 3.4 nm, FRET is particularly useful for those devices composed of mechanical elements with lengths between 10 bp and 30 bp. Current advanced fluorescence spectroscopic methods allow for the characterization of single molecules, and have recently been applied to the study of DNA-based nanodevices^{8,9}. Since molecular devices act as individual units and display considerable variability because of their 'statistical' nature, single molecule studies are expected to become increasingly important in this field. Apart from FRET between fluorophores, other distance-dependent energy transfer phenomena have also been used, e.g. quenching of fluorescence by metal surfaces^{10,11}, and coupling between surface plasmons in metal

nanoparticles¹². These additional energy-transfer events may allow one to investigate conformational changes on length scales other than those amenable to FRET studies. In some cases, the structure of DNA-based nanodevices in their various conformational states can be directly monitored using atomic force microscopy (AFM)^{13,14}. This is only possible if the devices and their conformational changes are large enough to be observed by the AFM – e.g. by adding large supramolecular 'pointers' to the DNA structures, or by incorporating the switching elements into ordered, two-dimensional DNA lattices. Finally, the forces exerted by DNA-based actuators have actually been measured using the DNA-induced bending of microcantilevers¹⁵. This represents the first experimental proof that DNA-based nanodevices could eventually act as 'molecular motors'.

Toward molecular motors based on DNA

DNA-based nanodevices that can move or change conformation have been developed rapidly since the first example was reported in 1998¹⁶. However, none have reached the point of being of practical use and thus 'toward' is to be emphasized in the section title. So far, a number of different prototypes have been developed. These include devices that are driven by DNA hybridization and branch migration, walk and rotate, use Hoogsteen bonding to form multiplex (rather than double helix) DNA structures, and respond to environmental conditions. At least some of these concepts will need to be combined and/or new ones developed before such devices will be of practical use.

Three major features arising from Watson-Crick base pairing have been put into use: the different mechanical properties of ssDNA and dsDNA; single-stranded extensions ('toeholds'); and strand displacement ('branch migration'). For branch migration, single-stranded extensions at the end of dsDNA are used as points of attachment for 'effector strands' that specifically remove single DNA strands from the duplex.

In 2000, Yurke *et al.*¹⁷ collated these ideas to build 'DNA tweezers' in which two DNA duplexes are connected by a short single strand acting as a flexible hinge (Fig. 1). The resulting structure is similar in form to a pair of open tweezers. By adding a 'set' strand to which the tweezers' ends hybridize, the tweezers can be closed. A 'reset' strand that attaches to a toehold on the set strand is then added. This reset strand displaces the set strand from the tweezers through branch migration, freeing them to open again. The tweezers' ends are labeled with a donor/acceptor fluorophore pair, and their relative movement is measured using FRET techniques.

Using similar concepts, Simmel and Yurke¹⁸ have developed a nanoactuator that switches from a relaxed, circular form to a stretched conformation. 'DNA scissors' have been demonstrated by Mitchell and Yurke¹⁹ in which two sets of tweezer structures are joined at their hinges with short carbon linkers. The motion of one set of tweezers is transduced to the other part, resulting in a scissor movement. Recently, a DNA-based nanodevice resembling tweezers has been applied as a

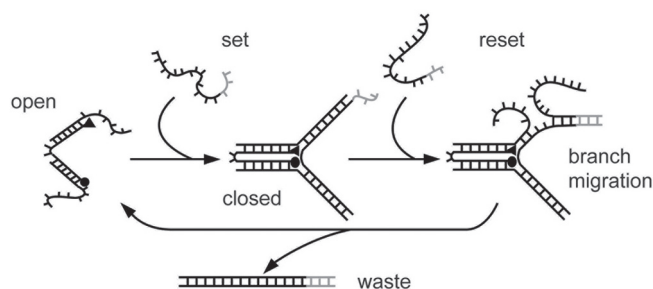


Fig. 1 In the open state DNA tweezers are composed of three strands of DNA forming two double-helical arms connected by a short single-stranded hinge. Hybridization with a 'set' strand closes the two arms. The set strand can be removed via branch migration using the fully complementary 'reset' strand, thus restoring the open state under formation of a 'waste' product. (Reprinted with permission from⁶⁵. © 2006 Wiley-VCH Verlag.)

'force gauge' to establish how much work a DNA-distorting protein can do when it binds to DNA²⁰.

The tweezers have been refined by Chen *et al.*²¹ who used the action of a DNAzyme (DNA molecule with enzymatic activity) to drive the device autonomously. Single molecule analysis of tweezers developed by Müller *et al.*⁹ has led to the conclusion that addition of the closing strand does not always lead to perfect closure of the tweezers. Instead, other structures can occur, such as bonding of multiple closing strands per tweezer device, without the device closing. These unwanted forms need to be addressed with improved sequence-design of the device. Chhabra *et al.*²² have now developed fully addressable DNA-based molecular tweezers along a DNA track to actuate coupling reactions in a programmable fashion.

A more complicated device structure has been developed by Yan *et al.*¹³ based on 'paranemic-crossover' DNA. This is a DNA structure that can be formed by reciprocal exchange between strands of the same polarity on two DNA double helices at every possible position²³. When parts of this structure are removed and replaced by DNA sections without crossovers, molecules in a 'juxtaposed' structure are produced in which two helices are rotated by 180° with respect to the previous structure.

There have also been considerable efforts to realize 'walking devices' that attach to 'track' strands, inspired by naturally occurring biological molecular motors such as kinesin. To achieve motion, enzymes are added in some cases to assist by providing new 'joining' and 'cutting' capabilities.

Shin and Pierce²⁴ introduced a simple walker (Fig. 2) that is a double-strand with two single-stranded extensions (acting as 'legs'). Specific 'fuel' attachment strands bind the legs to single-stranded extensions ('footholds') periodically placed along a double-strand track. Specific 'removal' strands unbind the legs using branch migration. Brownian motion provides movement, and the order of the adding attachment and removal strands directionality. A similar, more complex device has been developed by Sherman and Seeman²⁵. Tian and

Mao²⁶ have demonstrated molecular gears using essentially the same principles.

An autonomous device using ligase to bind connections, and restriction enzymes to cleave connections, has been developed by Yin *et al.*²⁷. In contrast, Tian *et al.*²⁸ have produced DNAzyme walkers that move along a track consisting of RNA. Notably, the enzymatic properties of the walker provide cleaving as required, doing away with the need for extra restriction enzymes and ligases. A similar concept was recently used to construct 'molecular spiders'²⁹.

Under certain conditions DNA can form triplexes and quadruplexes. A shape-changing device similar in principle to DNA tweezers has been developed by Li and Tan³⁰ and Makita *et al.*³¹. The device is based on a structure known as the G-quartet, and functions using an added strand and branch migration. By using a protection strand as discussed previously, Wang *et al.*³² have managed to improve the speed of such devices.

Structures other than G-quartets are possible; these are generally operated by changing the environmental conditions. Changing the buffer environment by addition and removal of intercalators, proteins, salt, and ion species have so far been used to activate devices, along with changes in pH levels and temperature. In 1998, Yang *et al.*¹⁶ developed a system consisting of a circular duplex in the shape of a cruciform. By adding and removing ethidium, double-stranded branch migration extrudes the cruciform under negative super-coiling conditions. Niemeyer *et al.*³³ changed the concentration of Mg ions to induce a structural transition between two states in superhelical DNA.

The very first well-structured device involved a transition from right-handed B-DNA to left handed Z-DNA. Using a double-crossover (DX) structure with a poly-CG sequence, Mao *et al.*³⁴ switched the device by adding $[\text{Co}(\text{NH}_3)_6]^{3+}$.

As already mentioned, DNA can also form triplexes. In a DNA triplex, a third DNA strand binds along the major groove of a regular 'B'-form double helix by Hoogsteen bonding, a base-pairing mode alternative to the Watson-Crick scheme. Chen *et al.*³⁵ varied the pH to form an ordered triplex helix from a duplex and a disordered strand, resulting in nanomechanical motion. This has been used to control chemical reactivity³⁶.

A further structure is the 'i-motif', in which four DNA strands are held together by an unconventional base pair between a protonated

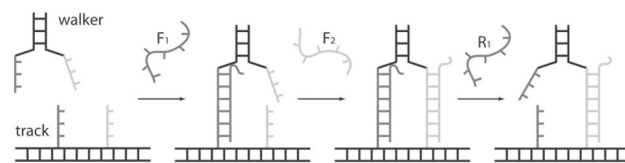


Fig. 2 A simple molecular walker based on DNA. The walker can be connected to single-stranded protrusions of a dsDNA 'track' using 'fuel' strands. The 'feet' can be selectively unlinked from the track using 'removal' strands and reconnected to other anchor points using new fuel strands. (Reprinted with permission from⁶⁵. © 2006 Wiley-VCH Verlag.)

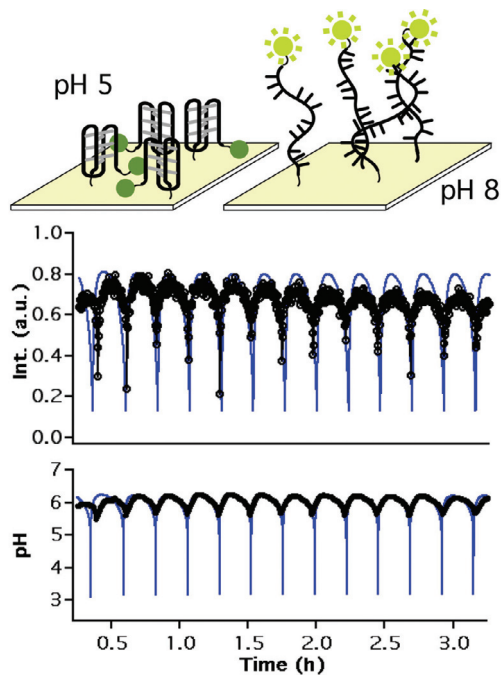


Fig. 3 At low pH values, the surface-tethered *i*-motif adopts its closed conformation, which forces the pH independent dye into close proximity with a Au surface. The resulting quenching of the dye (upper trace) can be monitored over multiple cycles of a pH-oscillation (lower trace) driven by a chemical oscillator. (Adapted from¹¹.)

and an unprotonated cytosine base. This pH-dependent structure has been studied intensively by Liu *et al.*^{10,15,37}. Liedl *et al.*^{11,38} used a chemical oscillator to drive proton concentration changes that generate a pH-based conformational transition between a random conformation and the *i*-motif. The system has been improved by attaching DNA to a solid substrate (Fig. 3) in a continuous flow stirred tank reactor, in principle allowing an infinite number of autonomous conformational switching events. Xiao *et al.*³⁹ have developed a thrombin-binding 'aptamer' (see next section) on a surface based on the G-quartet, while Fahlman *et al.*⁴⁰ used the same structure for a shape-changing device dependent on Sr ions and ethylenediaminetetraacetic acid (EDTA).

Recently, the pH-dependent self-assembly of Au nanoparticles based on the *i*-motif has been achieved by Seela and Budow⁴¹. The solution containing nanoparticles modified with the *i*-motif is observed to change from red to blue within a narrow pH range and is reversible.

Novel biosensors involving DNA-based nanodevices

Because of the properties described above and its inherent biocompatibility, DNA is perfectly suited for sensing tasks and information processing in a biological environment. In nature, DNA strands interact with a variety of proteins, e.g. during transcription or during repair of single- and double-strand ruptures. If a particular

DNA strand does not natively interact with a protein, then it may be possible to link the protein synthetically to the DNA⁴². Another approach toward DNA (or RNA)-protein-hybrids is the use of 'aptamers': strands of nucleic acid that fold into structures that bind strongly to a protein. Aptamers have been isolated successfully in *in vitro* selection experiments (SELEX) for a large variety of proteins and for other small ligands like ATP or cocaine⁴³⁻⁴⁷. In many cases, aptamers have an affinity to their targets comparable to that of antibodies towards their antigens⁴⁸. Thus, aptamers may participate in two different kinds of molecular recognition events: (i) binding to their aptamer target; and (ii) binding to their Watson-Crick complementary strand. Competition between these two types of recognition can be used to construct sensors and switches. Nutiu and Li⁴⁹⁻⁵¹ monitored the binding of biomolecules to an aptamer and the subsequent release of its complementary strand using FRET. Dittmer *et al.*⁵² used a similar concept to bind and release the human blood-clotting factor α -thrombin cyclically. The thrombin aptamer consists of a G-rich 15-mer that, in the presence of K ions, folds into two stacked intramolecular G-quadruplexes connected by three loops (Fig. 4). In this conformation, the aptamer binds to α -thrombin. A single-stranded 'toehold' on one end of the aptamer facilitates the binding of a partly complementary effector strand. The resulting duplex is not able to bind to the α -thrombin, which is consequently released. When a third strand fully complementary to the effector strand is added, the aptamer is displaced from the effector by branch migration. Now the aptamer can fold into the thrombin-binding conformation again and the cycle can be repeated. In recent experiments, Yan and coworkers^{53,54} incorporated the thrombin-aptamer into DNA-scaffolds, which can form micron-sized DNA arrays. With these arrays, they

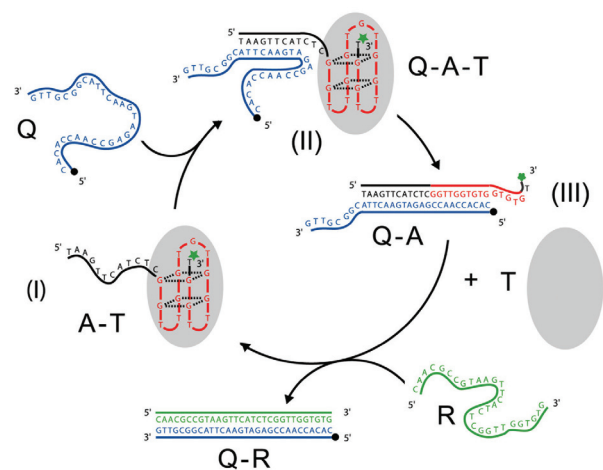


Fig. 4 Cyclical release and binding of human α -thrombin (T). The thrombin aptamer-thrombin complex (A-T) dissociates after the addition of an oligonucleotide Q, that replaces thrombin (I-III) via branch migration. A removal strand R forms a fully complementary double helix (Q-R) with the strand R, thus setting the aptamer strand (A) free, which can bind the thrombin again. (Reprinted with permission from⁵². © 2004 Wiley-VCH Verlag.)

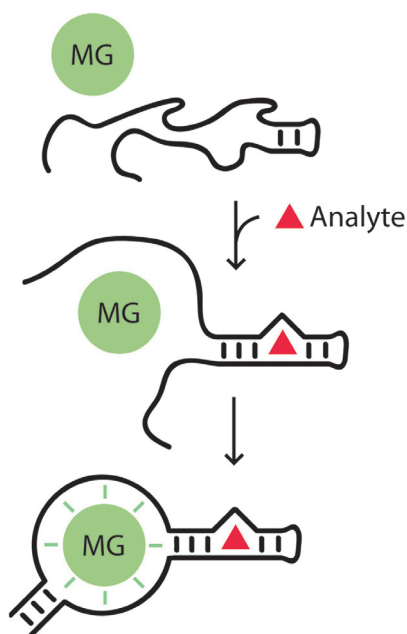


Fig. 5 The MGA as a reporter system for analyte binding. The RNA strand comprises an aptamer sequence for an analyte in its middle section and aptamer sequences for the malachite green molecule at its two end regions. In the absence of the analyte, neither the analyte aptamer nor – as a consequence – the MGA can bind. Upon introduction and binding of the analyte, the MGA can form and bind the reporter molecule malachite green, which is accompanied by a strong fluorescence increase. (Adapted from⁵⁵.)

were able to detect thrombin in nanomolar concentrations using fluorescence microscopy.

Stojanovic and Kolpashchikov⁵⁵ recently presented a versatile concept for the specific sensing of three different molecules: (i) adenosine triphosphate (ATP); (ii) flavin mononucleotide; and (iii) theophylline. The recognition of an analyte to a DNA or RNA aptamer is transduced via a short RNA communication module to a reporting domain, in this case the malachite green aptamer (MGA) (Fig. 5). Upon binding of the dye malachite green to the aptamer, its quantum yield increases up to 2000-fold. The two stems of MGA are reduced to only a few base pairs each, thus significantly lowering the probability for MGA folding into its malachite green binding conformation. In order to act as a reporter for a biomolecule, one of the two MGA stems should be elongated with the sequence of a second aptamer that binds to the target analyte. This second aptamer folds only in the presence of its analyte, which in turn enables the MGA to adopt its binding conformation. The strong increase of the fluorescence intensity of the bound malachite green dye can be monitored with standard fluorescence techniques.

There are a number of recent studies that use the action of DNA modifying enzymes for elaborate sensing processes. With the help of the restriction enzyme FokI, Beyer and Simmel⁵⁶ have been able to translate an arbitrary DNA sequence into a DNA

oligonucleotide triggering the release of thrombin by an aptamer. Stojanovic *et al.*⁵⁷ have used the catalytic properties of a hammerhead-type deoxyribozyme to discriminate between 15-mers with single base pair resolution. Recently, Weizmann *et al.*⁵⁸ detected single-stranded viral DNA with a detection limit of 10 fM using the autocatalytic synthesis of a DNAzyme. All these examples impressively demonstrate the outstanding potential of DNA-based nanodevices as an easy-to-handle, cost-efficient, and reliable sensor molecule for complex sensing tasks in the life sciences.

Using genetic mechanisms to control DNA-based nanodevices

The complex interaction of activation, inhibition, transcription, and translation of genes involving proteins, DNA, and RNA ensures the survival and proliferation of cells and organisms in a variable environment. By adapting parts of these mechanisms, we can not only learn more about the underlying biochemical networks, but also engineer novel molecular machinery *in vitro* and potentially *in vivo*.

Pioneering work has been performed by the Libchaber group^{59,60}, in which they demonstrate the 'principles of cell-free genetic circuit assembly'. Along similar lines, Dittmer *et al.*⁶¹ realized a simple gene regulatory 'switch' to actuate DNA tweezers (see above) using short RNA strands transcribed from an artificial DNA template (Fig. 6). The dsDNA template includes a promoter sequence for RNA polymerase from phage T7, directly followed by a sequence encoding the LacI

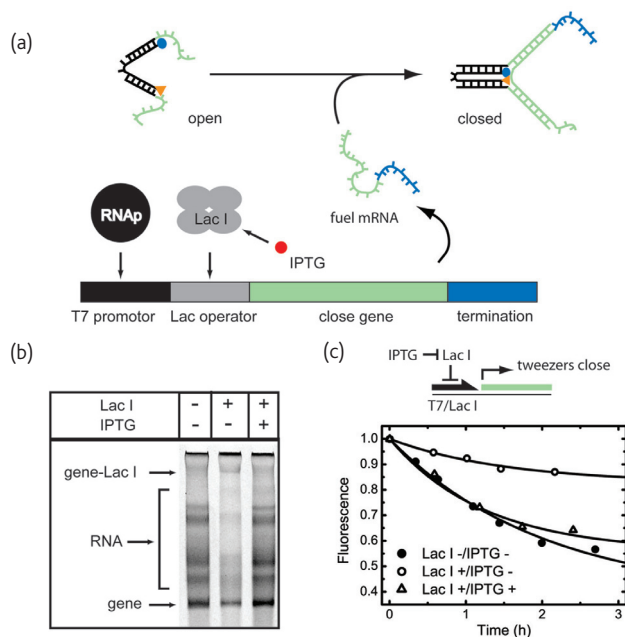


Fig. 6 (a) Working principle of a regulated gene encoding the closing sequence for DNA tweezers (see text for explanation). (b) Gel electrophoresis and (c) FRET experiments prove the regulatory behavior and functionality of the network. (Reprinted with permission from⁶¹. © 2005 Wiley-VCH Verlag.)

operator. In the absence of *lacI*, T7 RNA polymerase can transcribe the 'close gene', which is located downstream of the *lac* operator. The RNA synthesized from the template closes the tweezers, which can be monitored by a decrease in fluorescence. In the presence of *lacI* protein, the transcription is hindered, unless the small molecule isopropyl β -D-thiogalactoside (IPTG), which inhibits the binding of *lacI* to the operator, is added. These experiments show that artificially synthesized DNA machines can be controlled by genetic mechanisms *in vitro*. Kim *et al.*^{62,63} have proposed artificial transcriptional circuits composed of mutually inhibiting and activating genes that can provide controlled amounts of various actuator RNA strands for networks of DNA-based nanodevices. From these initial experiments, it is expected that autonomous molecular systems will be developed that are able to react to various environmental stimuli and could potentially find application as intelligent sensing devices or in drug delivery systems.

Conclusions

Much has happened during the last decade in the emerging field of DNA nanotechnology. Starting from relatively simple conformational changes, DNA-based nanodevices can already accomplish complex movements like unidirectional walking and fulfill highly sensitive sensory tasks. The successful combination of DNA-based nanodevices with genetic machinery, and implementation of concepts developed in DNA computing⁶⁴, promise the ultimate realization of intelligent molecular-sized devices that can sense environmental information and react according to their implemented molecular programs. **nt**

Acknowledgments

The authors gratefully acknowledge support by the Deutsche Forschungsgemeinschaft, the Munich International Graduate School for Nanobiotechnology, and the members of the LMU Center for Nanoscience.

REFERENCES

- Balzani, V., *et al.*, *Molecular Devices and Machines*. Wiley-VCH, Weinheim, (2003)
- Finer, J. T., *et al.*, *Nature* (1994) **368**, 113
- Svoboda, K., *et al.*, *Nature* (1993) **365**, 721
- Howard, J., *Mechanics of Motor Proteins and the Cytoskeleton*, Sinauer, Sunderland, (2001)
- Wuite, G. J. L., *et al.*, *Nature* (2000) **404**, 103
- Beissenhirtz, M. K., and Willner, I., *Org. Biomol. Chem.* (2006) **4**, 3392
- Mandal, M., and Breaker, R. R., *Nat. Rev. Mol. Cell Biol.* (2004) **5**, 451
- Buranachai, C., *et al.*, *Nano Lett.* (2006) **6**, 496
- Müller, B. K., *et al.*, *Nano Lett.* (2006) **6**, 2814
- Liu, D. S., *et al.*, *J. Am. Chem. Soc.* (2006) **128**, 2067
- Liedl, T., *et al.*, *Angew. Chem. Int. Ed.* (2006) **45**, 5007
- Hazarika, P., *et al.*, *Angew. Chem. Int. Ed.* (2004) **43**, 6469
- Yan, H., *et al.*, *Nature* (2002) **415**, 62
- Feng, L. P., *et al.*, *Angew. Chem. Int. Ed.* (2003) **42**, 4342
- Shu, W. M., *et al.*, *J. Am. Chem. Soc.* (2005) **127**, 17054
- Yang, X. P., *et al.*, *Biopolymers* (1998) **45**, 69
- Yurke, B., *et al.*, *Nature* (2000) **406**, 605
- Simmel, F. C., and Yurke, B., *Phys. Rev. E* (2001) **63**, 041913
- Mitchell, J. C., and Yurke, B., In *DNA Computing-7th International Workshop on DNA-Based Computers*, Springer, Heidelberg, (2002), **2340**, 258
- Shen, W. Q., *et al.*, *Angew. Chem. Int. Ed.* (2004) **43**, 4750
- Chen, Y., *et al.*, *Angew. Chem. Int. Ed.* (2004) **43**, 3554
- Chhabra, R., *et al.*, *Nano Lett.* (2006) **6**, 978
- Seeman, N. C., *Trends Biochem. Sci.* (2005) **30**, 119
- Shin, J. S., and Pierce, N. A., *J. Am. Chem. Soc.* (2004) **126**, 10834
- Sherman, W. B., and Seeman, N. C., *Nano Lett.* (2004) **4**, 1203
- Tian, Y., and Mao, C., *J. Am. Chem. Soc.* (2004) **126**, 11410
- Yin, P., *et al.*, *Angew. Chem. Int. Ed.* (2004) **43**, 4906
- Tian, Y., *et al.*, *Angew. Chem. Int. Ed.* (2005) **44**, 4355
- Pei, R., *et al.*, *J. Am. Chem. Soc.* (2006) **128**, 12693
- Li, J. W. J., and Tan, W. H., *Nano Lett.* (2002) **2**, 315
- Makita, N., *et al.*, *Nucleic Acids Symp. Ser.* (2004) **48**, 173
- Wang, Y. F., *et al.*, *Phys. Rev. E* (2005) **72**, 046140
- Niemeyer, C. M., *et al.*, *ChemBioChem* (2001) **2**, 260
- Mao, C. D., *et al.*, *Nature* (1999) **397**, 144
- Chen, Y., *et al.*, *Angew. Chem. Int. Ed.* (2004) **43**, 5335
- Chen, Y., and Mao, C., *J. Am. Chem. Soc.* (2004) **126**, 13240
- Liu, D. S., and Balasubramanian, S., *Angew. Chem. Int. Ed.* (2003) **42**, 5734
- Liedl, T., and Simmel, F. C., *Nano Lett.* (2005) **5**, 1894
- Xiao, Y. M., *et al.*, *Prog. Chem.* (2005) **17**, 692
- Fahlman, R. P., *et al.*, *Nano Lett.* (2003) **3**, 1073
- Seela, F., and Budow, S., *Helv. Chim. Acta* (2006) **89**, 1978
- Kukolka, F., *et al.*, *Small* (2006) **2**, 1083
- Tsai, D. E., *et al.*, *Proc. Natl. Acad. Sci., USA* (1992) **89**, 8864
- Xu, W., and Ellington, A. D., *Proc. Natl. Acad. Sci., USA* (1996) **93**, 7475
- Potyriilo, R. A., *et al.*, *Anal. Chem.* (1998) **70**, 3419
- Jhaveri, S., *et al.*, *Nat. Biotechnol.* (2000) **18**, 1293
- Stojanovic, M. N., *et al.*, *J. Am. Chem. Soc.* (2001) **123**, 4928
- Wilson, D. S., and Szostak, J. W., *Annu. Rev. Biochem.* (1999) **68**, 611
- Nutiu, R., and Li, Y. F., *J. Am. Chem. Soc.* (2003) **125**, 4771
- Nutiu, R., and Li, Y. F., *Chem. Eur. J.* (2004) **10**, 1868
- Nutiu, R., and Li, Y. F., *Angew. Chem. Int. Ed.* (2005) **44**, 5464
- Dittmer, W. U., *et al.*, *Angew. Chem. Int. Ed.* (2004) **43**, 3550
- Liu, Y., *et al.*, *Angew. Chem. Int. Ed.* (2005) **44**, 4333
- Lin, C. X., *et al.*, *Angew. Chem. Int. Ed.* (2006) **45**, 5296
- Stojanovic, M. N., and Kolpashchikov, D. M., *J. Am. Chem. Soc.* (2004) **126**, 9266
- Beyer, S., and Simmel, F. C., *Nucleic Acids Res.* (2006) **34**, 1581
- Stojanovic, M. N., *et al.*, *ChemBioChem* (2001) **2**, 411
- Weizmann, Y., *et al.*, *Angew. Chem. Int. Ed.* (2006) **45**, 7384
- Noireaux, V., and Libchaber, A., *Proc. Natl. Acad. Sci. USA* (2004) **101**, 17669
- Noireaux, V., *et al.*, *Proc. Natl. Acad. Sci., USA* (2003) **100**, 12672
- Dittmer, W. U., *et al.*, *Small* (2005) **1**, 709
- Kim, J., *et al.*, *Adv. Neural Info. Proc. Syst.* (2004) **17**, 681
- Kim, J., *et al.*, *Mol. Syst. Biol.* **2**, (2006) doi:10.1038/msb4100099
- Seelig, G., *et al.*, *Science* (2006) **314**, 1585
- Simmel, F. C., *DNA Nanodevices: Prototypes and Applications*. In *Nanodevices for the Life Sciences*, 1st edition, Kumar, C. S. S. R. (ed.) Wiley-VCH, Weinheim, (2006), 89

Determination of DNA Melting Temperatures in Diffusion-Generated Chemical Gradients

Tim Liedl and Friedrich C. Simmel

Department Physik and Center for Nanoscience, LMU Munich,

Geschwister-Scholl-Platz 1, 80539 Munich, Germany

Tel: +49 89 21803735; E-mail: tim.liedl@physik.uni-muenchen.de & simmel@lmu.de

For fast and reliable determination of DNA melting temperatures with single nucleotide resolution in a microfluidic setup, stable gradients of the denaturing agent formamide were generated by means of diffusion. Formamide lowers the melting temperature of DNA and a given formamide concentration can be mapped to a corresponding virtual temperature along the formamide gradient. We applied this concept to determine the melting temperatures of five sets of dye- and quencher-labeled oligonucleotides of different lengths. Differences in the length of complementary sequences of only one nucleotide as well as a single nucleotide mismatch can be detected with this method. Comparison with conventional melting temperature measurements based on temperature scans yield very good agreement.

Introduction

Due to their central role in biochemistry and molecular biology, the interactions between single strands of DNA with complementary sequences are extremely well studied. At low temperatures, and under favorable buffer conditions, two complementary DNA strands will usually form a double-helical duplex structure, which is stabilized by the hydrogen bonds between these bases and by stacking interactions between neighboring base pairs. A variety of factors such as temperature or denaturing agents, however, can destabilize the DNA double helix. The separation of the duplex into single strands can be regarded as a phase transition and is referred to as “melting” of the double helix. The so-called “melting temperature” T_M of a DNA duplex is defined as the temperature at which half of the double strands are separated into single strands. T_M is a convenient measure for the stability of a DNA duplex, which is important in a variety of contexts. The stability of a DNA duplex will also be reduced, when the two single strands composing the duplex are not fully sequence-complementary. A single base mismatch may already lead to a significant reduction in melting temperature. Another source of destabilization is the presence of denaturing chemicals such as formamide or urea, which may also form hydrogen bonds with the bases and therefore compete with Watson-Crick pairing.

Knowledge of the melting temperature T_M of a given DNA or RNA sequence is important for many biotechnological applications. For example, it is crucial for polymerase chain reaction (PCR) experiments, as the PCR amplification principle is based upon DNA denaturation and renaturation cycles. As the melting temperature of a duplex is very sensitive to base mismatches, determination of T_M is also of great interest for the detection of sequence mutations or variations such as single nucleotide polymorphisms (SNPs). Knowledge of the stability of DNA structures is also of great importance in the emerging area of DNA nanotechnology, in which DNA is used as a building material for artificial supramolecular structures and devices¹.

In many cases, the T_M of a DNA or RNA duplex can be accurately determined within a theoretical model. While for sequences shorter than 15 bases the simple Wallace Rule² often yields satisfactory results, for longer sequences more complex models have to be used. One of the most accurate models presented by SantaLucia and coworkers is based on the nearest neighbor thermodynamic parameters for Watson-Crick pairs^{3, 4}. In many cases, however, a computational approach is not feasible or accurate, e.g. when nonstandard buffer conditions are used, or when two DNA strands are mismatched or contain extensive secondary structure. In these cases, experimental determination of T_M is necessary.

The common experimental method to determine T_M is to slowly heat a sample of buffer solution containing the duplex of interest, while recording its absorbance at a wavelength of 260 nm. Absorption at this wavelength is due to in-plane transitions of the π electrons of the bases. Since the absorbance of two single strands is higher than the absorbance of the same strands forming a double helix, the cooperative melting of a DNA duplex can be monitored as an increase of absorption with

temperature. For accurate T_M measurements a slow temperature sweep - typically 0.1 – 0.5 °C / min - is important to allow the system to equilibrate. Measuring the melting temperature of a given sequence between room temperature and 90 °C thus can easily take 12 hours. A further disadvantage of the absorbance method is its relatively high sample consumption. Thermal cycler platforms containing an integrated microvolume fluorometer work with sample volumes of only 10 μ l and allow for the fast analysis of PCR products during their amplification⁵⁻⁷. An essential disadvantage of such devices is their high acquisition cost. Dodge *et al.* used a microfluidic setup with an integrated heating unit to perform dehybridization experiments with surface-bound DNA⁸.

Here we present a method to determine the T_M of DNA duplexes in solution in an inexpensive, reusable and easy-to-build microfluidic setup. The concept is based on the fact that formamide lowers the melting temperature of DNA double strands 0.6 °C per 1% formamide in the buffer^{9, 10}. By building up a stable, linear gradient of formamide in a solution containing the DNA strands of interest, it is possible to read out T_M by analyzing the ratio of double stranded and single stranded DNA along the formamide gradient. For practical reasons, we did not monitor the melting transition of DNA by measuring the absorbance at 260 nm. Instead, the dissociation of fluorescently labeled duplex DNA into single strands was monitored with Förster Resonance Energy Transfer (FRET)¹¹ (cf. Results and Discussion), both in the microfluidic setup on an epifluorescence microscope, and using a fluorescence spectrometer. The obvious disadvantage of this method is the expensive labeling of the corresponding DNA strands with proper FRET donors and acceptors. However, the setup used here could in principle be adapted to allow also for absorbance measurements.

Experimental Section

Preparation of PDMS chambers

We fabricated multilayer microfluidic chambers containing on-off valves as described in¹².

Two silicon wafers - one for the control channels and one for the flow channels - were prepared by exposing a 20 μ m thick layer (spin coating for 45 s at 900 rpm, soft bake for 2 min at 60 °C, 5 at 115 °C and 2 min at 60 °C) of SPR 220-7.0 (Microresist, Germany) for 25 s to light from a mercury lamp projected through a photo-plotted transparency (Zitzmann GmbH, Germany) using a standard mask aligner (Carl Suss, Germany). Exposed wafers were developed for 3 min in SD 334 (Microresist, Germany), washed in H₂O and dried with N₂. Prior to PDMS-contact, the processed wafers were exposed to the vapor of Trichloro-(perfluorooctyl)silane (Sigma-Aldrich, Germany) for 2 min to facilitate the later removal of the cured PDMS.

A 2 cm thick 5A:1B-mixture of PDMS (Sylgard 184, Dow Corning, Germany) was poured onto the wafer bearing the structure for the control channels. After a 60 min curing step at 80 °C this control layer was peeled off from the wafer. The second wafer supporting the flow channels was covered by a layer of PDMS (1:20), which was spin-coated (60 s, 2100 rpm) and cured (30 min, 80°C). After punching the holes for the air-control tubing into the control layer, the control layer was aligned manually onto the flow-channel wafer. During additional curing for 30 minutes, the flow layer conjoins with the control layer and the joint layers were peeled off the wafer. After punching the holes for the flow tubing, the joint layers were placed on a glass object carrier (50 mm x 75 mm, Marienfeld, Germany), which was covered by a layer of spin-coated (60 s, 2400 rpm) and cured (30 min, 80°C) PDMS (1:20). The whole microfluidic chamber was cured another 2 hours at 80 °C, cooled down and left overnight.

Chemical gradient measurements

A home-built valve controller with electrically actuated microvalves (LHDA121111H, Lee Valves, Germany) as core elements was used to address the microfluidic chamber. The control channels and the tubes connected to the common ports of the valves were filled with water. A few microliters of PBS-buffer (150 mM NaCl, 10 mM KCl) containing 2.5 μ M of strand M with the sequence 5' RG - CCC TAA CCC TAA CCC TAA CCC 3', 2.5 μ M and one of the five quencher-labeled strands (M'₁₁: 5' GTT AGG GTT AG BHQ-1 3', M'₁₂: 5' G GTT AGG GTT AG-BHQ-1 3', M'₁₄: 5' AGG GTT AGG GTT AG-BHQ-1 3', M'_{14mm}: 5' AGG GTA AGG GTT AG-BHQ-1 3', M'₁₇: 5' GTT AGG GTT AGG GTT AG BHQ-1 3') were filled into the reservoirs, separated by the pushed down valve in the middle (oligos purchased from biomers.net, Germany). The buffer in the right chamber additionally contained 75 % formamide. After closing both inlet and both outlet valves the middle valve was

opened, which led to a fast, diffusion-driven build-up of a stable formamide gradient in the connection channel between the two reservoirs. Fluorescence microscopy was performed with an Olympus IX 71 microscope using a 10x objective. Images were recorded with a CCD camera (Photometrics CoolSnap HQ). Below 250 nM concentration of labeled DNA the extracted line scans became noisy and hard to interpret. However, the sensitivity of our device could be enhanced by an improved optical setup.

Temperature sweep measurements

The temperature scans were performed with a fluorescence spectrometer (Fluorolog-3, Jobin Yvon, Germany). For each scan a solution of 300 μ l PBS buffer containing 2.5 μ M of the RG-labeled oligo, 2.5 μ M of one of the three quencher labeled strands, 150 mM NaCl, and 10 mM KCl was filled into a glass cuvette, which was placed in the excitation beam (480 nm). While slowly heating the sample from 20 $^{\circ}$ C to 65 $^{\circ}$ C (1 $^{\circ}$ C every 3 min) the fluorescence was recorded at 525 nm.

T_M calculations

Theoretical values were obtained using the Melting Temperature Calculator provided by IDT (<http://www.idtdna.com/analyzer/Applications/OligoAnalyzer/Default.aspx>) using the following settings: Target type: DNA, Oligo concentration: (2.5 μ M+2.5 μ M)/4, NaCl: 150 mM. The model used for the calculations is described in ³.

Results and Discussion

To create a stable concentration gradient, we prepared a multilayer microfluidic chip ¹² (Fig. 1) and mounted it on a fluorescence microscope. The flow layer consists of two inlets and two outlets accessing two reservoirs, which are separated by a connecting channel. If pressure is applied to the channels of the control layer, which cross the flow channels at designated points, the PDMS membrane separating the two layers is pushed down and acts as a closing valve at these points. If the valve between the two reservoirs is pushed down during the filling process, the liquids in the two reservoirs stay separated ¹³. In a calibration experiment (Fig. 2) we filled the left reservoir with PBS-buffer alone and the right reservoir with PBS-buffer containing 2.5 μ M of the 21-mer DNA strand M labeled at the 5' end with the fluorescent dye Rhodamine Green™ (RG). Within one minute after opening the intersecting valve, the two solutions mixed diffusively and a linear gradient of the labeled oligo along the connection channel was established, which could be monitored with the fluorescence microscope. Since the reservoirs are large in comparison to the connection channel, the concentrations of the analytes in the reservoirs did not change significantly during the first minutes while the gradient was already established. Due to the low Reynolds numbers in microfluidic systems, convection is negligible in our setup.

In a simplified model, the channel can be considered as a one-dimensional tube of length L , containing molecules or particles with a constant diffusion coefficient D and fixed concentrations $c(x=0,t)=0$ and $c(x=L,t)=c_0$ at its ends. With these boundary conditions, the solution to the 1D diffusion equation $\frac{\partial c(x,t)}{\partial t} = D \frac{\partial^2 c(x,t)}{\partial x^2}$ is time independent and reads $c(x) = c_0 \cdot \frac{x}{L}$ for $0 \leq x \leq L$. Hence, a linear gradient is expected in the channel. In order to make sure that this is also true for our experimental channel geometry, the two-dimensional diffusion equation was solved using the finite element simulation program package FEMLAB. The boundary condition along the margin of the left reservoir was set to a constant concentration of zero while the concentration along the margin of the right reservoir was set to one. Indeed, the simulation revealed a linear concentration gradient along the connection channel, which was reproduced perfectly in the experiment (Fig 2d). The equilibration of the concentrations in the two reservoirs during experiments took 40 minutes for the small formamide molecule and 6.1 hours for the dye-labeled 21 -mer. This shows, that in principle our microfluidic setup could also be used to determine the diffusion constant of a molecule of interest. Changing the dimensions of the connection channel and reservoirs can shorten or lengthen the equilibration times, and can therefore be adjusted to the requirements of the application aimed at. The continuity of the gradient and the fact that sustained input of liquid is not needed to maintain the gradient distinguishes our approach from previously proposed methods, which mostly create stepwise gradients under continuous flow ^{14, 15}.

To determine the melting temperatures of strand M paired with either of four complementary strands M'_{11} , M'_{12} , M'_{14} , M'_{17} , consisting of 11, 12, 14, and 17 nucleotides and labeled with the quencher BHQ-1™ at their 3' ends we prepared two buffer solutions for each pair of oligonucleotides: one contained 0%, the other 75% formamide while both contained the same amount of DNA. At low formamide concentrations the DNA was present in the double stranded conformation and the dye at the 5' end of strand M and the quencher at the 3' ends of strands M'_{11} , M'_{12} , M'_{14} , M'_{17} were in close proximity, which led to strong fluorescence quenching due to FRET. At high formamide concentrations the duplexes dissociated into single strands and the fluorescence was unquenched due to the spatial separation of dyes and quenchers (Fig 3a).

In contrast to conventional temperature scan experiments, where typically several hundred microliters of buffer are needed, the separated reservoirs of the microfluidic setup could be filled with only a few microliters of the two corresponding solutions. After the separating valve was opened a formamide gradient established and meaningful fluorescence images could already be recorded after one minute. The intensity profiles along the connecting channel were extracted, normalized and plotted and the linear formamide gradient along the channel was mapped onto a temperature scale. From this plot the melting temperature of the DNA duplexes could be determined (Fig. 3b).

We also determined conventional DNA melting curves with a fluorescence spectrometer, with which the fluorescence of the dye-labeled DNA strands was recorded while slowly sweeping the temperature. Plotting these melting curves in the same graph as the curves obtained from the gradient measurements revealed very good agreement of the two different techniques. Sigmoidal fits yielded the melting temperatures listed in table 1. The deviations between the values obtained from the two techniques were always less than 2%. The values for T_M calculated with the nearest neighbor method³ agreed well with the experimental data for all strands but for the shortest M'_{11} and M'_{12} . The deviation of 10 % between the calculated value and the value measured with both methods - temperature sweep and gradient experiment - demonstrates the need for experimental determination of T_M under certain circumstances.

We also performed an experiments in which a single nucleotide mismatche was introduced into the sequence of one of two otherwise complementary strands. The resulting change in the melting temperature could be easily detected in the diffusion generated formamide gradient (Fig. 4). This demonstrates the potential of our method for the detection of point mutations or SNPs.

Conclusion

We have shown that the melting temperature of DNA duplexes can be determined with a linear formamide gradient created in a microfluidic chip. The low sample consumption of the method, the ability to detect single base mismatches and length differences, and the fact that all gradient measurements displayed in this work were done within less than two hours inside the same chamber without any loss in performance clarifies the potential of the method presented here. The characterization of longer oligonucleotides sequences with higher melting temperatures could be accomplished by maintaining the microfluidic chip at a higher temperature or increasing the maximum formamide concentration or both. Further improvements of this technique are necessary to circumvent the time and cost intensive labeling of the DNA strands and could include the use of the double-strand specific dye SYBR Green I⁶, the utilization of molecular beacons^{16, 17}, or the application of UV absorption measurements along the gradient. The generated gradients are stable, linear, and continuous and should be applicable to other solutes. Measurements on protein and RNA degradation¹⁸ are conceivable as well as studies of biological morphogenesis, which relies on diffusive gradients of gene transcription factors.

References

- (1) Seeman, N. C. *Nature* **2003**, *421*, 427-431.
- (2) Wallace, R. B.; Shaffer, J.; Murphy, R. F.; Bonner, J.; Hirose, T.; Itakura, K. *Nucl. Ac. Res.* **1979**, *6*, 3543-3557.
- (3) Allawi, H. T.; SantaLucia, J. *Biochemistry* **1997**, *36*, 10581-10594.
- (4) SantaLucia, J.; Hicks, D. *Ann. Rev. Biophys. Biomol. Struct.* **2004**, *33*, 415-440.
- (5) Wittwer, C. T.; Ririe, K. M.; Andrew, R. V.; David, D. A.; Gundry, R. A.; Balis, U. J. *Biotechniques* **1997**, *22*, 176-181.
- (6) Ririe, K. M.; Rasmussen, R. P.; Wittwer, C. T. *Anal. Biochem.* **1997**, *245*, 154-160.
- (7) Crockett, A. O.; Wittwer, C. T. *Anal. Biochem.* **2001**, *290*, 89-97.
- (8) Dodge, A.; Turcatti, G.; Lawrence, I.; de Rooij, N. F.; Verpoorte, E. *Anal. Chem.* **2004**, *76*, 1778-1787.
- (9) McConaughy, B. L.; Laird, C. D.; McCarthy, B. J. *Biochemistry* **1969**, *8*, 3289-&.
- (10) Blake, R. D.; Delcourt, S. G. *Nucl. Ac. Res.* **1996**, *24*, 2095-2103.
- (11) Lakowicz, J. R. *Principles of Fluorescence Spectroscopy*, 2 ed.; Kluwer Academic: New York, 1999.
- (12) Unger, M. A.; Chou, H. P.; Thorsen, T.; Scherer, A.; Quake, S. R. *Science* **2000**, *288*, 113-116.
- (13) Hansen, C. L.; Skordalakes, E.; Berger, J. M.; Quake, S. R. *Proc. Natl. Acad. Sci. Of The U.S.A.* **2002**, *99*, 16531-16536.
- (14) Jeon, N. L.; Dertinger, S. K. W.; Chiu, D. T.; Choi, I. S.; Stroock, A. D.; Whitesides, G. M. *Langmuir* **2000**, *16*, 8311-8316.
- (15) Dertinger, S. K. W.; Chiu, D. T.; Jeon, N. L.; Whitesides, G. M. *Anal. Chem.* **2001**, *73*, 1240-1246.
- (16) Tyagi, S.; Kramer, F. R. *Nature Biotech.* **1996**, *14*, 303-308.
- (17) Leone, G.; van Schijndel, H.; van Gemen, B.; Kramer, F. R.; Schoen, C. D. *Nucl. Ac. Res.* **1998**, *26*, 2150-2155.
- (18) Casey, J.; Davidson, N. *Nucl. Ac. Res.* **1977**, *4*, 1539-1552.

Acknowledgment

We thank Alireza Ghaffari and Gabriel A. Kwong (Caltech) for introducing us to the multilayer microfluidics technique and Jongmin Kim and Erik Winfree (Caltech) for helpful discussions. This work was partially supported by the Deutsche Forschungsgemeinschaft (DFG SI 761/2-1) and the Munich International Graduate School for Nanobiotechnology. We gratefully acknowledge support by the Center for Nanoscience and the Nanosystems Initiative Munich.

Captions

Table 1:

Melting temperatures of four pairs of oligonucleotides of different lengths obtained from formamide gradient measurements, conventional temperature scans and theoretical calculations.

Figure 1:

Schematic representation of the two-layered microfluidic setup. The blue flow channels and reservoirs are located beneath the red-colored control channels, separated at the intersections by a thin layer of PDMS. All channels are 100 μm wide and 20 μm high. The diameter of both reservoirs is 750 μm . After subtracting the volume occupied by the supporting columns of 110 μm edge length (white squares), the volume of each reservoir is 7.9 nl while the volume of the 300 μm long connecting channel is only 0.6 nl.

Figure 2:

Calibration of the device.

a) and b) Overlaid fluorescence (green) and bright field (blue) images of the reservoirs and the connection channel. a) The left reservoir was filled with buffer, the right reservoir with buffer containing a fluorescently labeled oligonucleotide while the valve in the middle was closed. b) One minute after opening the valve a stable, linear gradient is established between the reservoirs. c) FEMLAB simulation of the concentration gradient. d) Intensity profiles along the dashed lines in b) and c).

Figure 3:

a) Two complementary DNA strands - one labeled with a fluorophore, the other with a dark quencher - form a double-helical duplex structure at low temperatures and low formamide concentration (left). The quencher and the fluorophore are in close proximity and the fluorescence is quenched. At high temperatures and high formamide concentrations, the DNA duplex dissociates into single strands and no quenching occurs.

b) Melting temperature measurements from conventional temperature scans in a fluorescence spectrometer compared to measurements performed in diffusion-generated gradients of formamide in the microfluidic setup.

Figure 4:

Detection of a single base mismatch. The 14 bp scan was performed with the DNA strand M'_{14} . Introduction of single nucleotide mismatch into the sequence of strand $M'_{14\text{mm}}$ (5' AGG GTA AGG GTT AG-BHQ-1 3') can be easily detected in the diffusion-generated formamide gradient. T_M for the strand $M'_{14\text{mm}}$ is 43.8 ± 0.1 °C in contrast to 51.5 ± 0.1 °C for the strand M'_{14} .

Table 1)

# complementary Oligonucleotides	Temperature Scan (°C)	Formamide Gradient (°C)	Calculation (°C)
11	41.9 ± 0.2	42.5 ± 0.1	37.9 ± 1.4
12	46.4 ± 0.2	45.4 ± 0.1	43.9 ± 1.4
14	52.2 ± 0.2	51.5 ± 0.1	52.0 ± 1.4
17	58.5 ± 0.6	57.5 ± 0.3	55.5 ± 1.4

Fig. 1)

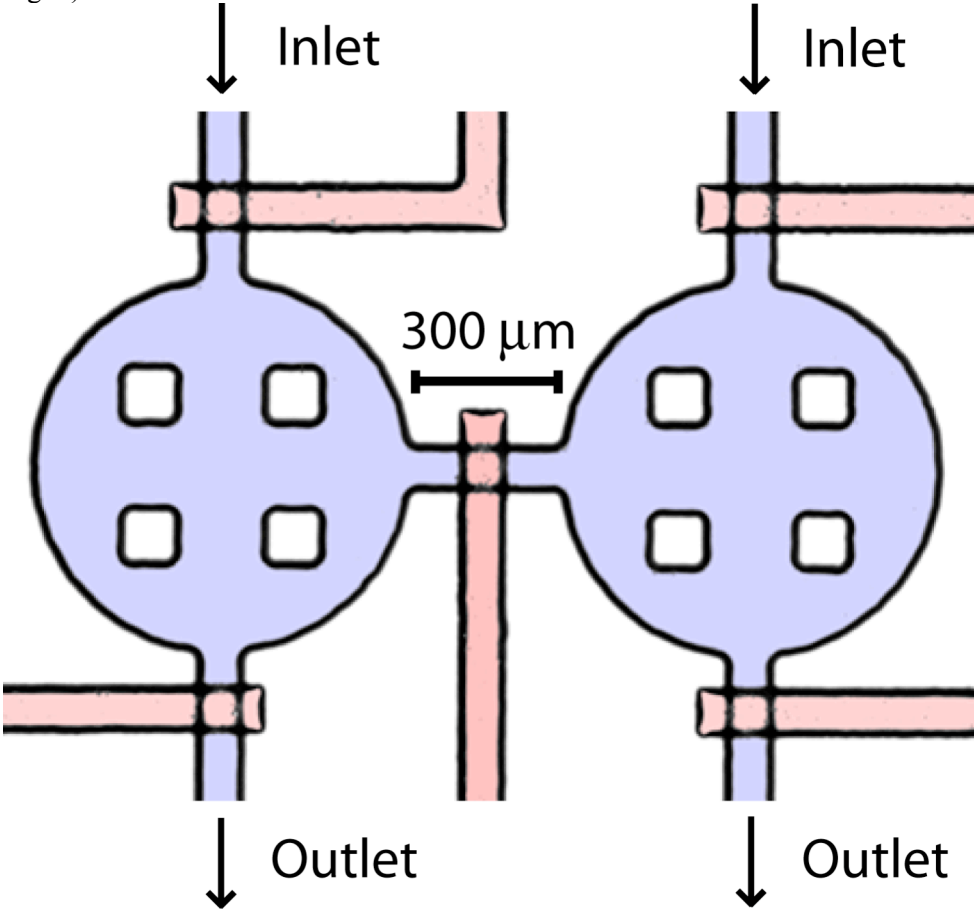


Fig. 2)

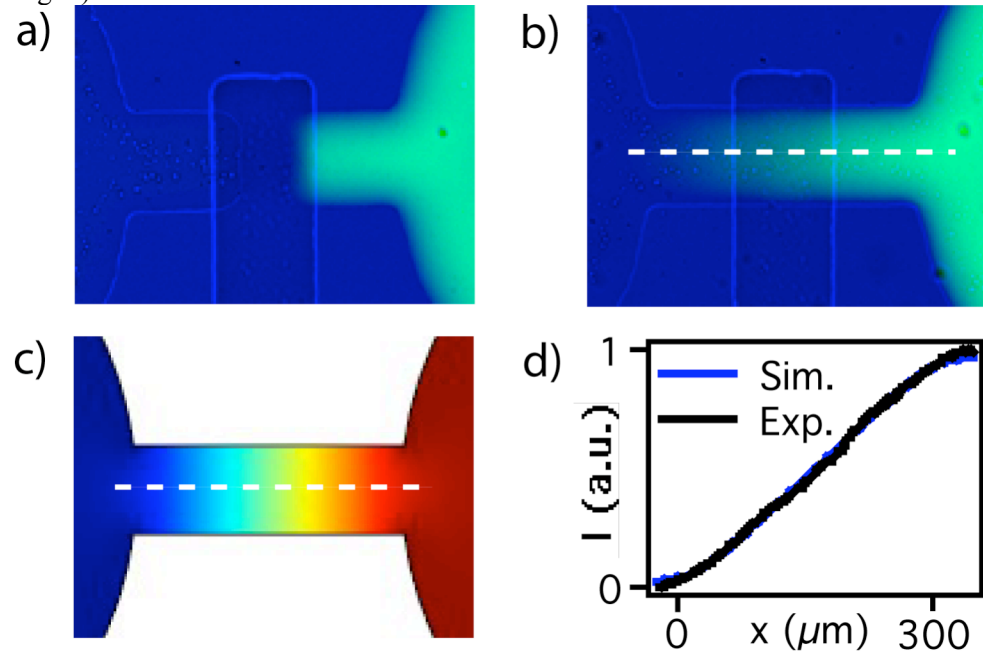
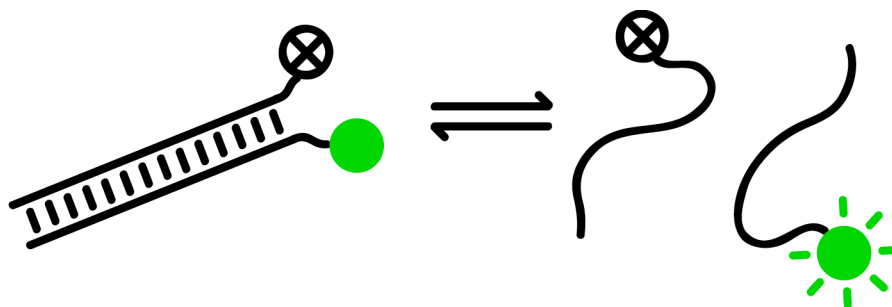


Fig. 3)

a)



b)

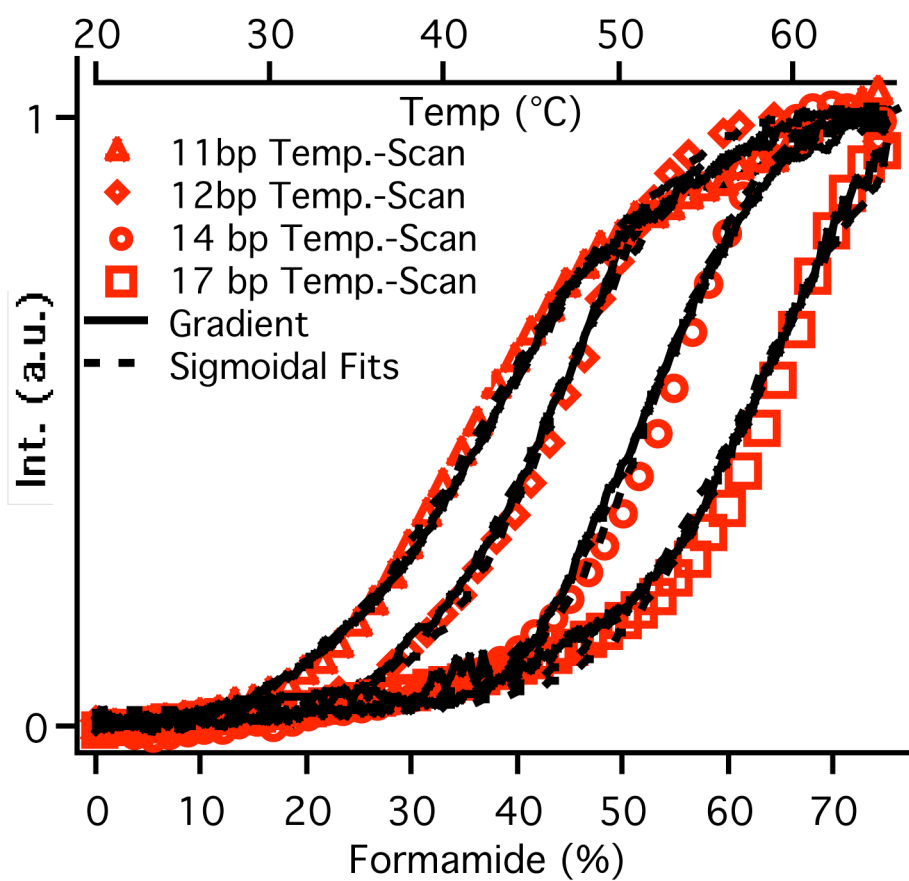
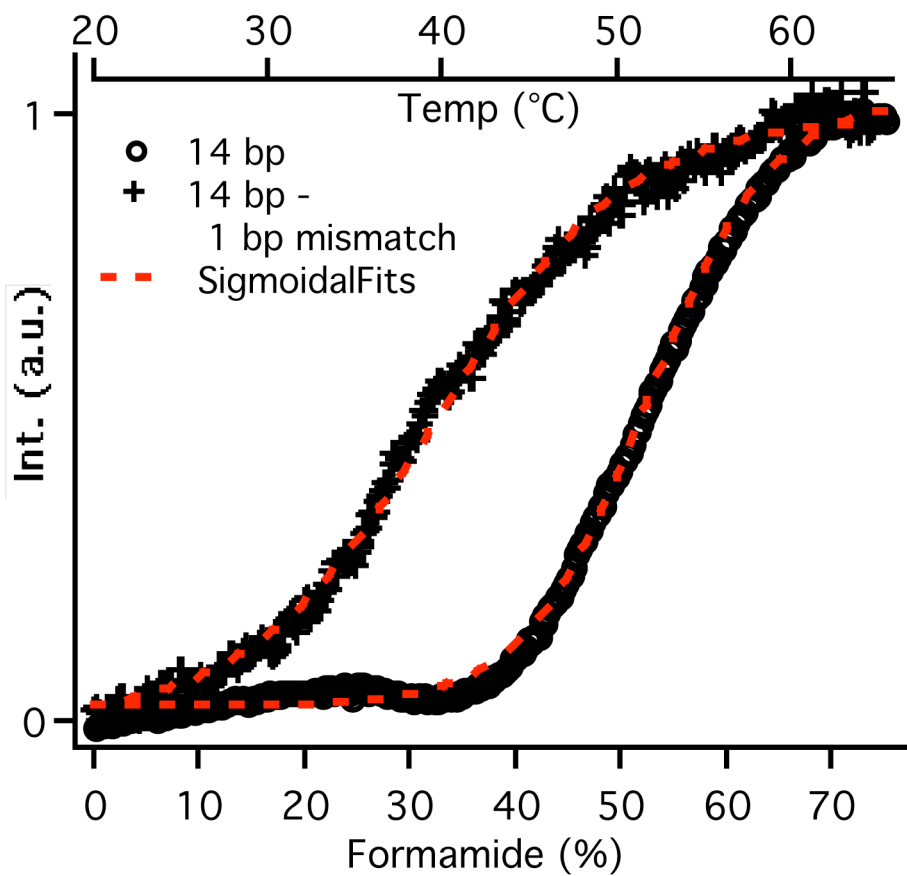


Fig. 4)



Switching the Conformation of a DNA Molecule with a Chemical Oscillator

Tim Liedl and Friedrich C. Simmel*

Department of Physics and Center for Nanoscience, Ludwig-Maximilians-Universität München, Geschwister-Scholl-Platz 1, 80539 München, Germany

Received June 22, 2005; Revised Manuscript Received September 5, 2005

ABSTRACT

pH oscillations generated by a nonequilibrium chemical reaction are used to switch a pH-sensitive DNA structure between two distinct conformations. The utilization of a chemical oscillator represents a novel method for achieving autonomous motion in molecular devices. The oscillatory reaction is a variant of the Landolt reaction and produces pH variations in the range between pH 5 and 7. In this range, a cytosine-rich DNA strand can be switched between a random coil conformation and the folded i-motif structure. The conformational changes are monitored simultaneously with the pH value in fluorescence-resonance energy-transfer experiments.

DNA-based nanomachines are DNA supramolecular structures, which can cyclically undergo large conformational changes in the presence of certain trigger molecules such as other DNA strands or small molecules. These conformational changes are accompanied by rotatory,^{1,2} stretching,^{3–12} or, as demonstrated quite recently, even translatory^{13–18} movements. In most cases, these molecular machines have to be controlled externally, that is, an external operator has to add certain chemical compounds to the reaction mixtures to cycle the devices through their various mechanical states. Autonomous behavior of nanodevices has been achieved in only a few cases with the help of deoxyribozymes^{9,17,19} or enzymes.^{14,18} Here we present a novel approach to achieving autonomous motion by demonstrating how a proton-fueled DNA conformational change can be driven by pH variations generated by a nonequilibrium oscillatory chemical reaction.

Conformational changes in artificially constructed DNA nanomachines are usually enforced by the addition of a DNA “fuel” strand, leading to the stiffening of a previously flexible single-stranded part of the device or connecting distant sections of it. Other DNA devices are driven by a change of buffer conditions, which favor one of several possible conformational states. To achieve cyclical operation, fuel strands had to be removed by “anti-fuel” strands using DNA branch migration or the original buffer conditions had to be restored. Continuous operation of these devices requires keeping track of the state of the devices and the external addition of fuel at the right moment. Under closed conditions, waste products accumulate and soon become the dominant chemical species in the system. In a conceptually different approach, here we demonstrate how the conformational

transition of a single-stranded DNA molecule can be driven autonomously by an oscillating chemical reaction occurring in a continuously fed reactor.

Inspired by spatiotemporal ordering processes in biological systems, oscillatory chemical reactions have been under investigation for a long time.²⁰ The canonical example is the Belousov–Zhabotinsky (BZ) reaction,^{21,22} but there are numerous other examples of reactions in which chemical concentrations oscillate in time^{23,24} or travel in space as chemical waves.²⁵ Several criteria have to be met in order to drive DNA-based devices with these chemical oscillators: First, the oscillating chemical species should be able to drive or influence a DNA conformational transition. Among the possibilities are to use the influence of certain ion species on DNA whose concentration may be varied by coupling pH oscillations to complexation and precipitation equilibria²⁴ or to use the oscillations in pH itself, as is done in the present work. Second, the pH range in which the oscillator operates should be compatible with biochemistry; this rules out, for example, the original BZ reaction. Furthermore, the reaction solution should be sufficiently “biocompatible” to avoid rapid degradation of DNA by oxidation. This requirement rules out, for example, oscillators using hydrogen peroxide in the presence of copper ions.²⁶ On the basis of these considerations, here we adopt an oscillatory variant of the Landolt reaction to change the pH value periodically in a continuously fed chemical reactor.^{26–28} The oscillating proton concentration is then utilized to drive proton-fueled DNA nanodevices through their conformational states periodically.

Our artificial reaction network is depicted schematically in Figure 1a. The alternating oxidation of sulfite and thiosulfate by iodate is accompanied by a periodic production

* Corresponding author. E-mail: simmel@lmu.de; fax: (+49) 89 2180 3182.

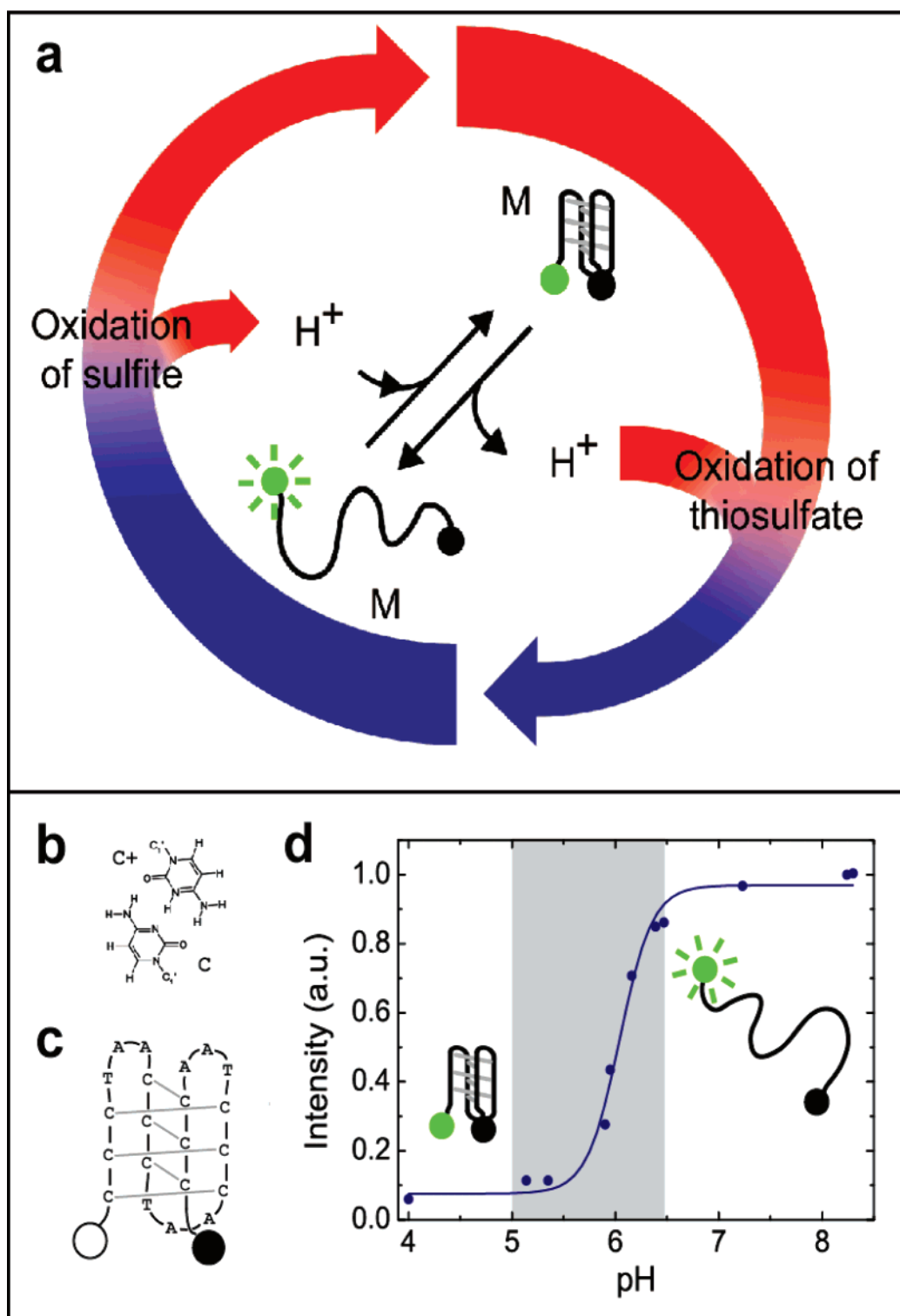


Figure 1. Principle of operation. (a) Operation cycle for DNA switch M driven by a chemical oscillator. An oscillatory variant of the Landolt reaction changes the pH value of the reaction solution periodically. In one-half of the reaction cycle, protons produced during the oxidation of sulfite induce a conformational transition to a folded DNA structure, the so-called i-motif (see part c of this Figure). In the other half of the reaction cycle, the oxidation of thiosulfate consumes protons and leads to an unfolding of the i-motif. (b) Base-pairing scheme between protonated and nonprotonated cytosin. (c) Sequence and folding scheme of DNA strand M. Strand M is labeled with Alexa 488 on the 5' end and BHQ on the 3' end. At low pH values, M folds into the i-motif upon formation of six C⁺-C pairs (gray lines). In this conformation, the dye and the quencher are in close proximity and the fluorescence intensity is considerably lower than that in the open state. (d) Fluorescence titration of strand M against the pH value. At low pH, the conformational switch M assumes the i-motif conformation. Between pH 5.5 and 6.5, strand M unfolds into a random coil conformation. Because strand M is labeled with a fluorescent dye and a quencher, the transition can be monitored in the fluorescence signal (dots). In the folded state, fluorescence is quenched, whereas in the random coil conformation it is not. A sigmoidal fit to the titration values is drawn as a continuous line.

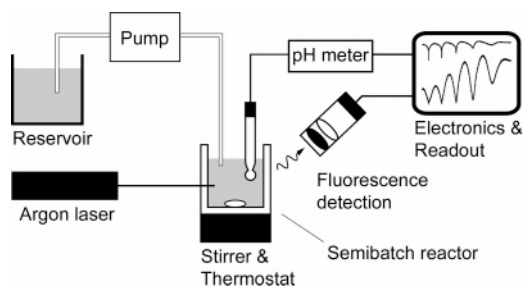


Figure 2. Experimental setup. A solution of sodium sulfite, sodium thiosulfate, and sulfuric acid is pumped from a reservoir into a continuously stirred reactor containing a solution of sodium iodate and the fluorescent-labeled DNA switches M. Fluorescence is excited with an argon ion laser, detected, and recorded simultaneously with the pH value.

or consumption of protons. This pH oscillation is coupled to a DNA conformational change. As the proton-sensitive DNA structure, a molecular device based on the *i*-motif is chosen.^{7,29} The *i*-motif is a four-stranded DNA structure that forms because of intramolecular noncanonical base-pairing between protonated and unprotonated cytosine residues (Figure 1b). In the particular case of the device used here, a DNA strand containing 12 cytosines can form 6 intramolecular C⁺–C base-pairs, resulting in the folded DNA structure depicted in Figure 1c. The *pK* value for cytosine is approximately 4.2, and the transition to the *i*-motif conformation, in which only half of the cytosines are protonated, takes place in the pH range between 6 and 7. At higher pH values, the cytosines are deprotonated and the DNA strand adopts a random coil conformation. To monitor its conformational transition, we labeled the DNA molecule with a pH-insensitive fluorophore at the 5' end and a quencher at the 3' end. If the fluorophore and quencher are in close proximity, then the fluorescence of the fluorophore is suppressed by the quencher because of energy transfer. If the two chromophores are far apart, then the fluorescence intensity is high. The transition between the folded single-stranded *i*-motif structure and the relaxed coil structure is therefore accompanied by a strong increase in fluorescence (Figure 1d).

The experimental setup is displayed in Figure 2. For the reaction, a solution of Na₂SO₃, Na₂S₂O₃, and H₂SO₄ is fed slowly with a pump into a continuously stirred reaction vessel initially containing only a solution of NaIO₃. Qualitatively, the chemical processes taking place are the following: At low H⁺ concentrations, iodate predominantly oxidizes hydrogen sulfite to sulfate, a reaction that produces iodide plus protons and therefore lowers the pH. At high H⁺ concentrations, however, the oxidation of iodide to iodine and of thiosulfate to tetrathionate becomes dominant, consuming protons and thus raising the pH value again.^{30,31} Because we wish to keep the same population of DNA molecules in the reactor permanently, we currently use a “semibatch” reactor that has an inlet but no outlet.²⁶ As shown in Figure 3, in this setup the oscillations slowly die out because of the continuous decrease in reactant concentrations. This behavior can be well reproduced in model calculations based on a set of rate equations^{30,31} describing the dominant kinetic pro-

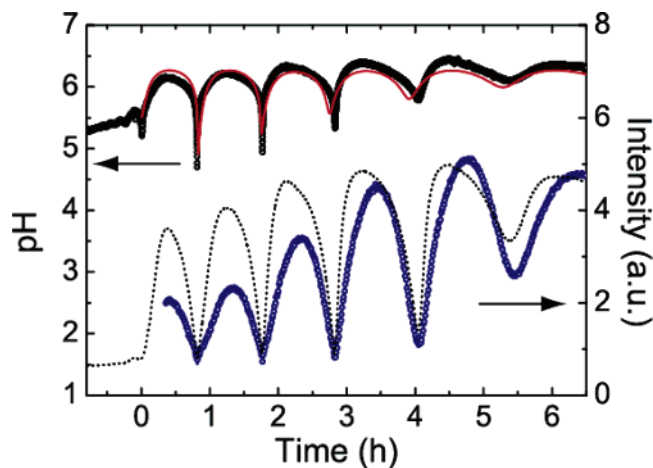


Figure 3. Measurements. Upper curves: measured (circles) and simulated (red solid line) time course of the pH value of the chemical oscillator in the semibatch configuration. See the Supporting Information for a detailed description of the kinetic model used for the simulation. Lower curves: fluorescence trace (blue circles) recorded simultaneously with the pH oscillations monitoring the motion of the DNA switches. Also shown is the fluorescence intensity expected from the pH values using the titration data from Figure 1 (dotted line). The measured fluorescence values roughly agree with the calculated values, in particular for the later oscillations that have a larger temporal spacing and reach slightly higher pH values. This indicates that the unfolding kinetics may not be fast enough at lower pH values in order for the DNA switches to follow the oscillator.

cesses of the reaction that we adapted for the semibatch case. If the reaction is performed in an open reactor with an inlet and an outlet, then pH oscillations with a very regular amplitude can be produced (see the Supporting Information).

With our choice of experimental conditions, the oscillator varies the pH value between 5 and 7 periodically with a temporal period of about 1 h. In consequence, the conformational transitions of the DNA strands are enforced periodically by the oscillator. In Figure 3, the pH oscillations in the reactor are displayed together with the simultaneously measured fluorescence-intensity signal. The fluorescence signal indeed follows the pH value, indicating that the DNA strands present in solution undergo their conformational change as designed. Also indicated in Figure 3 is the fluorescence signal calculated from the titration curve in Figure 1d on the basis of the pH oscillations. Obviously, for the first few oscillations (corresponding to lower pH values) the amplitude of the fluorescence oscillations is lower than expected. We assume that in this regime the kinetics of the conformational change between the *i*-motif and the relaxed coil is actually slower than the time-scale of the oscillations. Control experiments with the fluorophore alone and with DNA strands not prone to fold into the *i*-motif confirmed that the observed oscillations in the fluorescence signal are in fact caused by the structural transition of the DNA switch (see the Supporting Information for control experiments).

The *i*-motif has been used previously for the construction of a DNA-based molecular machine that could stretch and contract cyclically, driven in response to changes in the pH value.⁷ In this case, the stretching motion was caused by hybridization of the *i*-motif strand to its complement strand.

We therefore also added the complement of M to our oscillator solution. The fluorescence signals recorded from the two DNA strands were indistinguishable from the signals recorded from strand M alone, indicating that hybridization does not take place under the present reaction conditions (Supporting Information Figure 2). To make full use of chemical oscillators for the autonomous operation of DNA nanomachines, the main challenge will be the optimization of the reaction conditions to allow for efficient DNA hybridization. Optimization of the reaction conditions will also be necessary to achieve faster oscillations, which may be more relevant technologically. Temporal periods of 2–5 min have been demonstrated for pH oscillations very similar to the ones used in this work.³¹ Among the parameters influencing the period are temperature and flow speed. Another challenge will be the immobilization of DNA nanodevices to solid supports. Immobilized devices could, in principle, be driven indefinitely by the regular pH oscillations that occur in a flow-through reactor (Supporting Information Figure 1). A general limitation of this approach, as generally is the case for DNA devices that are driven by changes in buffer composition, is that no use is made of sequence specificity and DNA devices cannot be addressed individually within the reaction solution.

Here we have shown how a proton-sensitive DNA structure can be driven autonomously through its conformational states by a chemical oscillator. This constitutes the first example of a DNA device maintained in nonequilibrium within a permanently fed chemical reactor and opens up a novel field of applications for oscillating and pattern-generating chemical reactions. It should be possible to generalize the approach presented here to operate DNA nanodevices within spatiotemporal chemical patterns or oscillations that could be helpful for applications in which molecular machines assist in nanoassembly tasks or in which transport of nanocomponents along supramolecular tracks is desired. Our approach should be applicable to other pH-dependent DNA machines such as devices based on the duplex–triplex transition;^{10,12} however, it need not be restricted to DNA-based systems. It should also be possible to drive other pH-dependent molecular machines by chemical oscillators, for example, the recently demonstrated rotaxane-based supramolecular “elevator”.³²

Experimental Section. Unless stated otherwise, all chemicals were purchased from Sigma-Aldrich, Germany. DNA strand M with the sequence 5'-CCCTAACCCTAAC-CCTAACCC-3' was synthesized by biomers.net, Ulm, Germany and labeled at the 5' end with Alexa Fluor 488 (Molecular Probes, Eugene, OR) and at the 3'-end with BHQ-1 (Biosearch Technologies, Novato, CA).

The semibatch reactor consisted of a reservoir, a reactor, and a peristaltic pump (Minipuls 2, Gilson, Bad Camberg, Germany). The reservoir contained a solution of 30 mL of 26 mM Na₂SO₃, 15 mM Na₂S₂O₃, and 5 mM sulfuric H₂SO₄. This solution was pumped at 30 μL/min into the reactor containing 30 mL of a 50 mM solution of NaIO₃. The reaction solution was stirred constantly at 300 rpm. After approximately 4 h, the pH value started to oscillate and DNA

strand M was added to the reactor at an initial concentration of 10 nM. The titration of strand M was performed in a solution of 100 mM NaCl, and the pH was adjusted by the addition of NaOH and HCl.

For oscillator measurements, fluorescence was excited with an argon ion laser ($\lambda = 488$ nm) and detected with a Si photodiode at an angle of 90°. The signal was amplified, detected by a lock-in amplifier, and recorded with a data acquisition card. The pH value was measured and recorded simultaneously with a pH-Electrode (Schott, Mainz, Germany). Fluorescence titrations were performed with a spectrofluorometer (Fluorolog 3, Jobin Yvon GmbH, Munich, Germany).

Acknowledgment. This work was supported by the Deutsche Forschungsgemeinschaft through the Emmy Noether program (DFG SI 761/2-2) and by the Bavarian Ministry for Science, Research and Arts through the program “Neue Werkstoffe”. T.L. acknowledges funding through the CeNS International Graduate School for NanoBioTechnology. We wish to thank Jörg P. Kotthaus and Joachim O. Rädler for critically reading the manuscript.

Supporting Information Available: Simulation of the kinetics of the oscillator, reaction with the complementary strand of M, and control experiments. This material is available free of charge via the Internet at <http://pubs.acs.org>.

References

- (1) Mao, C. D.; Sun, W. Q.; Shen, Z. Y.; Seeman, N. C. *Nature* **1999**, *397*, 144–146.
- (2) Yan, H.; Zhang, X. P.; Shen, Z. Y.; Seeman, N. C. *Nature* **2002**, *415*, 62–65.
- (3) Yurke, B.; Turberfield, A. J.; Mills, A. P.; Simmel, F. C.; Neumann, J. L. *Nature* **2000**, *406*, 605–608.
- (4) Simmel, F. C.; Yurke, B. *Appl. Phys. Lett.* **2002**, *80*, 883–885.
- (5) Li, J. W. J.; Tan, W. H. *Nano Lett.* **2002**, *2*, 315–318.
- (6) Alberti, P.; Mergny, J. L. *Proc. Natl. Acad. Sci. U.S.A.* **2003**, *100*, 1569–1573.
- (7) Liu, D. S.; Balasubramanian, S. *Angew. Chem., Int. Ed.* **2003**, *42*, 5734–5736.
- (8) Feng, L. P.; Park, S. H.; Reif, J. H.; Yan, H. *Angew. Chem., Int. Ed.* **2003**, *42*, 4342–4346.
- (9) Chen, Y.; Wang, M. S.; Mao, C. D. *Angew. Chem., Int. Ed.* **2004**, *43*, 3554–3557.
- (10) Chen, Y.; Lee, S. H.; Mao, C. D. *Angew. Chem., Int. Ed.* **2004**, *43*, 5335–5338.
- (11) Shen, W. Q.; Bruist, M. F.; Goodman, S. D.; Seeman, N. C. *Angew. Chem., Int. Ed.* **2004**, *43*, 4750–4752.
- (12) Brucale, M.; Zuccheri, G.; Samori, B. *Org. Biomol. Chem.* **2005**, *3*, 575–577.
- (13) Sherman, W. B.; Seeman, N. C. *Nano Lett.* **2004**, *4*, 1203–1207.
- (14) Yin, P.; Yan, H.; Daniell, X. G.; Turberfield, A. J.; Reif, J. H. *Angew. Chem., Int. Ed.* **2004**, *43*, 4906–4911.
- (15) Shin, J. S.; Pierce, N. A. *J. Am. Chem. Soc.* **2004**, *126*, 10834–10835.
- (16) Tian, Y.; Mao, C. D. *J. Am. Chem. Soc.* **2004**, *126*, 11410–11411.
- (17) Tian, Y.; He, Y.; Chen, Y.; Yin, P.; Mao, C. D. *Angew. Chem., Int. Ed.* **2005**, *44*, 4355–4358.
- (18) Bath, J.; Green, S. J.; Turberfield, A. J. *Angew. Chem., Int. Ed.* **2005**, *44*, 4358–4361.
- (19) Turberfield, A. J.; Mitchell, J. C.; Yurke, B.; Mills, A. P.; Blakey, M. I.; Simmel, F. C. *Phys. Rev. Lett.* **2003**, *90*.
- (20) Winfree, A. T. *The Geometry of Biological Time*, 2nd ed.; Springer: New York, 2000.
- (21) Zaikin, A. N.; Zhabotinsky, A. M. *Nature* **1970**, *225*, 535.
- (22) Winfree, A. T. *Science* **1972**, *175*, 634.
- (23) Rabai, G.; Orban, M.; Epstein, I. R. *Acc. Chem. Res.* **1990**, *23*, 258–263.

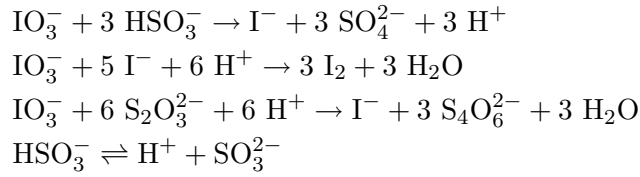
- (24) Kurin-Csorgei, K.; Epstein, I. R.; Orban, M. *Nature* **2005**, *433*, 139–142.
- (25) Kadar, S.; Wang, J. C.; Showalter, K. *Nature* **1998**, *391*, 770–772.
- (26) Rabai, G.; Epstein, I. R. *J. Am. Chem. Soc.* **1992**, *114*, 1529–1530.
- (27) Edblom, E. C.; Orban, M.; Epstein, I. R. *J. Am. Chem. Soc.* **1986**, *108*, 2826–2830.
- (28) Rabai, G.; Beck, M. T. *J. Phys. Chem.* **1988**, *92*, 4831–4835.
- (29) Gehring, K.; Leroy, J. L.; Gueron, M. *Nature* **1993**, *363*, 561–565.
- (30) Gaspar, V.; Showalter, K. *J. Am. Chem. Soc.* **1987**, *109*, 4869–4876.
- (31) Rabai, G.; Beck, M. T. *J. Phys. Chem.* **1988**, *92*, 2804–2807.
- (32) Badjic, J. D.; Balzani, V.; Credi, A.; Silvi, S.; Stoddart, J. F. *Science* **2004**, *303*, 1845–1849.

NL051180J

Supplementary information for Liedl & Simmel

Modeling of the oscillatory reaction

For the oscillatory reaction, a solution of sodium sulfite, sodium thiosulfite and sulfuric acid is continuously added to a reactor containing sodium iodate. The dominant reactions taking place in the reactor are:



To model the pH oscillator we adapted the empirical kinetic model from the original publications by Rabai and Beck (J. Phys. Chem. 92, 2804-2807 (1988); J. Phys. Chem. 92, 4831-4835 (1988)) for the semibatch case. To this end, the volume V and the rate of its change v are introduced as dynamic variables and used to incorporate the effect of the increasing volume on the concentrations of the reactants.

$$\begin{aligned}j &= [\text{IO}_3^-] \times \text{M}^{-1} \\ y &= [\text{HSO}_3^-] \times \text{M}^{-1} \\ s &= [\text{SO}_3^{2-}] \times \text{M}^{-1} \\ t &= [\text{S}_2\text{O}_3^{2-}] \times \text{M}^{-1} \\ h &= [\text{H}^+] \times \text{M}^{-1}\end{aligned}$$

$$\begin{aligned}v_1 &= k_{1a}jyh + k_{1b}jy^2 + k_cjyth^2 \\ v_2 &= k_2y \\ v_{-2} &= k_{-2}sh \\ v_3 &= \frac{k_3jt^2h^2}{1 + k_iy}\end{aligned}$$

$$\begin{aligned}\frac{d}{dt} j &= -v_1 - v_3 \frac{jv}{V} \\ \frac{d}{dt} y &= -3v_1 - v_2 + v_{-2} + \frac{(y_0 - y)v}{V} \\ \frac{d}{dt} s &= v_2 - v_{-2} + \frac{(s_0 - s)v}{V} \\ \frac{d}{dt} t &= -6v_3 + \frac{(t_0 - t)v}{V} \\ \frac{d}{dt} h &= 3v_1 - 6v_2 + v_2 - v_{-2} + \frac{(h_0 - h)v}{V} \\ \frac{d}{dt} V &= v\end{aligned}$$

The rate constants were chosen as follows

$$\begin{aligned}
k_{1a} &= 8.8 \times 10^3 \text{ s}^{-1} \\
k_{1b} &= 11 \text{ s}^{-1} \\
k_c &= 1 \times 10^{11} \text{ s}^{-1} \\
k_2 &= 20 \times 10^3 \text{ s}^{-1} \\
k_{-2} &= 5 \times 10^{10} \text{ s}^{-1} \\
k_3 &= 3.4 \times 10^{12} \text{ s}^{-1} \\
k_i &= 5 \times 10^4
\end{aligned}$$

The inhibitory constant k_i is dimensionless. For the calculation for Fig. 3 in the paper, initial conditions were chosen as follows: The concentrations in the added reaction solution were

$$\begin{aligned}
j_0 &= 0 \\
y_0 &= 0 \\
s_0 &= 0.026 \\
t_0 &= 0.015 \\
h_0 &= 0.008
\end{aligned}$$

The initial concentrations in the reactor were:

$$\begin{aligned}
j(0) &= 0.05 \\
y(0) &= 0 \\
s(0) &= 0 \\
t(0) &= 0 \\
h(0) &= 7 \times 10^{-4}
\end{aligned}$$

and, finally, the initial reaction volume was $V = 0.03$ l and the flow rate was $v = 14$ $\mu\text{l}/\text{min}$. The values for the calculation are therefore very close to the experimental conditions, albeit not identical. The oscillatory patterns observed in the experiments can be well reproduced by this system of rate equations. Some of the features, however, differ. In particular, a long pre-oscillatory period in the reaction is not accurately reproduced by the calculations. Nevertheless, the calculations can be used to test the influence of certain reaction parameters such as flow rate or total volume.

Using the same model for a flow-through reactor (i.e. without dilution terms), we can also predict what would be observed in a reactor with an inlet and an outlet and immobilized DNA nanoswitches. In this case, the oscillator produces very regular pH oscillations. Plugging in the pH dependence of the fluorescence of the nanoswitches (from Fig. 1 in the paper), one can plot the expected fluorescence curves for this case (see figure). For this calculation, the initial conditions have to be chosen slightly differently:

$$\begin{aligned}
j_0 &= 0.0125 \\
y_0 &= 0
\end{aligned}$$

$$\begin{aligned}
 s_0 &= 0.025 \\
 t_0 &= 0.0104 \\
 h_0 &= 0.0105
 \end{aligned}$$

and

$$\begin{aligned}
 j(0) &= 0.05 \\
 y(0) &= 0 \\
 s(0) &= 0 \\
 t(0) &= 0 \\
 h(0) &= 1 \times 10^{-7}
 \end{aligned}$$

The rate equations were implemented and solved with a MATLAB (The MathWorks, Natick, MA) program on a conventional personal computer.

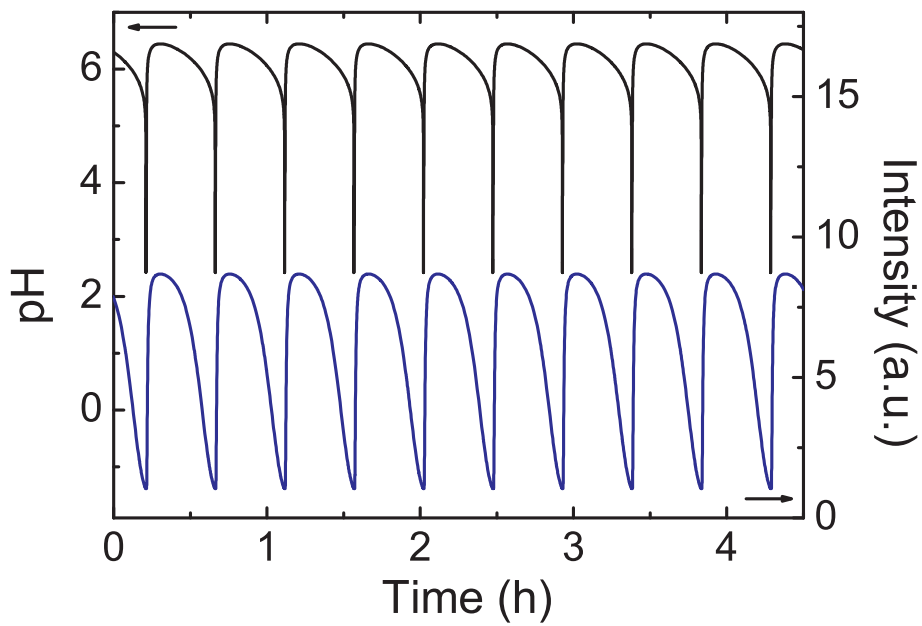


Figure 1: Calculated pH oscillations (black line) for a reactor with inlet and outlet and corresponding expected fluorescence signal (blue line) from the DNA switch.

Reaction with the complement of strand M

We also tried to operate the DNA conformational switch in “machine mode” (as in Ref. 7 of the manuscript) by adding a slightly mismatched complement of M (5'- GTTAGTGTTAGT-GTTAG -3'). This strand has two mismatches and is 4 nt shorter than the full complement of M. It is the same strand as used in Ref. 7 of the article. The mismatches are introduced into the complementary strand to ensure decay of the duplex into single strands at low pH. The result is shown in Fig. 2 - the oscillations are virtually indistinguishable from the oscillations obtained with M alone (the differences arise from the slightly different pH range over which the oscillations occur). Using the 17 nt complementary strand 5'- GTTAGGGT-TAGGGTTAG -3' (with no mismatches) for our oscillatory reaction also does not lead to any improvement.

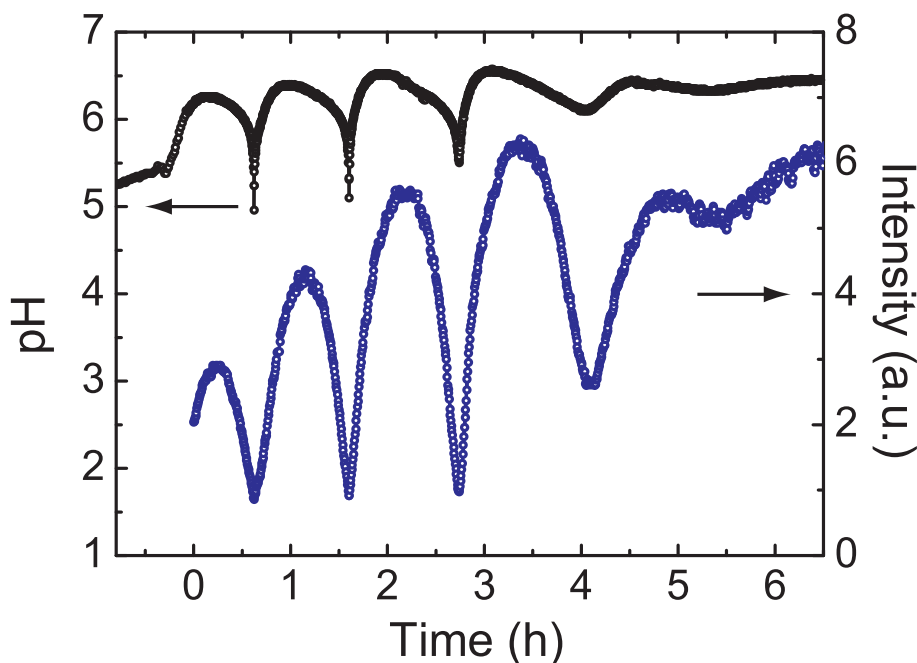


Figure 2: pH oscillations and corresponding fluorescence oscillations obtained from DNA switch M in the presence of its slightly mismatched complementary strand.

Control experiments

pH (in)dependence of Alexa 488 fluorescence

We also checked that the fluorescent dye Alexa 488 is pH independent and monitored the fluorescence of the dye alone added to the reaction mixture. As can be seen in Fig. 3, the fluorescence of the dye Alexa 488 is almost independent from pH in the range of interest. Furthermore, its fluorescence does not seem to be degraded by the reaction mixture.

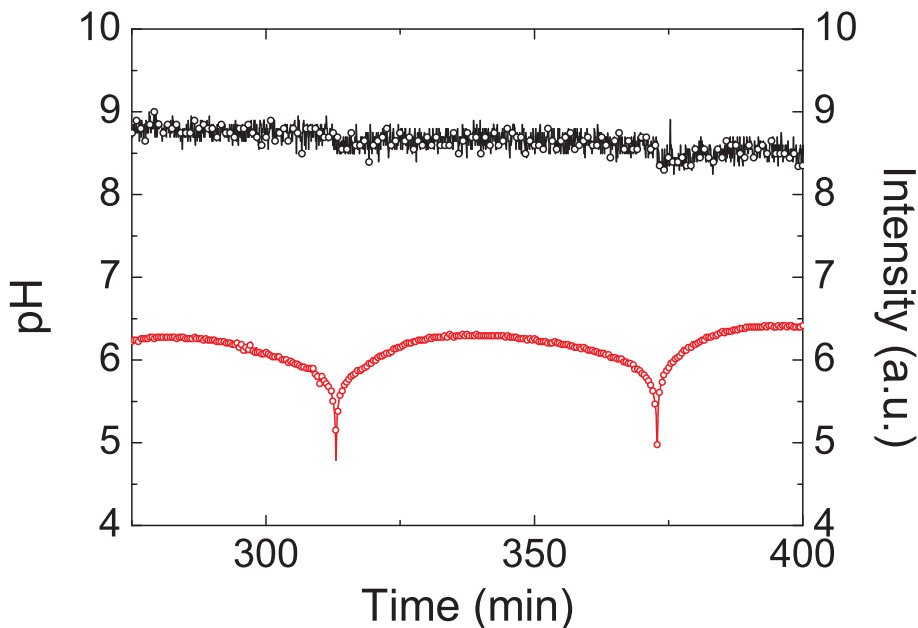


Figure 3: pH oscillations (lower curve) and fluorescence signal (upper curve) recorded from Alexa 488 dye mixed to the reaction solution. Almost no dependence on the pH is observed.

A control strand

Fig. 4 shows a comparison of the pH dependence of the fluorescence of strand M compared to a control strand with the randomly chosen sequence Alexa 488-5'-CTTTAACAAATAATGATA ATT-3'-BHQ 1. This sequence has the same length as M, but only contains 2 cytosines (instead of 12 in M). It does not form any significant secondary structure and it cannot fold into the i-motif. The signals in Fig. 4 have been normalized to be equal at pH 8.3. It can clearly be seen that the fluorescence variation is smaller and considerably shallower for the control strand. In particular, no transition can be seen around pH 6 as is the case for strand M (and the i-motif). The sigmoidal shape may be explained by a cooperative transition to the other conformation, but it also reflects the distance dependence of energy transfer between the end labels of M. The slight change in fluorescence for the control strand may reflect the protonation of adenine at low pH (adenine: $pK_a=3.5$ and cytosine $pK_a=4.2$) which results in an effective change of the charge of the DNA backbone which in turn reduces the electrostatic contributions to its persistence length. This effect may also be present for the cytosine rich strand M, but it does not explain its transition around $pH=6$.

Distance calibration

To further confirm that the observed transition is consistent with the i-motif, we used the fluorescence data at pH 8 for a distance calibration. In Fig. 5 fluorescence values for strand M as single strand and hybridized to its 17 nt complement as well the fluorescence of the control strand with and without its 22 nt complement are shown together with the fluorescence of a strand singly labeled with Alexa 488. We estimate the end-to-end distances d for single-stranded DNA as $d = \sqrt{2l_pNa}$, where l_p is the persistence length, N is the number of bases and

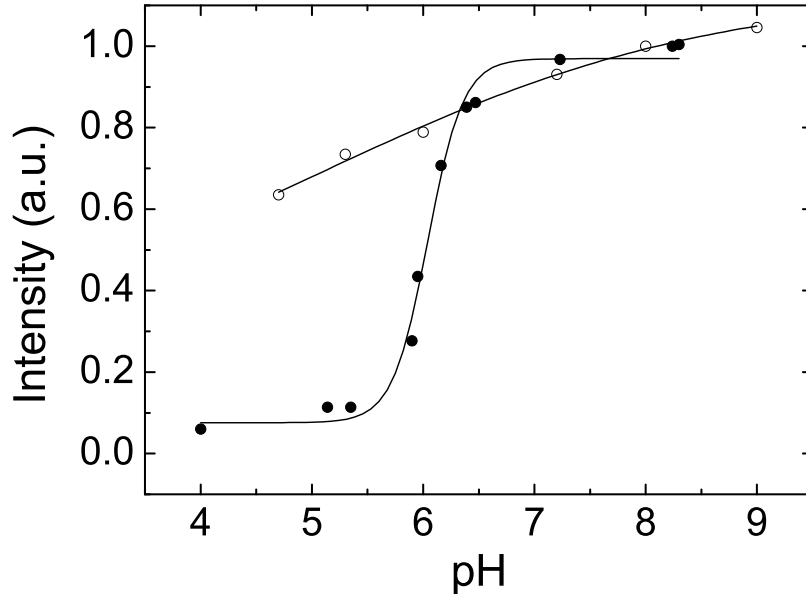


Figure 4: Fluorescence titrations in the range of the i-motif transition for strand M and a control strand.

$a = 0.43$ nm is the distance between bases in single-stranded DNA (cf. Tinland, B.; Pluen, A.; Sturm, J.; Weill, G. *Macromolecules* 1997, 30, (19), 5763-5765). For double-stranded DNA we multiply the number of base-pairs by 0.34 nm. A good fit to the data by the Förster curve $(r/r_0)^6/(1 + (r/r_0)^6)$ is possible, when we choose $l_p = 1.3$ nm for single-stranded DNA. A fit with the single parameter r_0 yields a Förster distance of $r_0 = 5.7$ nm. From this value, we estimate the distance between dye and quencher in the low pH conformation to be about 2.5 nm which is consistent with an i-motif conformation.

To summarize: Alexa 488 is not pH dependent in the range in question. M seems to undergo a large conformational transition around pH 6, whereas a control strand with only two cytosines, is not. As it is known for strand M that it folds into the i-motif, we assume that we here also observe the i-motif transition. The distance estimated from the fluorescence in the quenched state also corresponds to the distance expected for the i-motif. The fluorescence trace obtained for M during the operation of the oscillator is completely consistent with the titration data, indicating that the strand basically displays the same behavior under these reaction conditions as during the titration.

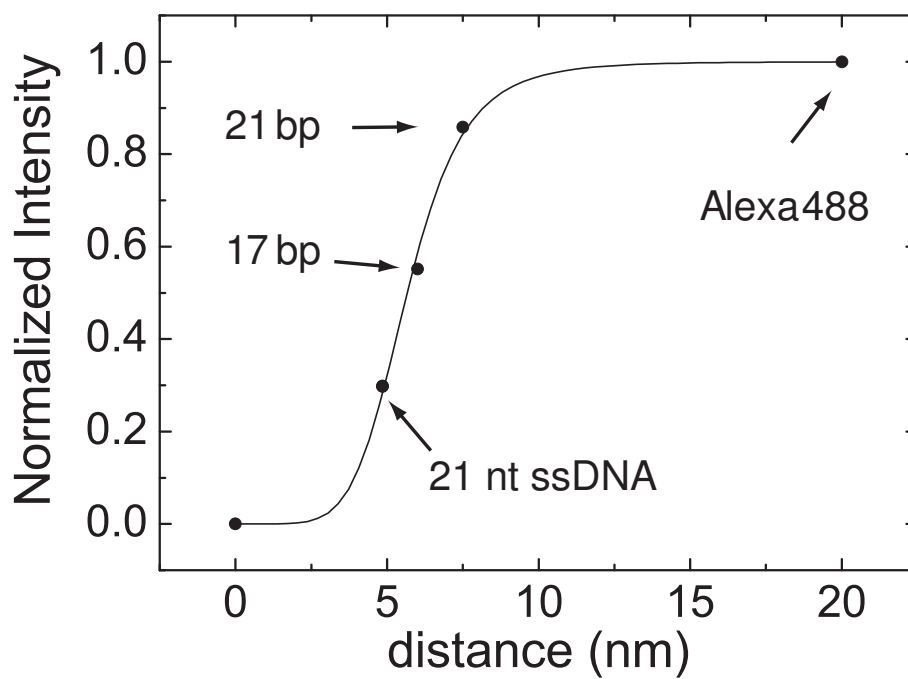


Figure 5: Fluorescence values for various distances between Alexa 488 and BHQ-1 (normalized to the maximum value obtained for a singly Alexa 488-labeled strand). For the fit, the distance for the singly-labeled strand has been arbitrarily set to a large value. The fluorescence values for 21 nt single-stranded M and control strand coincide.

DOI: 10.1002/anie.200600353

A Surface-Bound DNA Switch Driven by a Chemical Oscillator**

Tim Liedl, Michael Olapinski, and Friedrich C. Simmel*

The fabrication of autonomously moving molecular structures is one of the central challenges in the field of DNA nanodevices.^[1] Some of the concepts introduced recently to achieve this goal rely on the sequence-dependent catalytic action of DNA-modifying enzymes such as restriction endonucleases or nicking enzymes^[2] while others use the catalytic power of DNA itself by incorporating DNA enzyme sequences into DNA devices.^[3] Both approaches have also been used to realize autonomous molecular computers.^[4] Another strategy is based on controlled inhibition of DNA hybridization by formation of secondary structure and its acceleration by catalytic DNA strands.^[5] These concepts were developed for the autonomous operation of DNA devices fueled by DNA hybridization. A different approach was recently taken by our research group^[6] and we could show that the pH-sensitive conformational transition of a cytosine-rich DNA strand between a random conformation and the so-called “i motif” could be driven by the oscillating proton concentration generated by a chemical oscillator. In such a system, the temporal succession of the states of the DNA devices is determined by a nonlinear dynamical system rather than by an external operator. We report here how this system can be significantly improved by attaching the DNA conformational switches to a solid substrate. This attachment allows us to operate the chemical oscillator in a continuous flow stirred tank reactor (CSTR) into which a glass chip supporting the DNA devices is placed. In principle, the surface-bound DNA structures can undergo an infinite number of autonomous conformational switching events in this configuration.

We showed recently how proton-fueled DNA devices can be driven by an oscillating chemical reaction^[6] by using a variant of the Landolt reaction to periodically change the pH value in a continuously fed reactor. To retain the DNA switches within the reaction solution, a reactor without an outlet had to be used. In such a configuration, one cannot reach a steady state since the continuous influx of reaction

solution means the average concentrations of the reactants vary. As a result, this dynamic chemical system is driven out of its oscillatory region, thus causing the oscillations to die away after a few periods.

To overcome this limitation in the present work we operated the oscillator in a CSTR with two inlets and one outlet. In principle, an infinite number of homogeneous pH oscillations can be generated by using a continuous filling combined with the simultaneous removal of waste materials. However, the DNA devices had to be attached to a solid substrate to prevent loss of the DNA through the reactor's outlet. For these experiments, we used thiol-modified, fluorescently labeled DNA switches bound to an ultrathin transparent gold layer on a glass substrate. This allowed a firm covalent attachment of the DNA to the surface while at the same time energy transfer between the fluorophores and the gold layer^[7] could be used to characterize the conformational transitions of the switches.

Schematic representations of the surface-bound DNA switches in their two states at low and high pH values are shown in Figure 1 a. The switches consist of 21 nucleotide (nt)

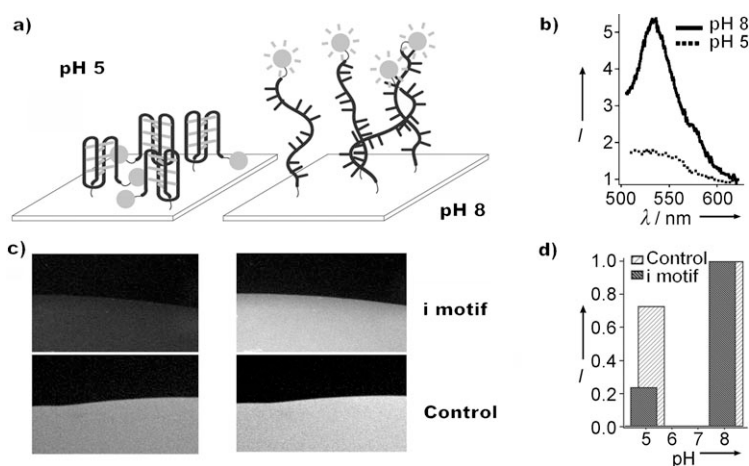


Figure 1. a) Schematic representation of single-stranded DNA bound to the gold/glass substrate through a 5'-thiol-C₆ spacer. In the closed i motif conformation at low pH values the dye attached to the 3' end is in proximity to the surface and is thus quenched. In contrast, the fluorescence strongly increases at higher pH values where the DNA strand adopts a random single-stranded conformation. b) Emission spectra recorded from the i motif attached to the substrate at pH 8 (random) and pH 5 (i motif). c) Fluorescence microscopy images of the i motif (top) and a control strand (bottom) at pH 5 (left) and pH 8 (right). d) Corresponding normalized fluorescence intensities.

long DNA strands with the sequence 5'-CCCTAACCC-TAACCCCTAACCC-3' (strand M). Below pH 6.5, DNA molecules of this sequence are known to undergo a conformational transition to the so-called “i motif”, in which four DNA strands are held together by a number of semiprotonated C-C⁺ base pairs (in this case six intramolecular C-C⁺ pairs). This particular DNA sequence has been utilized previously for the fabrication of other DNA-based nanodevices^[8] and is also the same sequence as used in our previous bulk experiments.^[6] The DNA strands were modified with a thiol-C₆

[*] T. Liedl, M. Olapinski, Dr. F. C. Simmel
Department of Physics and Center for Nanoscience
LMU Munich
Geschwister Scholl Platz 1, 80539 Munich (Germany)
Fax: (+49) 89-2180-3182
E-mail: simmel@lmu.de

[**] This work was supported by the Deutsche Forschungsgemeinschaft (Emmy Noether grant DFG SI 761/2-2). T.L. and M.O. are supported by the LMU International Graduate School “Nanobiotechnology”.

Supporting information for this article is available on the WWW under <http://www.angewandte.org> or from the author.

spacer at the 5' end and with the fluorescent dye Rhodamine Green (RG) at the 3' end. The fluorescence of RG is pH-insensitive between pH 4 and 9 (see the Supporting Information). At low pH values, the transition to the *i* motif brings the 3' end of the molecule into proximity to the 5' end (ca. 1.5 nm^[9]). The fluorophore is brought closer to the substrate when the DNA switches are attached to a surface through the 5' end.

A glass coverslip with an ultrathin layer of gold was used as the substrate. To prepare the substrate, first a thin gold layer was evaporated onto a clean coverslip, and then nearly completely removed by sputtering with argon ions (experimental details are given in the Supporting Information). The substrate is then nearly transparent, but it is still possible to attach DNA strands to the remaining gold on the surface (see the Supporting Information). The modified coverslips were mounted on an epifluorescence microscope and the fluorescence was monitored while subsequently adding phosphate buffer of pH 8 and pH 5. Switching the DNA strands between a random conformation at high pH values and the *i* motif at low pH values resulted in strong changes in the fluorescence intensity (Figure 1 c,d). Such clear changes in the intensity could be monitored only at sites on the chip spotted with the *i* motif strand. Sites spotted with a control strand with a random sequence only showed a small change in intensity.

A fluorescence spectrometer was extended with a custom built module which allowed characterization of the sample when placed in a CSTR to allow for fluorescence spectroscopic and energy-transfer measurements during the operation of the pH oscillator. The setup is shown schematically in Figure 2. Fluorescence spectra recorded with this setup for the substrate-attached *i*-motif switches at low and high pH values are displayed in Figure 1 b.

The pH oscillator was operated by pumping two separate solutions at 150 $\mu\text{L min}^{-1}$ into the cuvette, which was initially filled with 20 mL H₂O. One solution contained 19 mM NaIO₃ while the other contained 30 mM Na₂SO₃, 21 mM Na₂S₂O₃, and 5 mM H₂SO₄. A second pump removed excess volume at 300 $\mu\text{L min}^{-1}$. Typically, after a period of 4 h prior to oscillation, the pH value started to oscillate between pH 6.3 and pH 5.5 with a period of 20 minutes. The oscillations persisted until the reactant reservoirs were exhausted (typically after 24 h).

Figure 3 shows the fluorescence intensity recorded from the surface-immobilized DNA switches together with the oscillations in the pH value. The fluorescence strongly oscillates in concordance with the pH value, thus indicating that the chemical oscillator enforces the conformational transition of the switches as designed. We performed a variety of test experiments to verify that these fluorescence oscillations are indeed caused by the conformational transitions of the switches to the *i* motif and back. A conventional fluorescence titration experiment shows

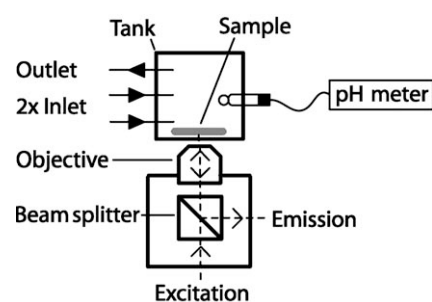


Figure 2. Experimental setup: Excitation light coming from a fluorescence spectrometer is focused onto the sample chip with a long working distance objective. Light emitted from the chip is collected by the same objective and reflected into the spectrometer with a beam splitter. The sample chip resides in a CSTR which consists of a large volume ($V=25$ mL) fluorescence cuvette with two inlets and one outlet for the reactants. The pH value is monitored with a conventional pH meter.

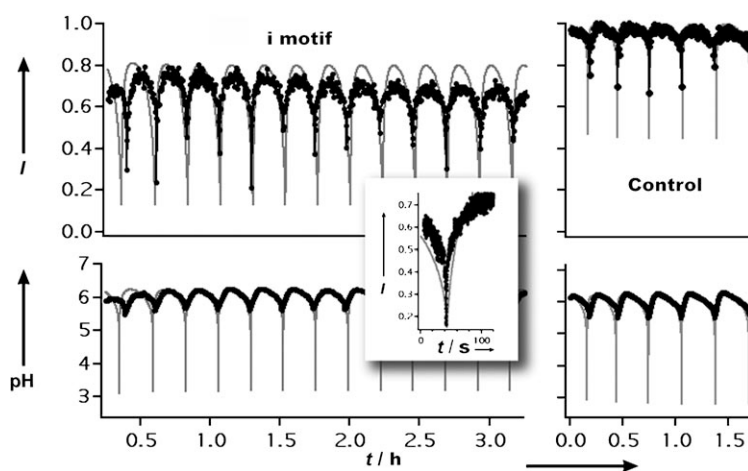


Figure 3. Left: In the CSTR setup, a large number of pH oscillations can be generated (bottom, black trace). The simultaneously recorded fluorescence intensity originating from the *i* motif bound to a gold/glass chip follows the pH oscillations (top, black trace). The simulated pH values (bottom, gray trace) coincide with the measured values except for regions where the low pH spikes occur. This deviation is caused by the slow response of the pH meter. The simulated fluorescence trace in the top graph (gray) is generated from data from a titration experiment (see the Supporting Information). Inset: In an experiment at higher time resolution it became apparent that the fluorescence intensity at the position of the low pH spikes indeed drops to 20% of its maximum value, as expected from the simulation. Right: Measured (bottom, black trace) and predicted (bottom, gray trace) pH oscillations and corresponding fluorescence intensity (top, black trace: experimental data, gray curve: calculated values) of the control strands. The fluorescence is normalized to the maximum value at pH 7.4 for both the device and control strand. In the case of the device strand, the *i* motif is already partly formed under the conditions of the oscillator, which results in a decreased fluorescence signal. The fluorescence values of both strands are in complete agreement with the titration experiments (see the Supporting Information), which shows that the strands essentially behave in the same way in the CSTR as under ordinary buffer conditions. The fluorescence of the device strand is consistent with its transition to the *i* motif, while the control strand does not show such a behavior.

that the immobilized DNA switches undergo a conformational change when the pH value is lowered below about 6.5, as expected (see the Supporting Information). A plot of the

fluorescence intensity obtained in the CSTR during the operation of the pH oscillator essentially shows the same transition (see the Supporting Information). By contrast, the immobilized control strands show a less pronounced response to pH changes, in particular no transition around pH 6 is observed. Accordingly, a different fluorescence trace is recorded when they are put under the influence of the oscillator (Figure 3). The fluorescence for the control strand only drops to about 50% of its maximum value, whereas the signal decreases to below 20% for the device strand. Both fluorescence traces are fully consistent with those obtained by conventional titration experiments, thus indicating that the immobilized DNA molecules undergo the same conformational changes when driven by the oscillator. It has to be noted, however, that when the pH is below 4 the fluorescence may not reflect conformational changes of the DNA alone, but can be influenced by a variety of other factors (see the Supporting information).

Simulated time traces of the pH oscillations based on a model developed by Rabai and Beck^[10] are also shown in Figure 3. Experimentally obtained data agree well with the model's prediction at pH values above 5.5. However, the model also predicts sharp "spikes" down to pH values of about 3. In fact, these spikes also occur experimentally, but their short duration ($t_{1/2} \approx 2$ s) means they cannot be resolved by our pH meter, which has a response time of 30 s. We independently checked the occurrence of the spikes at low pH values with the pH-sensitive dye methyl orange, which changes its color from yellow to pink at pH 4.4.^[10] Indeed, during the operation of the oscillator we observed this color change for fractions of a second at the position of the low pH spikes. This also explains why we observe fluorescence values at the minima of the pH oscillations which are lower than those expected from the recorded pH values. For comparison, the upper panel of Figure 3 contains time traces calculated from the simulated pH values and the titration curves for DNA strand M and the control strand. The experimental intensities agree well with the simulated values, except that the experimental traces again do not follow the low intensity spikes. This is simply caused by "undersampling". Only a limited number of data points could be taken for observations over long times, because of excessive photobleaching, and therefore the spacing of the data points is not close enough to resolve the pH spikes. In the inset of Figure 3, a fluorescence trace recorded at a higher rate is shown which reproduces very well the predicted values. This also indicates that the response time of the immobilized switches is on the order of a second.

Further evidence for the formation of the *i* motif in the surface-bound DNA switches is obtained from temperature-dependent measurements: a sharp melting transition is observed for DNA switches immobilized on the chip surface and in solution, whereas no such transition is seen for the control strand (Figure 4). These observations are in agreement with previous circular dichroism studies on the *i* motif.^[11]

In summary, a chemical oscillation generated in a continuous flow stirred tank reactor was utilized to periodically switch a DNA molecular structure immobilized on a

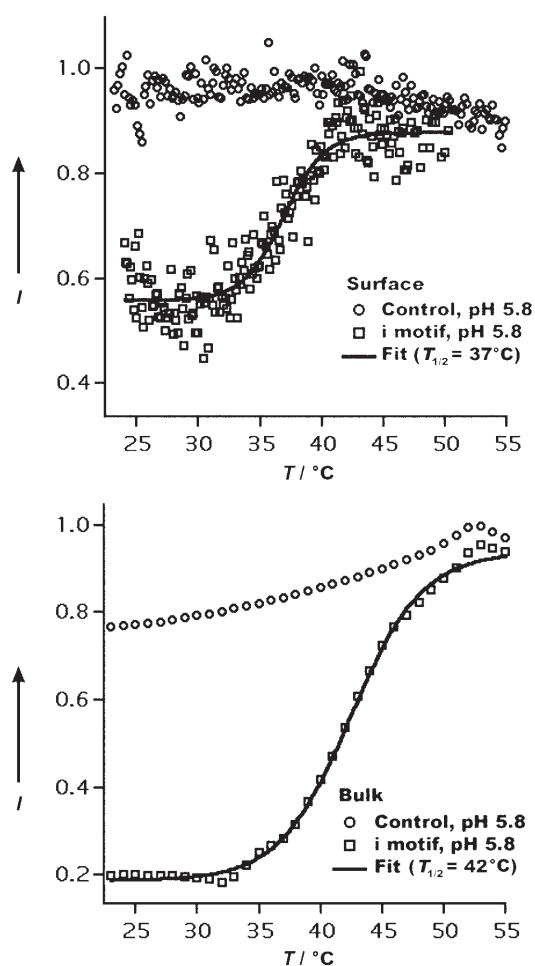


Figure 4. Fluorescence intensities of the *i* motif and the control strand in a melting experiment at pH 5.8 and comparison between surface-bound and solution-phase switches. Top: The surface-bound *i* motif unfolds at 37°C, while a surface-bound control strand does not show any change in fluorescence. Bottom: For the experiment in solution, the *i* motif strand labeled with a dye on one end and a quencher on the other end^[10] displays essentially the same behavior and unfolds at a slightly higher temperature than on the surface. The control strand exhibits only a small change in the fluorescence in the solution experiment.

glass chip between two distinct conformations. In a CSTR, these oscillations occur with a regular period and can in principle occur infinitely often. To realize and characterize this molecular-switching system experimentally, the DNA oligonucleotides were immobilized on a glass surface covered with an ultrathin gold layer, which allowed characterization of the surface-bound switches within a CSTR in an epifluorescence setup. This system represents the first example of an autonomously driven DNA switch immobilized on a solid substrate. It was shown recently in a related study by Shu et al.^[8b] that an immobilized DNA device based on the *i* motif can cyclically generate forces during the consumption of H⁺ ions and can thus even be construed as a periodically working motor. Such and similar systems may find application as actuators or sensors in biomolecular hybrid nanostructures. It is expected that surface-immobilized DNA switches could

also display spatiotemporal patterns and oscillations under the influence of chemical reaction waves.

Received: January 26, 2006

Revised: April 4, 2006

Published online: June 29, 2006

Keywords: chemical oscillations · DNA · molecular switches · nanotechnology

-
- [1] a) N. C. Seeman, *Trends Biochem. Sci.* **2005**, *30*, 119–125; b) F. C. Simmel, W. U. Dittmer, *Small* **2005**, *1*, 284–299.
- [2] a) P. Yin, H. Yan, X. G. Daniell, A. J. Turberfield, J. H. Reif, *Angew. Chem.* **2004**, *116*, 5014–5019; *Angew. Chem. Int. Ed.* **2004**, *43*, 4906–4911; ; b) J. Bath, S. J. Green, A. J. Turberfield, *Angew. Chem.* **2005**, *117*, 4432–4435; *Angew. Chem. Int. Ed.* **2005**, *44*, 4358–4361.
- [3] a) Y. Chen, M. S. Wang, C. D. Mao, *Angew. Chem.* **2004**, *116*, 3638–3641; *Angew. Chem. Int. Ed.* **2004**, *43*, 3554–3557; b) Y. Tian, Y. He, Y. Chen, P. Yin, C. D. Mao, *Angew. Chem.* **2005**, *117*, 4429–4432; *Angew. Chem. Int. Ed.* **2005**, *44*, 4355–4358.
- [4] a) Y. Benenson, T. Paz-Elizur, R. Adar, E. Keinan, Z. Livneh, E. Shapiro, *Nature* **2001**, *414*, 430–434; b) M. N. Stojanovic, D. Stefanovic, *Nat. Biotechnol.* **2003**, *21*, 1069–1074.
- [5] A. J. Turberfield, J. C. Mitchell, B. Yurke, A. P. Mills, M. I. Blakey, F. C. Simmel, *Phys. Rev. Lett.* **2003**, *90*, 118102.
- [6] T. Liedl, F. C. Simmel, *Nano Lett.* **2005**, *5*, 1894–1898.
- [7] a) B. Dubertret, M. Calame, A. J. Libchaber, *Nat. Biotechnol.* **2001**, *19*, 365–370; b) H. Du, M. D. Disney, B. L. Miller, T. D. Krauss, *J. Am. Chem. Soc.* **2003**, *125*, 4012–4013; c) C. S. Yun, A. Javier, T. Jennings, M. Fisher, S. Hira, S. Peterson, B. Hopkins, N. O. Reich, G. F. Strouse, *J. Am. Chem. Soc.* **2005**, *127*, 3115–3119.
- [8] a) D. S. Liu, S. Balasubramanian, *Angew. Chem.* **2003**, *115*, 5912–5914; *Angew. Chem. Int. Ed.* **2003**, *42*, 5734–5736; b) W. M. Shu, D. S. Liu, M. Watari, C. K. Riener, T. Strunz, M. E. Welland, S. Balasubramanian, R. A. McKendry, *J. Am. Chem. Soc.* **2005**, *127*, 17054–17060; c) D. Liu, A. Bruckbauer, C. Abell, S. Balasubramanian, D. Kang, D. Klenerman, D. Zhou, *J. Am. Chem. Soc.* **2006**, *128*, 2067–2071.
- [9] K. Gehring, J. L. Leroy, M. Gueron, *Nature* **1993**, *363*, 561–565.
- [10] a) G. Rabai, M. T. Beck, *J. Phys. Chem.* **1988**, *92*, 2804–2807; b) G. Rabai, M. T. Beck, *J. Phys. Chem.* **1988**, *92*, 4831–4835.
- [11] G. Manzini, N. Yathindra, L. E. Xodo, *Nucleic Acids Res.* **1994**, *22*, 4634–4640.
-



Supporting Information

© Wiley-VCH 2006

69451 Weinheim, Germany

Supporting information for Liedl, Olapinski & Simmel

1. Materials and Methods

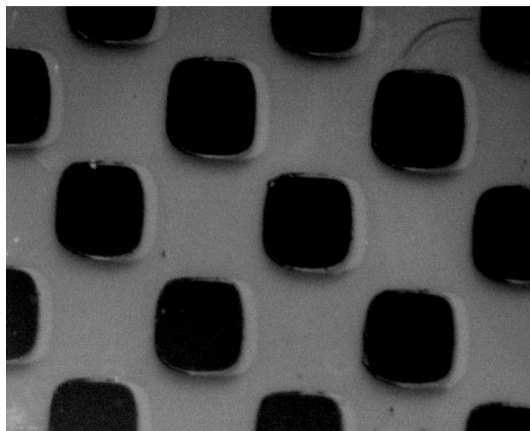


Figure 1: Binding of thiol-labeled DNA to a patterned, but transparent surface: A Au pattern was defined on a glass coverslip with standard lithography techniques. Then the sample was sputtered with Ar ions until no pattern was visible anymore. The modified surface was exposed to a DNA strand labeled with a dye on one end and a thiol-group on the other end. The pattern is revealed again under a fluorescence microscope. The side-length of the squares is $50\mu\text{m}$

Chemicals:

Unless stated otherwise, all chemicals were purchased from Sigma-Aldrich, Germany. The DNA strand M with the sequence 5' - CCC TAA CCC TAA CCC TAA CCC - 3' and the strand Control with the sequence 5' - CTT TAA CAA ATA ATG ATA ATT - 3' was synthesized by IBA GmbH, Göttingen, Germany and labeled at the 3' end with Rhodamine Green (Molecular Probes, Eugene, OR) and a Thiol-C6 spacer at the 5'-end.

Sample preparation:

The surface was prepared for attachment as follows: 8 nm Au was deposited on glass coverslips (Superior, Marienfeld, Germany) by thermal evaporation. The coverslips were subsequently sputtered with Ar-Ions at 200 W, 7×10^{-7} mbar for 45 s, thus removing almost all Au from the surface. Afterwards, the coverslips were placed in 65% HNO_3 for 2 h. After rinsing with de-ionized water 1 μl droplets of 25 μM DNA in PBS buffer containing 500 mM NaCl were spotted onto the coverslips and kept under 100% air moisture overnight. Then the coverslips were thoroughly rinsed with PBS and placed in PBS containing 10 mM Mercaptohexanol for 1/2 h to saturate the remaining Au-binding sites and remove unspecifically bound DNA. After rinsing with PBS the slides were ready for use.

Fluorescence microscopy:

The samples prepared as described above were mounted face up under a 200 μl PBS droplet on a object carrier on a fluorescence microscope (Olympus IX 71) and observed with a 10x objective. The images were recorded with a CCD camera (Photometrics CoolSnap HQ). To change the pH the samples were removed and rinsed under a buffer with the desired pH and placed again on the microscope under a 200 μl droplet of a buffer with the desired pH.

Chemical Oscillations:

The continuous stirred tank reactor consisted of two reservoirs, a reactor and two pumps (Minipuls 2, Gilson, Bad Camberg, Germany and XXS-EL20 E, thin xxs GmbH, Germany). Initially the cubic reactor contained 20 ml of Milipore water. One reservoir contained 19 mM NaIO_3 . The other reservoir contained 30 mM Na_2SO_3 , 21 mM $\text{Na}_2\text{S}_2\text{O}_3$, and 5 mM H_2SO_4 . Both solutions were pumped at $150 \mu\text{l}/\text{min}$ into the reactor while the a second pump removed the excess volume at a speed of $300 \mu\text{l}/\text{min}$. The reaction solution was constantly stirred at 150 rpm. After approximately 4 h the pH oscillation started and the glass-slide with the immobilized DNA strands were glued with silica-glu inside the reactor with the DNA facing the solution.

Energy transfer measurements:

For detection a modified fluorescence spectrometer (Jobin Yvon Fluorolog 3) was used: A 50/50 beam splitter was placed at the site normally used for the cuvette, guiding the excitation light (480 nm) through an objective (Leitz H32x/NA=0.60, WD=5.7 mm) onto the sample. The emitted light was collected through the same objective and reflected into the detection unit of the spectrometer with the beam splitter. The data was recorded with the spectrometer's software. The pH-value was measured and recorded simultaneously with a pH-Electrode (Schott, Mainz, Germany).

2. Formation of the i-motif in substrate-bound oligonucleotides

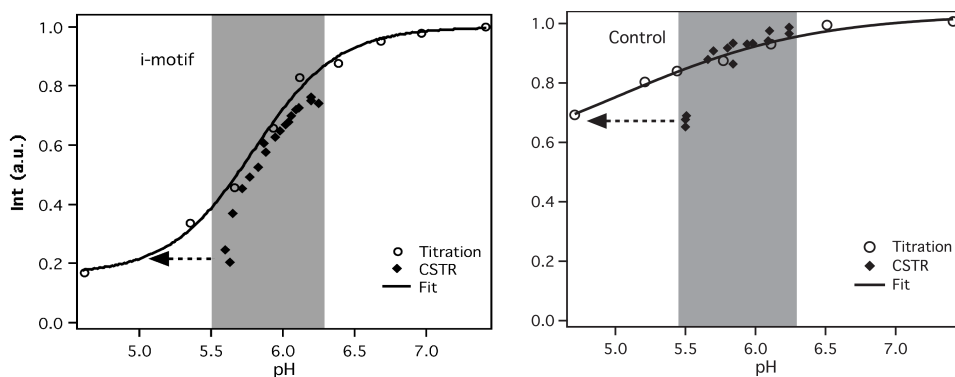


Figure 2: pH dependence of fluorescence of surface-bound labeled DNA strands. Left: The i-motif. Right: A control strand. The open symbols are data points recorded from a conventional titration while the closed symbols are directly taken from the device and control strand under the influence of the oscillator. Obviously, the behavior in the CSTR is consistent with that found in the titration experiment. The lowest fluorescence values recorded in the CSTR correspond to lower pH values than measured by the pH meter. As explained in the main text, this is due to the slowness of the response of the pH meter.

Fig. 2 shows the fluorescence of the i-motif and the control strand as a function of the pH value. Data marked with circles originate from a simple titration experiment where the pH in the solution surrounding the surface-bound DNA strands was altered by slowly adding HCl

and NaOH. The signal has been normalized to the value attained at pH 7.4. In case of the i-motif strand a strong increase of fluorescence can be observed around pH 6, whereas no such behavior is visible for the control strand. The sigmoidal shape (fit, solid line) of the curve, corresponding to strand M (the i-motif), may be explained by a cooperative transition to the other conformation, but at the same time it reflects the distance dependence of energy transfer between the dye and the gold/glass surface. The slight change in fluorescence for the control strand may reflect the protonation of adenine at low pH (adenine: $pK_a = 3.5$ and cytosine $pK_a = 4.2$), which results in an effective change of the charge of the DNA backbone which in turn reduces the electrostatic contributions to its persistence length. The same effect influences the cytosine rich i-motif, but it does not explain the sharp transition around pH 6. Data denoted by diamonds in Fig. S1 are obtained directly from a plot of the fluorescence intensity values against the pH taken from the CSTR experiments (Fig. 3 in the paper) for a few oscillation cycles. Both the i-motif and the control strand show the same pH dependence when driven by the pH oscillator as in the simple titration experiment. A few of these data points are “too low” when compared to the titration curve. As is argued in the paper, the pH values corresponding to these fluorescence intensities are actually lower than recorded by the pH-meter whose response time is too large to resolve the low pH spikes exhibited by the oscillator. These low pH spikes could be monitored, however, using the pH sensitive dye methyl orange which changes its color from yellow to pink between pH 4.4 and pH 3. This finding is also in agreement with the measurements of Rabai and Beck. Although the pH-dependence of Rhodamine Green is stated to be stable between pH 4 and pH 9, there is an effect on the fluorescence intensity of this dye below pH 4, which augments the uncertainty of the fluorescence data obtained for the low pH spikes.

To further confirm the formation of the i-motif by the surface-bound DNA strands M, temperature-dependent measurements were performed. A cuvette was filled with phosphate buffer (pH 5.8, 135 mM NaCl, 2.7 mM KCl), and 1 μ M of DNA in case of the bulk measurements. The pH value of 5.8 was chosen near the transition point of the i-motif and was not altered during the experiments. When heating the cuvette a sharp increase in fluorescence is observed at $T = 37^\circ\text{C}$ for the i-motif bound to the surface, while the control strand does not show any change in fluorescence under the same conditions (Fig. 4 in the paper). A DNA strand with the same sequence as the i-motif, but modified with a dye and a quencher on both ends shows a strong increase in fluorescence at slightly higher temperatures in a bulk experiment, whereas the fluorescence signal originating from an equally modified control strand does not change significantly. This is in agreement with previous circular dichroism measurements on the i-motif (G. Manzini, N. Yathindra, L. E. Xodo, *Nucleic Acids Research*, 1994, 22, 4634-4640).

For the energy transfer efficiency between a fluorescent dye and a gold surface, the distance dependence

$$E_T = \frac{1}{1 + (r/r_0)^4} \quad (1)$$

is expected. If one assumes energy transfer between dye and metal according to Yun et al. (Ref. 7c in the paper), the characteristic length r_0 is given by

$$r_0 = \left(\frac{0.525 c^3 \Phi_D}{\omega^2 \omega_F k_F} \right)^{1/4}, \quad (2)$$

where ω_F and k_F are Fermi frequency and wavenumber of the metal, Φ_D and ω are the quantum efficiency and the fluorescence emission frequency of the dye, respectively. This

length is on the order of 9 – 10 nm in our case. Due to a number of uncertainties, however, it is not easy to quantify the fluorescence data obtained in the experiments. A simple estimate would be that the distance between the fluorescent dye to the gold surface changes from roughly 0 – 1 nm in the folded state to roughly 5 nm (the end-to-end distance for a random coil of single-stranded DNA with 22 nt) in the relaxed state. The latter distance may be considerably smaller, when the DNA strands make an angle with the surface, or larger when they are stretched, e.g., due to mutual repulsion.

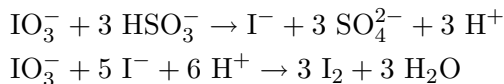
Addition of the complementary strand increased the fluorescence signal in the case of the control strand but reproducibly decreased the signal for the i-motif at pH 8. Whereas the increased fluorescence for the control strand is easily explained by a stretching of the DNA due to duplex formation, and hence a larger distance of the fluorophore from the gold surface, it is not straightforward to explain the decrease in fluorescence for the i-motif strand. It is conceivable that due to the repetitive sequence of the i-motif strand the DNA molecules are crosslinked by the complementary strands, resulting in a reduced effective distance of the fluorophores to the surface. By the addition of a denaturing 8M solution of urea to the sample, the complementary strands can be removed and the fluorescence of both the i-motif and the control strand return to their original value.

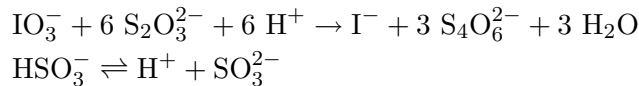
3. pH dependence of fluorescence

Several effects influence the fluorescence recorded in our system: First of all, the dye Rhodamine Green is known to be pH insensitive between pH 4 and pH 9. Most of the time our system oscillates in this range but for fractions of a second the pH drops below pH 4 (compare text in paper) which makes an interpretation of fluorescence data obtained during these time intervals difficult. Another effect is the influence of the nucleobases on the fluorescence of a dye attached to a DNA strand (cf. C. A. M. Seidel et al., *J. Phys. Chem.*, 1996, 100, pp. 5541-5553). The fluorescence intensity of a dye can be altered by photo-induced electron transfer which is dependent on the redox potential of the bases. This in turn is dependent on the pH value. As mentioned in the previous paragraph, protonation of one of the bases (adenine or cytosine) will also lead to a reduction of the overall charge of the oligonucleotides which will result in a reduced mean end-to-end distance. All these effects may in parts be responsible for the change in fluorescence of the control and the i-motif system, but they cannot account for the conformational transition of our device around pH 6 (Fig. S 2) and around 37°C (Fig. 4 in the paper). Plotting the fluorescence values obtained from the immobilized device and control strands under the influence of the oscillator (filled symbols in Fig. S2) show that the recorded fluorescence variations are consistent with the i-motif transition in the case of the device strand and with no such transition in the case of the control strand.

4. Modeling of the oscillatory reaction

For the oscillatory reaction, a solution of sodium iodate and a solution of sodium sulfite, sodium thiosulfite and sulfuric acid are continuously added to a reactor. The excess volume is removed at the same rate as it is pumped in. The dominant reactions taking place in the reactor are:





To model the pH oscillator we used the empirical kinetic model from the publications by Rabai and Beck (J. Phys. Chem. 92, 2804-2807 (1988); J. Phys. Chem. 92, 4831-4835 (1988)) for the Continuous stirred tank reactor (CSTR). With the abbreviations $j = [\text{IO}_3^-] \times \text{M}^{-1}$; $y = [\text{HSO}_3^-] \times \text{M}^{-1}$; $s = [\text{SO}_3^{2-}] \times \text{M}^{-1}$; $t = [\text{S}_2\text{O}_3^{2-}] \times \text{M}^{-1}$; $h = [\text{H}^+] \times \text{M}^{-1}$ the rate equations read:

$$\begin{aligned} v_1 &= k_{1a}jyh + k_{1b}jy^2 + k_cjyth^2 \\ v_2 &= k_2y \\ v_{-2} &= k_{-2}sh \\ v_3 &= \frac{k_3jt^2h^2}{1 + k_iy} \end{aligned}$$

$$\begin{aligned} \frac{d}{dt} j &= -v_1 - v_3 + k_0(j_0 - j) \\ \frac{d}{dt} y &= -3v_1 - v_2 + v_{-2} - k_0y \\ \frac{d}{dt} s &= v_2 - v_{-2} + k_0(s_0 - s) \\ \frac{d}{dt} t &= -6v_3 + k_0(t_0 - t) \\ \frac{d}{dt} h &= 3v_1 - 6v_2 + v_2 - v_{-2} + k_0(h_0 - h) \end{aligned}$$

$k_0 = 1.3 \times 10^{-3} \text{ s}^{-1}$ denotes the pump speed divided by the volume of the reactor. The other rate constants were chosen as follows: $k_{1a} = 8.8 \times 10^3 \text{ s}^{-1}$; $k_{1b} = 18 \text{ s}^{-1}$; $k_c = 1 \times 10^{11} \text{ s}^{-1}$; $k_2 = 30 \times 10^3 \text{ s}^{-1}$; $k_{-2} = 5 \times 10^{10} \text{ s}^{-1}$; $k_3 = 3.4 \times 10^{12} \text{ s}^{-1}$; $k_i = 5 \times 10^4$. The inhibitory constant k_i is dimensionless. For the calculation for Fig. 3 in the paper and Fig. S3, the following initial conditions were chosen: $j(0) = 0$; $y(0) = 0$; $s(0) = 0$; $t(0) = 0$; $h(0) = 1 \times 10^{-7}$. The concentrations in the added reaction solution were $j_0 = 0.019$; $s_0 = 0.03$; $t_0 = 0.02$; $h_0 = 0.008$.

In the experiment, the reactor initially only contained water, the volume was 20 ml and was kept constant all over the time. The flow rate was 150 $\mu\text{l}/\text{min}$ for both inlet tubes and 300 $\mu\text{l}/\text{min}$ for the outlet tube. The values for the calculation are therefore close to the experimental conditions, albeit not identical. The very regular oscillations observed in the experiments can be well reproduced by this system of rate equations. Plugging in the pH dependence of the fluorescence of the DNA switches (from Fig. S1), one can plot the expected fluorescence curves (see Fig. 3 in the paper and Fig. S3). The rate equations were implemented and solved with a MATLAB (The MathWorks, Natick, MA) program on a personal computer.

DOI: 10.1002/sml.200500108

Fluorescent Nanocrystals as Colloidal Probes in Complex Fluids Measured by Fluorescence Correlation Spectroscopy

Tim Liedl, Simon Keller, Friedrich C. Simmel, Joachim O. Rädler, and Wolfgang J. Parak*

The diffusion properties of fluorescent colloidal CdSe and CdSe/ZnS nanocrystals (QDs) with different hydrophilic coatings were characterized in complex fluids such as actin solutions using fluorescence correlation spectroscopy (FCS). The hydrodynamic radii of the QDs were determined both in organic solvents and water. Attention was given to the potential artifacts arising from the fluorescence properties of the QDs. With increasing excitation intensities, the apparent particle concentration and diffusion times are overestimated if using a simple diffusion model. This can be explained by a numerical simulation. The diffusion behavior of QDs in actin networks of different concentrations was determined to demonstrate the potential use of nanocrystals as probes in soft biological matter. The decreasing diffusion coefficient of the nanocrystals with increasing actin concentration results in an intrinsic polymer viscosity of $0.12 \pm 0.02 \text{ ml mg}^{-1}$, in accordance with literature values.

Keywords:

- actin
- diffusion
- fluorescence
- nanocrystals
- semiconductors

1. Introduction

Fluorescent colloidal semiconductor nanocrystals — so-called quantum dots (QDs) — are unique nanoscale probes for the investigation of biological matter. Their fluorescence properties, such as high quantum yield and reduced photobleaching, make them ideal for applications in which high sensitivity and long observation times are required. Another advantage is that due to their nanoscale size they are suited for addressing specific biophysical questions, such as the local viscous properties of biopolymer networks. For example, in migrating cells actin networks are continuously assembled underneath the plasma membrane by polymerization and depolymerized towards the cell interior. The

actin concentration and the degree of its polymerization therefore vary widely throughout the cell. The degree of polymerization of such a complex network is reflected in its local viscous properties. The typical size scales involved are given by the diameter of the monomers (which is 6 nm in the case of actin) and the mesh size of the network (several 100 nm). Hence, a fluorescent probe for the local viscous properties of the network has to be sensitive on this nanometer scale. One strategy for local viscosity studies is to measure the diffusion constant of small particles within the polymer matrix, since the diffusion of the particles is influenced by the viscosity of the network. The size of the particles has to be large enough to probe the polymer network efficiently and it has to be small enough to fit through its pores. In the case of the actin network of cells, the diameter of the particles should be in the nanometer range.

In this work we describe how the diffusion coefficient of colloidal fluorescent nanoparticles embedded in polymer networks can be measured using fluorescence correlation

[*] T. Liedl, Dr. S. Keller, Dr. F. C. Simmel, Prof. J. O. Rädler, Dr. W. J. Parak
LMU München, Department für Physik
Amalienstrasse 54, 80799 München (Germany)
Fax: (+49) 89-2180-2050
E-mail: wolfgang.parak@physik.uni-muenchen.de

spectroscopy (FCS). The aim of this study is threefold. First, we describe how the diffusion coefficient of fluorescent colloidal nanoparticles dissolved in standard solvents, and thus their hydrodynamic radius, can be determined with FCS. Second, we discuss how fluorescence saturation effects for high illumination powers have to be taken into account in the interpretation of the FCS data. Finally, the colloidal nanoparticles are studied in actin networks and it is shown how the local actin concentration can be measured.

2. Results and Discussion

2.1. Theory of Fluorescence Correlation Spectroscopy

In fluorescence correlation spectroscopy (FCS) intensity fluctuations of fluorescent particles within a small volume of around $1 \mu\text{m}^3$ are recorded. The temporal autocorrelation function of these fluctuations is related to the diffusion properties of the fluorescing particles. The principle of FCS was invented and realized in the early 1970s by Magde, Elson, and Webb.^[1–3] As there are several good reviews in the literature we will give only a short introduction into the subject.^[4–6] The raw signal in a FCS experiment is the time-dependent fluorescence intensity signal $F(t)$ coming from a small and fixed volume element usually created by a laser focus of sub-micrometer waist size and detected with a confocal setup. In the ideal case the generated fluorescence intensity is proportional to the excitation intensity of the focused laser and the observation volume can then be approximated by a three-dimensional (3D) Gaussian ellipsoid with radius r_0 and height z_0 .^[7] Fluctuations in this signal are analyzed by using the normalized temporal autocorrelation function (ACF) $G(\tau)$:

$$G(\tau) = \frac{\langle F(t) \cdot F(t + \tau) \rangle_t}{\langle F(t) \rangle_t^2} \quad (1)$$

In the case of freely diffusing particles the autocorrelation can be written as:^[4]

$$G(\tau) = \frac{1}{N} \cdot G_{\text{Diff}}(\tau) \quad (2)$$

with

$$G(\tau) = \frac{1}{1 + \frac{\tau}{\tau_D}} \cdot \frac{1}{\sqrt{1 + \frac{r_0^2}{z_0^2} \frac{\tau}{\tau_D}}} \quad (3)$$

Here N denotes the mean number of particles present in the observation volume. The diffusion time τ depends on the size of the observation volume and the diffusion coefficient D :

$$\tau = \frac{r_0^2}{4D} \quad (4)$$

Equation (3) represents the ideal situation of a single monodisperse species of diffusing particles. In a system with two fractions of different sizes the correlation function is the weighted sum of the two observed fractions:

$$G_{\text{Diff}}(\tau) = a \cdot G_{\text{Diff},1}(\tau) + (1 - a) \cdot G_{\text{Diff},2}(\tau) \quad (5)$$

The functions $G_{\text{Diff},i}(\tau)$ represent the autocorrelation resulting from the diffusion of fraction i with the diffusion time τ_i . The weighting factor a depends on both the relative concentrations and the brightness of the fractions. FCS is not only sensitive to intensity fluctuations caused by diffusion but also to photokinetic processes within the fluorescent particles. Changes in the brightness of the diffusing particle can be detected with FCS as long as they occur on a significantly faster timescale than the diffusion time. The most prominent and well-known process is the triplet decay of organic fluorophores, which results in an exponential decay of the autocorrelation function in the microsecond time range.^[8] In the following sections we discuss the unique properties of QDs.

2.2. Fluorescent Colloidal Nanocrystals as Fluorescent Probes for FCS

Fluorescent colloidal nanocrystals, such as CdSe or CdSe/ZnS quantum dots possess a broad absorption band in the UV region and a sharp emission band in all desirable colors between the blue and the near infrared; the color of emission is tunable by the size of the nanocrystals. Furthermore, colloidal QDs show a reduced tendency to photobleach.^[9,10] Due to the process used for the particle synthesis in this study the colloidal QDs originally have a hydrophobic surface and are only soluble in nonpolar solvents (e.g., chloroform or toluene). In biological applications an aqueous environment is desired, therefore the surface of the particles has to be rendered hydrophilic. To this end, different techniques can be applied, resulting in water-soluble colloidal nanoparticles with the same color of fluorescence but with different surface coatings.^[9] The small overall size of less than 20 nm of these water-soluble particles allows for a range of applications in the life sciences.^[10]

Fluorescent nanocrystals have been previously shown to be suitable probes for FCS measurements.^[11–13] However, standard FCS theory used for organic fluorophores has to be modified for colloidal nanocrystals to account for some of the specific properties of these particles. QDs exhibit no triplet behavior, but show blinking on all timescales from nanoseconds to seconds. The distribution of blinking times follows a power law.^[14,15] As for organic fluorophores, the fluorescence decay time of QDs of a few nanoseconds is too fast to be detected in a FCS measurement. As until now no analytical expression to fit FCS data obtained from fluorescent nanocrystals could be derived, we fitted the curves with a simple FCS model that only takes diffusion into account [Eq. (3)]. This fit procedure yielded satisfactory results for our purposes. In a recent publication, Doose et al. approached this problem using Monte Carlo simulations that include diffusion and power law on/off statistics to elucidate the effects of QD blinking on FCS.^[12] To extract diffusion times, these authors also used a simple diffusion model. The present work extends a previous report by our group in which

the peculiarities of QD photophysics had not been taken into account.^[13]

A fit to the experimental autocorrelation function $G(\tau)$ (obtained from the FCS raw data $F(t)$ via Equation (1)) using Equations (2), (3), and (4) yields the diffusion constant D of the particles. Since QDs are spherical, from knowledge of D the hydrodynamic radius r_h of the particles can be determined using the Stokes–Einstein relation:

$$r_h = \frac{kT}{6\pi\eta D} \quad (6)$$

where kT is the thermal energy and η denotes the viscosity of the surrounding fluid.

2.3. Materials and Methods

We used a commercial FCS setup by Carl Zeiss (Jena, Germany) consisting of a ConfoCor2 module^[16] and an Axiovert200 microscope with a Zeiss C-Apochromat (40 \times , NA 1.2) water immersion objective. The 488 nm line of an Ar ion laser and the 633 nm line of a HeNe laser were used for excitation. The maximum laser power corresponded to an illumination intensity of 2.91 mW at 488 nm and 1.42 mW at 633 nm. The emitted light was split up by a 50/50 mirror and fed into two identical independent detection channels with 505-nm-long pass filters and pinholes with a 70 μ m diameter. The intensities from the two avalanche photodiodes were cross-correlated. Artifacts like detector after-pulsing or other detection noise do not occur in the cross-correlation function.

For calibration of the sample volume (i.e., to determine the parameters r_0 and z_0) the dyes Alexa488 ($D = 316 \mu\text{m}^2\text{s}^{-1}$, Molecular Probes) and Cy5 ($D = 250 \mu\text{m}^2\text{s}^{-1}$, Amersham Biosciences) were used as fluorescent particles. For all measurements r_0 was found to be between 180 and 190 nm. The ratio z_0/r_0 was always between 7 and 8.

A customized teflon block with drilled holes of 7 mm diameter was used for the measurements of the fluorescent colloidal particles diluted in chloroform. A cover slide (thickness: 150 μ m) was glued to the bottom of the block with silica grease. Due to the different refraction indices of chloroform ($n_{\text{Cl}} = 1.445$ at 20 $^\circ\text{C}$) and water ($n_{\text{water}} = 1.33$ at 20 $^\circ\text{C}$), the radius of the focus in chloroform (r_{Cl}) changes. We assume that the focus radius is diffraction limited and the product of focus radius and refractive index is constant. Thus the focus radius r_{Cl} is given by $r_{\text{Cl}} = r_{\text{water}} \cdot n_{\text{water}} / n_{\text{Cl}}$. This is a rough approximation which does not consider various other aberrations studied in detail by others.^[17,18] The characteristic diffusion time varies quadratically with $n_{\text{water}}/n_{\text{Cl}}$ (see [Eq. (4)]). The measurements in water and actin were performed using conventional coverslip chambers (Nunc, Wiesbaden, Germany). Each sample was illuminated 10 times in a row for 20 s each with the appropriate laser. The recorded signals were averaged for each sample. The standard deviation was obtained by averaging the measurements of different sets. Each sample was measured at least three times.

Two batches of hydrophobic CdSe nanocrystals capped with trioctylphosphine oxide (TOPO) and dissolved in chloroform were used in this study,^[19] one having its first absorption maximum at 507 nm, the other one at 635 nm. In a first modification step, a shell of ZnS was grown around the CdSe cores yielding TOPO-capped CdSe/ZnS nanocrystals dissolved in chloroform.^[20] Due to shell growth, the first absorption maximum is slightly red-shifted (from 507 nm to 528 nm and from 635 nm to 645 nm for the green and red fluorescent nanoparticles, respectively). To transfer the nanocrystals into water they were capped with three different kinds of hydrophilic shells (for a detailed description see ref. [21]). The simplest modification strategy is to exchange the hydrophobic surfactant molecules covering the CdSe/ZnS nanocrystals with molecules bearing a reactive thiol group on one end and a hydrophilic group on the other end. Here mercaptopropionic acid (MPA) was used. Another possibility is to grow a silane shell around the crystal. Polyethylene glycol chains pointing out of the silane shell prevent agglomeration of the particles by steric repulsion. The third applied technique uses amphiphilic polymers. The hydrophobic ends of the polymer intercalate with the hydrophobic chains covering the ZnS shell, whereas the hydrophilic ends point outwards. To enhance stability, the polymers were crosslinked with bis(6-aminoethyl)amine. In total, we prepared green and red fluorescent nanoparticles with five different modifications for each color: CdSe and CdSe/ZnS particles with a TOPO coating dissolved in chloroform and CdSe/ZnS particles with mercaptopropionic acid (MPA), silica, and polymer coating dissolved in aqueous solution.^[13] With each resulting sample FCS measurements were performed.

Actin is a protein of the cytoskeleton and exists in a monomeric and a polymerized form: the globular actin monomer (G-actin, $M_w = 42$ kDa) polymerizes into long filaments (F-actin) and dense networks. Monomeric G-actin from rabbit muscle was a kind gift from the group of M. Bärmann (Physics Department E22, TU München, Germany). The sample was concentrated by centrifugation in G-buffer (2 mM Tris/HCl (pH 7.4), 0.5 mM ATP, 0.2 mM CaCl_2 , 0.2 mM dithiothreitol, and 0.2% NaN_3) to 4.55 mgml^{-1} . Polymerization was initiated by the addition of 10 vol. % of 10x F-buffer (G-buffer + 2 mM MgCl_2 and 100 mM KCl). After 20 min phalloidin (Molecular Probes, Eugene, OR, USA, P-3457) (phalloidin/G-actin = 1:4) was added to stabilize the filaments. These filaments could now be diluted in F-buffer without depolymerization.

2.4. Hydrodynamic Radii of Fluorescent Colloidal Nanocrystals Determined by FCS

The experimental data obtained for nanocrystals modified with different surface coatings are shown in Figures 1 and 2. The corresponding hydrodynamic radii are shown in Table 1. For the TOPO-capped CdSe nanocrystals dissolved in chloroform we obtained a hydrodynamic radius of 1.8 ± 0.7 nm and 4.2 ± 1.3 nm, respectively. After growing a layer of ZnS around the CdSe particles,^[20] the radius increases to

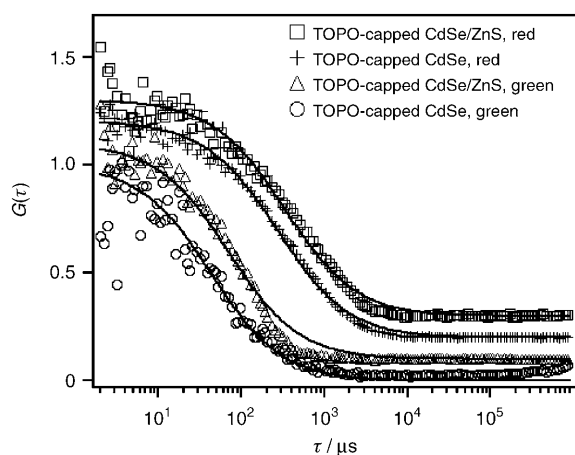


Figure 1. The autocorrelation functions of TOPO-capped green and red fluorescent CdSe and CdSe/ZnS nanocrystals and the respective fits with Equations (2) and (3) (solid lines). The fit parameters are τ and N . The offset between the individual curves for presentational purposes is 0.1. The measurements were performed in chloroform ($n=0.57$ mPa s).

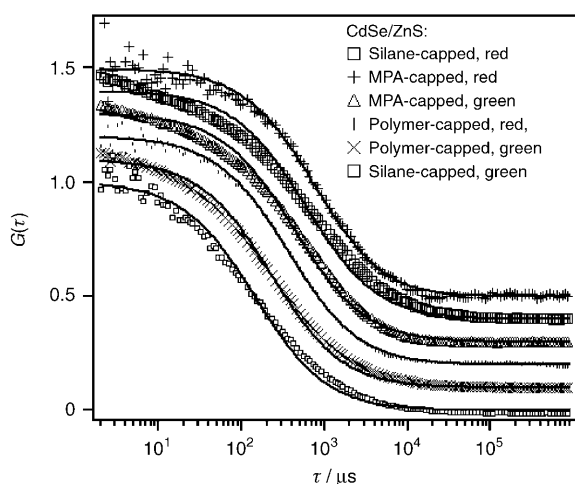


Figure 2. The autocorrelation function of green and red fluorescent CdSe/ZnS nanocrystals capped with different hydrophilic shells and the respective fits with Equations (2) and (3) (solid lines). The offset between the individual curves for presentational purposes is 0.1. The measurements were performed in water ($n=0.98$ mPa s).

2.8 ± 0.8 nm and 5.7 ± 2.3 nm. These results match well with the radii of CdSe and CdSe/ZnS nanocrystals obtained from transmission electron microscopy (TEM).^[22] It should be noted that due to a lack of contrast of the surface coating, TEM is only sensitive to the inorganic core and inorganic shell of the nanoparticles and thus the radii obtained by TEM describes the hard core radii of the CdSe and CdSe/ZnS particles. FCS on the other hand detects the effective hydrodynamic radius and thus also the surface coating around the inorganic cores (i.e., the TOPO molecules bound to the surface of the CdSe and CdSe/ZnS particles). The hydrodynamic radii of the particles in aqueous solution are larger than for those dissolved in chloroform. Apart from an increased thickness in the surface coating, interac-

Table 1. Hydrodynamic radii of fluorescent CdSe nanocrystals with various capping groups. The error is the standard deviation derived from different measurements.

NCs (Emission: 535 nm)	r_h [nm]	Error [nm]
TOPO-capped CdSe ^[a]	1.8	0.7
TOPO-capped CdSe/ZnS ^[a]	2.8	0.8
Polymer-capped CdSe/ZnS ^[b]	5.5	1.3
Silane-capped CdSe/ZnS ^[b]	5.2	1.9
MPA-capped CdSe/ZnS ^[b]	11.2	1.3
NCs (Emission: 645 nm)		
TOPO-capped CdSe ^[a]	4.2	1.3
TOPO-capped CdSe/ZnS ^[a]	5.7	2.3
Polymer-capped CdSe/ZnS ^[b]	10.8	1.4
Silane-capped CdSe/ZnS ^[b]	18.1	4.8
MPA-capped CdSe/ZnS ^[b]	12.9	1.6

[a] In chloroform ($n=0.57$ mPa s, 20°C) [b] In water ($n=0.98$ mPa s, 20°C).

tions between water and the particle surface are assumed to be responsible for this effect. Also a tendency of incompletely capped particles to agglomerate to small particle clusters might lead to an increase in the determined mean effective hydrodynamic radius.

In a previous study,^[13] we have determined the hydrodynamic radii of the same TOPO-capped CdSe/ZnS and polymer-capped CdSe/ZnS nanoparticles dissolved in chloroform and water, respectively, but with a fit function for $G(\tau)$ containing a triplet term. This procedure led to larger hydrodynamic radii as compared to those determined in the present study using Equations (2) and (3). As discussed above, QDs in fact do not display a triplet-like behavior and therefore only a simple diffusion model was applied. The results of Table 1 demonstrate that colloidal CdSe and CdSe/ZnS are appropriate probes for FCS measurements with hydrodynamic radii on the order of 10 nm. However, another potential pitfall has to be considered in the interpretation of the data, as discussed below.

2.5. Blinking and Saturation Effects

Artifacts of FCS due to blinking and optical saturation have been studied before for the case of organic dyes.^[23–25] Similar effects have been observed for inorganic QDs by Doose et al.^[12] and by our group, but the interpretation of the influence of blinking has to be modified in this case. For high laser intensities, the autocorrelation data cannot be fitted with the same quality as for low laser intensities. This was investigated experimentally with green fluorescent nanocrystals with a silane shell, by tuning the laser intensity from 0.1% to 100%, corresponding to a laser intensity of 2.91 μ W to 2.91 mW in the sample volume. As can be seen in Figure 3, the overall shape of experimentally obtained ACFs markedly changes with increasing excitation intensity. This is due mainly to two factors:

1) With increasing laser intensity the blinking behavior gains influence, which can be observed in a steepening of the curves in the range of 1 μ s to 10 μ s and a flattening of

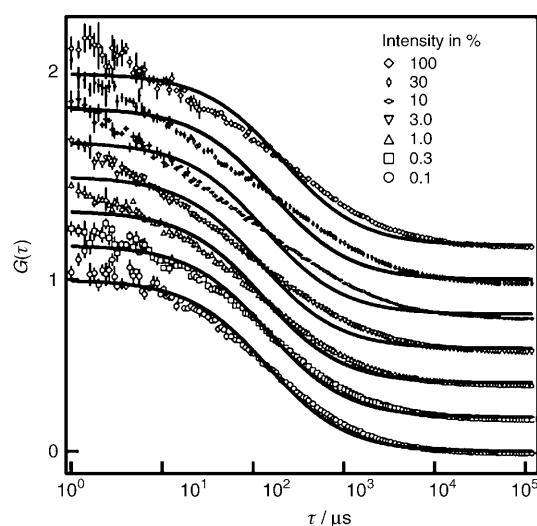


Figure 3. Correlation functions of silane-capped CdSe/ZnS nanocrystals (Emission: 535 nm) for different laser intensities. Solid lines are fits with the ideal model in Equation (3). The offset between the individual curves for presentational purposes is 0.1. The measurements were performed in water ($n=0.98$ mPa).

the whole curve. Doose et al. found similar behavior for peptide-coated NCs (CdSe/ZnS and CdSe/CdS/ZnS), for lipid-coated CdSe/ZnS NCs, and for commercially available polymer-coated NCs (Quantum Dot Corp).^[12]

2) With increasing laser intensity the assumption of a Gaussian-shaped observation volume is not valid any more. This can be understood as follows: If one assumes that the emission of each fluorescent particle saturates above a certain laser intensity, the emitted fluorescence is no longer proportional to the excitation intensity. In this case the assumption of a Gaussian-shaped observation volume is wrong. Saturation leads to a flattening of the effective intensity profile in the center of the observation volume.^[24] Qualitative statements about two immediate observables in the resulting correlation functions can be made: a) The recorded fluorescence signal $F(t)$ has a smaller variance than in the ideal case. This leads to systematically smaller amplitudes $G(0)$ of the correlation functions. The number of particles $N = \frac{1}{G(0)}$ is overestimated; b) the flattening of the effective intensity profile leads to an enlarged virtual observation volume. As a consequence, the correlation times increase and result in underestimated diffusion constants.

To test this hypothesis the experimental data were compared with simulated data (Figure 4). Saturation effects were simulated by a fluorescent particle performing a random walk through a detection volume with a cut-off Gaussian profile using the script language IDL. At low intensities the particle ‘sees’ a Gaussian excitation profile. Above a certain laser intensity, which is determined in the experiment, saturation sets in and the Gaussian profile starts to be cut off. For elevated laser intensities the Gaussian profile is increasingly cut off, which results in an almost rectangular shape of the excitation profile at the highest laser intensities. This simulation already yields good agreement with the measured diffusion times. The simulated

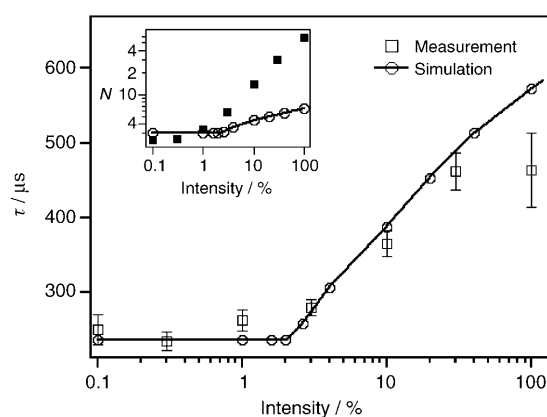


Figure 4. Due to saturation effects the measured diffusion time τ_D and number of particles N (inset) increases with increasing illumination laser intensity. Squares: experimentally obtained data from Figure 3; Line: simulation.

number of particles N , however, only qualitatively shows the same behavior as the measured data. There is a discrepancy between the absolute calculated values and the experimentally obtained data, which we are not able to explain. From the comparison of experiment and simulation, the saturation threshold, that is, the laser intensity at which the saturation effects set in, was determined to be 2% of the laser intensity. This corresponds to a laser intensity of 58.2 μW in the sample volume. Our simple model explains saturation effects already at low excitation energies and continuous wave excitation, as discussed by Gregor et al. in greater detail.^[25] For the subsequent measurements in actin networks the laser intensity was fixed at 1% to ensure that saturation effects can be neglected.

2.6. Diffusion In Concentrated Actin Networks

To demonstrate the potential of hydrophilic nanocrystals as probes for complex fluids, we determined diffusion times of green-fluorescent QDs coated with a silane shell in networks of polymerized actin (Figure 5). The mesh size ξ of actin networks (as a function of the actin concentration c_{actin}) is given by the empirical formula:^[26]

$$\xi = 0.34 \cdot \left(\frac{c_{\text{actin}}}{1 \text{ mg ml}^{-1}} \right)^{-1/2} \mu\text{m} \quad (7)$$

Autofluorescence of polymerized actin networks causes an experimental hurdle, since it could not be cut out by filters or by using particles of other emission wavelengths. However, the signal of the autofluorescence can be correlated with an intrinsic diffusion time and was measured separately each time before adding the nanocrystals according to Equation (5).

$$G(\tau) = 1 + \frac{1}{N} \cdot [a \cdot G_{\text{actin}}(\tau) + (1 - a) \cdot G_{\text{QD}}(\tau)] \quad (8)$$

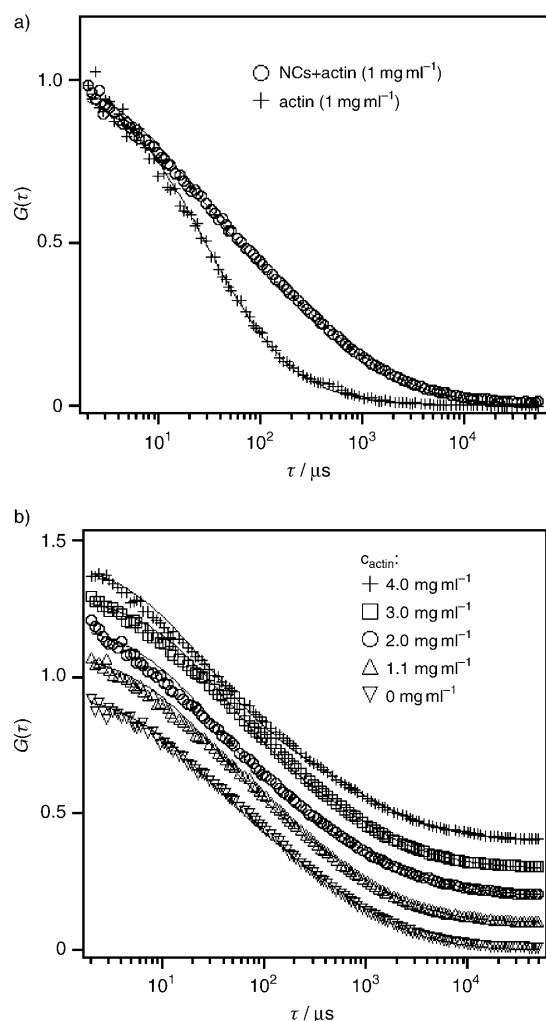


Figure 5. Autocorrelation function of silane-capped CdSe/ZnS nanocrystals (E_m : 535 nm) in polymerized actin networks. a) Measurements in a solution of F-actin with and without nanocrystals. Solid lines are fits; b) autocorrelation functions for different actin concentrations. Solid lines are fits with two fractions according to Equation (8). The diffusion time of the fast fraction was determined by previous measurements of the pure actin solution and then kept fixed. The offset between the individual curves for presentational purposes is 0.1.

The diffusion of colloidal particles in polymer solutions has been investigated in numerous polymeric systems. For particles with radii smaller than the mesh size of the polymer solution, $r_h < \xi$, the particles feel a viscosity that increases linearly with the polymer concentration c_p :^[27–29]

$$\eta_p = \eta_0(1 + \eta_{int} \cdot c_p) \quad (9)$$

where η_0 denotes the solvent viscosity and η_{int} the intrinsic viscosity of the polymer in solution. Using the Stokes–Einstein relation (Equation (6)), Equation (9) can be written as:

$$\frac{D_t}{D_0} = 1 - \eta_{int} \cdot c_{actin} \quad (10)$$

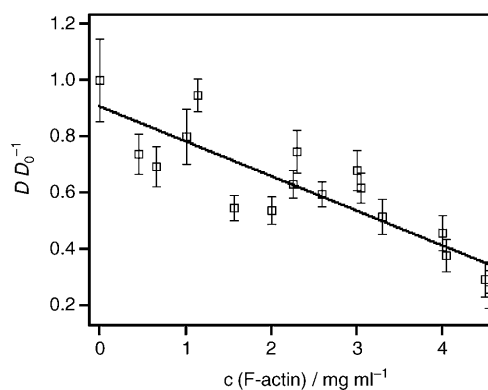


Figure 6. The normalized diffusion constant of water-soluble nanocrystals decreases with rising concentration of actin. The fitted line (Equation (10)) yields to an intrinsic viscosity of actin of $0.12 \pm 0.02 \text{ ml mg}^{-1}$. According to Equation (7), 1 mg ml^{-1} and 4.5 mg ml^{-1} corresponds to a mesh size of 340 nm and 160 nm, respectively.

The fit in Figure 6 yields an intrinsic viscosity for polymerized actin solutions of $\eta_{int} = 0.12 \pm 0.02 \text{ ml mg}^{-1}$. For comparison, Schmidt et al. measured values between 0.08 and 0.9 ml mg^{-1} with beads of diameters between 100 and 250 nm.^[26] Anomalous diffusion in actin has already been described for beads of comparable or even larger diameters than the mesh sizes of the actin network.^[30,31] Possible reasons for anomalous diffusion are obstacles^[32] or binding.^[33] The potential of FCS to characterize anomalous diffusion behavior has been shown before.^[29,34–36] The colloidal nanocrystals used in this study have a diameter of around 20 nm and are therefore considerably smaller than the resulting mesh size (160 nm), even at high concentrations of actin (4.5 mg ml^{-1}).

We tested the data for signatures of anomalous diffusion, for which the mean-square displacement of the particles is no longer proportional to time, but scales as $\langle \chi^2 \rangle \propto t^\beta$.^[29,36] Fits of this expression to the data yielded anomalous diffusion parameters β between 0.9 and 1.1. A value of $\beta = 1$ accounts for normal diffusion behavior, hence our data is consistent with normal diffusion rather than anomalous diffusion.

3. Conclusion

In summary, we used fluorescence correlation spectroscopy to characterize the hydrodynamic radius of fluorescent colloidal nanocrystals with various coatings, in both organic solvent and in an aqueous environment. The nanocrystals were used as probes for the viscosity of complex fluids such as actin networks. For data analysis, various artifacts that can systematically influence the results of FCS measurements were taken into account. In particular, we considered the problem of saturation effects, which increase the calculated number of particles within the effective sample volume and lead to longer diffusion times. Our results here agree with the findings by Doose et al.^[12]

Due to the small size of the nanocrystals used, the viscous properties of actin networks with mesh sizes smaller than 200 nm could be determined. The measured values for the intrinsic viscosity of the networks agree well with those obtained previously using other techniques. Anomalous diffusion was not observed as it only comes into play when particle size and mesh size are comparable. Our results show that fluorescent colloidal nanoparticles are well suited for the investigation of the local viscosity of biological samples or other complex fluids using FCS.

Acknowledgements

The authors are grateful to S. Kudera and A. Muñoz Javier for assistance in the synthesis of the colloidal nanoparticles. We thank Jörg Enderlein for helpful discussions. The work was funded by the DFG (Emmy Noether Research Grants to F.C.S. and W.J.P. and SFB 486 Grant to J.O.R.).

-
- [1] D. Magde, E. Elson, W. W. Webb, *Phys. Rev. Lett.* **1972**, *29*, 705.
 [2] E. Elson, D. Magde, *Biopolymers* **1974**, *13*, 1.
 [3] D. Magde, E. Elson, W. Webb, *Biopolymers* **1974**, *13*, 29.
 [4] P. Schwille, J. Bieschke, F. Oehlenschläger, *Biophys. Chem.* **1997**, *66*, 211.
 [5] O. Krichevsky, G. Bonnet, *Rep. Prog. Phys.* **2002**, *65*, 251.
 [6] N. L. Thompson, A. M. Lieto, N. W. Allen, *Curr. Opin. Struct. Biol.* **2002**, *12*, 634.
 [7] S. Hess, W. Webb, *Biophys. J.* **2002**, *83*, 2300.
 [8] J. Widengren, U. Mets, R. Rigler, *J. Phys. Chem.* **1995**, *99*, 13368.
 [9] T. Pellegrino, S. Kudera, T. Liedl, A. Muñoz, L. Manna, W. J. Parak, *Small* **2005**, *1*, 48.
 [10] W. J. Parak, T. Pellegrino, C. Planck, *Nanotechnology* **2005**, *16*, R9.
 [11] D. R. Larson, W. R. Zipfel, R. M. Williams, S. W. Clark, M. P. Bruchez, F. W. Wise, W. W. Webb, *Science* **2003**, *300*, 1434.
 [12] S. Doose, J. M. Tsay, F. Pinaud, S. Weiss, *Anal. Chem.* **2005**, *77*, 2235.
 [13] T. Pellegrino, L. Manna, S. Kudera, T. Liedl, D. Koktysh, A. Rogach, G. Natile, S. Keller, J. Rädler, W. J. Parak, *Nano Lett.* **2004**, *4*, 703.
 [14] M. Kuno, D. P. Fromm, H. F. Hamann, A. Gallagher, D. J. Nesbitt, *J. Chem. Phys.* **2000**, *112*, 3117.
 [15] M. Kuno, D. P. Fromm, H. F. Hamann, A. Gallagher, D. J. Nesbitt, *J. Chem. Phys.* **2001**, *115*, 1028.
 [16] T. Jankowski and R. Janka, in *Fluorescence Correlation Spectroscopy*, (Eds.: R. Rigler, E. Elson), Springer, Berlin, **2001**, pp. 331–345.
 [17] P. Reiss, J. Bleuse, A. Pron, *Nano Lett.* **2002**, *2*, 781.
 [18] S. Hell, G. Reiner, C. Cremer, E. H. K. Stelzer, *J. Microsc.* **1993**, *169*, 391–405.
 [19] M. J. Booth, T. Wilson, *J. Biomed. Opt.* **2001**, *6*, 266–272.
 [20] B. O. Dabbousi, J. Rodriguez-Viejo, F. V. Mikulec, J. R. Heine, H. Mattoussi, R. Ober, K. F. Jensen, M. G. Bawendi, *J. Phys. Chem. B* **1997**, *101*, 9463.
 [21] W. J. Parak, D. Gerion, T. Pellegrino, D. Zanchet, C. Micheel, S. C. Williams, R. Boudreau, M. A. L. Gros, C. A. Larabell, A. P. Alivisatos, *Nanotechnology* **2003**, *14*, R15.
 [22] W. W. Yu, L. Qu, W. Guo, X. Peng, *Chem. Mater.* **2003**, *15*, 2854.
 [23] J. Widengren, R. Rigler, *Bioimaging* **1996**, *4*, 149.
 [24] J. Enderlein, I. Gregor, P. Digambara, J. Fitter, *Curr. Pharm. Biotechnol.* **2004**, *5*, 155.
 [25] I. Gregor, D. Patra, J. Enderlein, *ChemPhysChem* **2005**, *6*, 164.
 [26] C. F. Schmidt, M. Bärmann, G. Isenberg, E. Sackmann, *Macromolecules* **1989**, *22*, 3638.
 [27] X. Ye, P. Tong, L. J. Fetters, *Macromolecules* **1998**, *31*, 5785.
 [28] N. A. Busch, T. Kim, and V. A. Bloomfield, *Macromolecules*, **2000**, *33*, 5932.
 [29] S. Mangenot, S. Keller, J. O. Rädler, *Biophys. J.* **2003**, *85*, 1817.
 [30] F. Amblard, A. C. Maggs, B. Yurke, A. N. Pargellis, S. Leibler, *Phys. Rev. Lett.* **1996**, *77*, 4470.
 [31] I. Y. Wong, M. L. Gardel, D. R. Reichman, E. R. Weeks, M. T. Valentine, A. R. Bausch, D. A. Weitz, *Phys. Rev. Lett.* **2004**, *92*, 178101.
 [32] M. J. Saxton, *Biophys. J.* **1994**, *66*, 394.
 [33] M. J. Saxton, *Biophys. J.* **1996**, *70*, 1250.
 [34] A. Gennerich, D. Schild, *Biophys. J.* **2000**, *79*, 3294.
 [35] M. Wachsmuth, W. Waldeck, J. Langowski, *J. Mol. Biol.* **2000**, *298*, 677.
 [36] P. Schwille, J. Korfach, W. W. Webb, *Cytometry* **1999** *36*, 176.

Received: March 31, 2005
 Revised: June 2, 2005
 Published online on August 11, 2005

Controlled trapping and release of quantum dots in a DNA-switchable hydrogel

Tim Liedl, Hendrik Dietz, Bernard Yurke, Friedrich C. Simmel*

DNA-switchable structures have been under extensive investigation in DNA nanotechnology^[1], where DNA-based supramolecular assemblies are switched between mechanically distinct conformational states through hybridization with DNA “fuel” strands. Reversibility is achieved by displacing previously added fuel strands from the assembly in a branch migration process^[2]. This operation principle has been recently applied to realize a switchable polyacrylamide (PAAm) hydrogel with controllable macroscopic rheological properties^[3]. In the present study, we investigate the nanoscopic aspects of this system in detail using fluorescent semiconductor quantum dots (QDs) as probe particles. The diffusion properties of the QDs in the gel are studied using single molecule fluorescence microscopy and fluorescence correlation spectroscopy. Trapping and DNA-triggered release of the nanoparticles is directly visualized, demonstrating the potential of the DNA-switchable gel as a controlled release system with possible applications in drug delivery.

PAAm gels are usually synthesized by mixing acrylamide monomers, crosslinkers and water at a certain ratio, followed by initiation of polymerization with a catalyst. The resulting polyacrylamide chains are chemically inert and biocompatible^[4]. Numerous crosslinking agents can be used to tune the properties of PAAm gels^[5]. Using double-stranded DNA as a reversible crosslinker provides a

number of advantages: the resulting gel is biocompatible and sequence programmable; the mechanical properties and the pore size of the crosslinked gel can be adjusted by the length of the DNA crosslinker strands and the melting temperature of the gel can be controlled by the sequence and length of the DNA crosslinkers.

For the synthesis of the DNA-switchable gel, first two non-complementary Acrydite(TM)-modified oligonucleotides^[6] A and B are separately copolymerized with acrylamide (4% w/v) and thereby incorporated into the PAAm chains. Mixing of the two solutions yields a highly viscous fluid, which in our experiments is complemented with fluorescent colloidal semiconductor quantum dots as tracer particles. Fluorescent QDs are easy to track with single molecule fluorescence techniques and they are available with a wide variety of functionalizations for biomedical applications^[7].

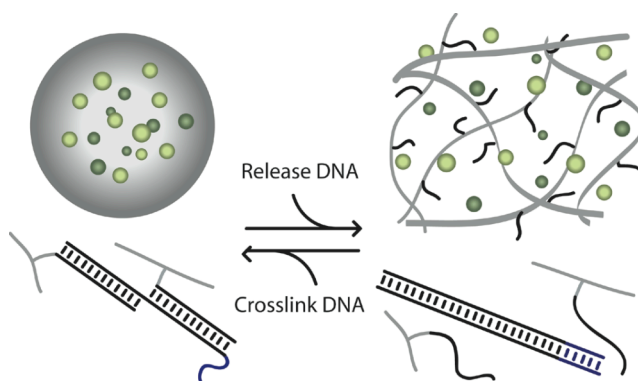


Figure 1. Operation principle of the DNA-switchable gel used for nanoparticle delivery. Water-soluble, polymer-coated nanocrystals trapped reversibly in a DNA crosslinked polyacrylamide hydrogel (left) can be liberated by unlinking the gel with DNA “release” strands. As a result, the particles can leave the unlinked gel (right), and a DNA waste duplex composed of the crosslinking and the release strand is formed. The unlinked gel can be re-organized by adding the crosslinking strand again.

Addition of gelation oligonucleotides complementary to the Acrydite strands transforms the fluid PAAm/nanoparticle mixture into a solid gel (Fig. 1), trapping the particles. The DNA crosslinker strands are equipped with an additional, unhybridized “toehold” section which acts as a “recognition tag” for DNA release strands^[2]. When release strands fully complementary to the crosslinker strands are added to the gel, they attach to the toeholds and remove the crosslinker strands via branch migration. The gel dissolves into a solution, liberating the trapped particles. For a 4% acrylamide “1 D” gel, i.e. for unlinked linear polymer strands, a typical pore size much larger than the particle diameter is expected, which is considerably reduced by the crosslinking process. The crosslinking density used in our experiments corresponds to a value of %C = 0.16 in a conventional PAAm gel crosslinked with N,N'-methylene bis(acrylamide). Compared to typical polyacrylamide gels used for gel electrophoresis, the DNA-PAAm gel is sparsely crosslinked. For a bis-crosslinked PAAm gel with the same parameters, a pore size of $r_p > 100$ nm would be expected^[8]. Nevertheless, we experimentally observe that the DNA-switchable gel is capable of controllably trapping and releasing nanoparticles with a diameter on the order of 10 nm.

[*] Dr. Tim Liedl, Dr. Friedrich C. Simmel
Department of Physics and Center for Nanoscience
Ludwig-Maximilians-Universität München
Geschwister-Scholl-Platz 1, 80539 München (Germany)
Fax: (+49)89-2180-3182
E-mail: simmel@lmu.de
Dr. Hendrik Dietz
Physik Department E22 and Center for Nanoscience
TU München
James-Franck-Straße, 85478 Garching (Germany)
Dr. Bernard Yurke
Bell Laboratories
Alcatel-Lucent
600 Mountain Ave, Murray Hill, NJ 07974 (USA)

[**] We thank R. Sperling and W. J. Parak for supply with quantum dots, T. Schubert for tracking software, J. O. Rädler, N. A. Langrana, R. A. Neher and M. Rief for helpful discussions. This work was funded by the IDK-NBT, the DFG (Emmy Noether Grant to FCS) and the Bavarian StMWFK (Neue Werkstoffe).

Supporting information for this article is available on the WWW under <http://www.small-journal.org> or from the author

To characterize the trapping and release process in detail, the diffusion behavior of our tracer particles was studied in the sol and gel states of the switchable gel. As tracer particles, we used CdSe/ZnS QDs ($\lambda_{em}=565$ nm) with a “bare” radius of roughly 6 nm. The QDs were made water soluble by a polymer coating^[9] which slightly increased their radius. As described previously^[10], the radius of the coated QDs was determined using fluorescence correlation spectroscopy (FCS). FCS measurements on free QDs in water yielded a diffusion constant of $D_{H_2O}=29 \pm 0.5 \mu\text{m}^2\text{s}^{-1}$ (Fig. 2b). Using the Stokes-Einstein (SE) equation this value can be translated into a hydrodynamic radius of the particles of 7.4 ± 0.6 nm. We then determined the diffusion properties of the QDs for the two states of the gel using both single molecule fluorescence microscopy and FCS^[10,11]. In the unlinked hydrogel matrix the diffusion constant dropped to $D_{FCS, \text{unlinked}}=6.6 \pm 0.3 \mu\text{m}^2\text{s}^{-1}$ (Fig. 2b). Again using the SE equation, one can estimate the (local^[12]) viscosity of the unlinked gel matrix to be $\eta=4.8 \pm 0.5$ mPa s. Tracking individual QDs in the unlinked gel matrix by fluorescence microscopy (Fig. 2 c,d) yields a diffusion constant of $D_{\text{Tracking, unlinked}}=6.3 \pm 0.4 \mu\text{m}^2\text{s}^{-1}$, which agrees well with the value obtained from FCS measurements. The unrestricted mobility of QDs in the unlinked gel is illustrated by collapsed fluorescence image time traces in Fig. 2a.

Addition of the gelation strand L to the PAAm-nanoparticle mixture induces crosslinking of the DNA-modified polyacrylamide strands. The impact of this process on the diffusion of the QDs is observed by fluorescence microscopy. During gelation, an increasing number of nanoparticles ceases to diffuse (Fig. 3a), they instead appear as spatially fixed fluorescent spots (Fig. 3c) that display the characteristic blinking behaviour (Fig. 3d) of single quantum dots^[13,14]. Complementary FCS measurements reveal decreasing diffusion constants and an increasing contribution of anomalous subdiffusion during gelation (Fig. 4a), i.e., the mean-square-displacement of a particle is no longer simply proportional to time, but scales as $\langle x^2 \rangle \propto t^\beta$, with $\beta < 1$. The exponent β was included in the fit function used for the analysis of the FCS data to obtain an estimate of the extent of anomalous behavior, which can be caused by inert obstacles that obstruct particle motion by an excluded volume interaction. Additional binding events to the obstacles may result in a decrease of the apparent diffusion coefficient^[15,16]. Depending on the amount of gelation strands added the crosslinking process is completed after 1-2 hours. At this point the diffusion constant determined by particle tracking drops to zero. FCS, however, does not allow for an accurate measurement of D anymore (Figs. 4a & b). All QDs are now tightly trapped in the crosslinked gel. Determination of the position of the center of single fluorescent spots reveals spatial confinement of the particles within 25 nm (Fig. 3e), which is on the order of the size of the quantum dots themselves. FCS control experiments with the organic dye Alexa 488 with a diameter of only 1 nm revealed no confinement or reduced diffusion constant (data not shown), when the gel was switched between the unlinked and the crosslinked state.

As already mentioned, the confinement of the QDs is stronger than expected from the average pore size of the sparsely crosslinked gel. It is possible that particles are trapped in small pores during the crosslinking process, from which they cannot escape. The distance between two crosslinking points is expected to be of the order of 20 bp, i.e., 7.5 nm. It is therefore conceivable that some of the gel pores are much smaller than the average pore

size. In addition, particles may be trapped in a gel even when the pore size is larger than the particle diameter, which can be attributed to the high entropic cost of motion in the gel^[17]. Finally, we cannot rule out a possible electrostatic interaction between the quantum dots and the charged DNA crosslinkers. However, permanent binding between QDs and DNA-polyacrylamide fibers is not observed.

Addition of the release strand R to the crosslinked gel triggers the liberation of the trapped particles. Strand R displaces the gelation strand L from strands A and B in the PAAm chains by branch migration^[2], resulting in a DNA waste duplex R-L and the gel mixture reverted to the initial fluid state. Due to the slow diffusion of R into the gel, the release process takes longer than the gelation process. Released QDs first start to diffuse again within micron-sized domains (Fig. 3b). A few hours after addition of the release strand, several distinct modes of motion are observed: unhindered, freely diffusing quantum dots, freely diffusing particles confined to volumes of $1 \text{ fl} - 1 \mu\text{l}$, and some particles still trapped in undissolved gel clusters.

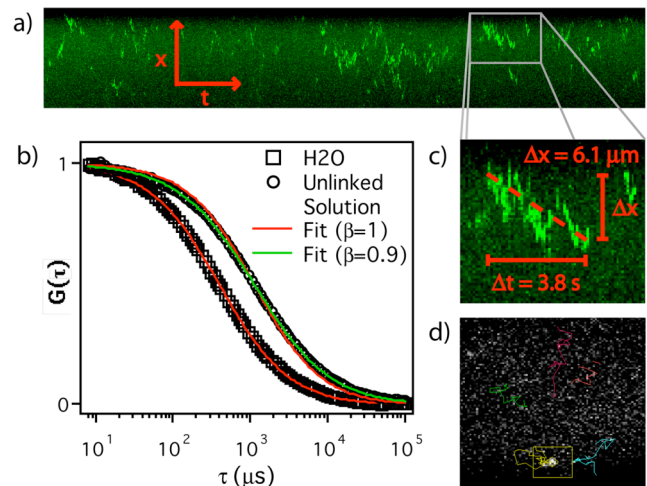


Figure 2. Time trace of QDs in the unlinked gel mixture. The time traces were obtained by stacking 3000 images ($128 \times 128 \text{ pixel}^2 = 28 \times 28 \mu\text{m}^2$, recorded at 35.7 Hz) with a distance of 0.28 Pixel and subsequent tilting of the stack by 90° around its x- or y-axis. The abscissa then corresponds to 100 ms per pixel from left to right, while the ordinate displays the projection of the former x- or y-axis. b) Autocorrelation functions obtained from FCS measurements of quantum dots in water and in the unlinked gel matrix fitted with Eq. 1. The diffusion constant in water is $D_{H_2O}=29 \pm 0.5 \mu\text{m}^2\text{s}^{-1}$ and $D_{FCS, \text{unlinked}}=6.6 \pm 0.3 \mu\text{m}^2\text{s}^{-1}$ in the unlinked gel solution. Already for the unlinked matrix the fit yields a value of $\beta < 1$, an indication of anomalous diffusion (cf. text). c) The bright traces coincide with 1D diffusion along one axis. By measuring the distances between the points where particles enter and leave the focal plane, one can calculate the diffusion constants with $D = x^2 / 2t$. By averaging over many particles and traces the obtained value D matches $\langle x^2 \rangle / 2t$. d) Computer aided particle tracking yields comparable diffusion constants as obtained by FCS and by the time trace method described in c).

The release of trapped nanoparticles can also be observed in a bulk experiment (Fig. 4c and Supplementary Videos 1 and 2). We prepared a crosslinked gel loaded with a high concentration of quantum dots and placed it into a buffer solution for several hours. No increase in fluorescence with time could be observed, corroborating the tight trapping of particles in the gel matrix as observed on the single particle level. Only after addition of the DNA

release strand, an increase of fluorescence in the solution surrounding the gel is observed, indicating release of the trapped particles and dissolution of the gel triggered by release DNA.

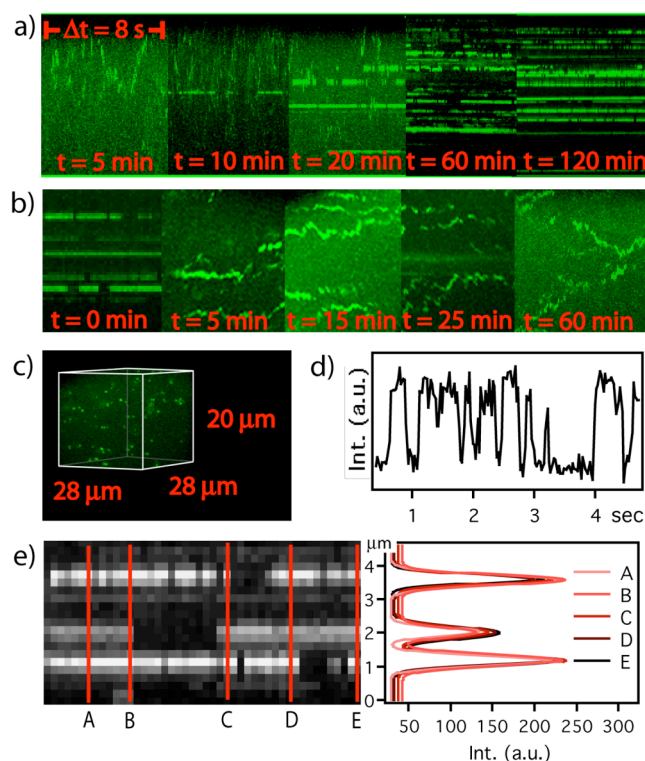


Figure 3. a) Five sections of time traces recorded during the crosslinking process. Each section is approximately 8 seconds long and was taken 5, 10, 20, 60, and 120 minutes after the addition of the crosslinking DNA strand. With ongoing crosslinking, more and more particles get trapped. b) Five sections of time traces recorded during the release process. Each section is around 8 seconds long and was taken 0, 5, 15, 25, and 60 minutes after the addition of the release DNA strand. With time the particles are uncaged, although the freedom of the unlinked matrix is not completely recovered. c) 1500 images of the crosslinked gel recorded at 35.7 Hz of a z-scan at 500 nm/s were stacked and tilted. Almost all QDs are fixed in the gel. d) On single bright spots, the well-known blinking behavior of QDs can be observed which indicates the trapping of single nanoparticles. e) Fitting the fluorescence intensities of the trapped QDs along the y-axis with Gaussians allows for the accurate determination of their position with a lateral precision < 30 nm. In the crosslinked gel the Gaussian peaks and thus the positions of the nanoparticles are fixed over time at least with this precision. Positions of the peaks \pm max error are: $1.18 \mu\text{m} \pm 10$ nm, $2.015 \mu\text{m} \pm 15$ nm, $3.585 \mu\text{m} \pm 15$ nm.

One of the potential applications of DNA-switchable gels lies in the area of controlled agent release. Hydrogels with variable pore size have been studied extensively as drug delivery systems^[18]. So far, however, gel swelling and component release has been controlled mainly by temperature or pH changes^[19], and only in a few cases by the presence of biologically relevant molecules such as saccharides or antigens^[20]. Our work demonstrates that a DNA-crosslinked PAAm gel could be used to release nanoparticles as potential drug delivery vehicles in response to the presence of trigger DNA or RNA molecules. Whether our system – implemented as DNA-crosslinked microgel beads – could be used for *in vivo* drug delivery depends on a variety of factors. Drug release could be triggered by

extracellular DNA or RNA, which is occasionally observed in cancer patients^[21]. Response to intracellular RNA signals, however, requires the uptake of the microgel beads by cells. In either case, the concentration of naturally occurring nucleic acids may be too low to trigger drug release efficiently. This could be remedied, e.g., by implementation of a DNA-based signal amplification scheme^[22]. A more realistic scenario involves incorporation of aptamers or allosteric aptazymes^[23]. Aptazymes could be used to release DNA or RNA strands in response to extracellular molecular signals. The released nucleic acids would then trigger the release of nanoparticles from the gel. The same strategy could be used to trigger the release of drugs from pure DNA hydrogels^[24] with smaller pore sizes.

In conclusion, we have studied the diffusion properties of fluorescent semiconductor nanoparticles in a DNA-switchable hydrogel using single QD tracking and fluorescence correlation spectroscopy. We have demonstrated that DNA-crosslinked hydrogels are capable of trapping and releasing nanoparticles on demand. Nanoparticles are trapped during the crosslinking process even though their diameter is smaller than the mean pore size. Our system or a modification thereof may find application as a switchable material for the controlled release of nanoscale agents.

Experimental Section

Sample preparation: CdSe/ZnS nanocrystals (Quantum Dot Corporation (Invitrogen), Berkeley, CA; emission maximum 565 nm) were capped with a polymer coating as described in Ref. [9]. Acrydite (TM)-modified DNA (A: 5'-Acrydite-CGG CCT GAA GCC TCC GTG TG-3', B: 5'-Acrydite-AAG CAC TCT TCT CCT CTC TG 3') was purchased from IDT (Coralville, IA), linker strand (L: 5'-ATC GCA CGC CCA GAG AGG AGA AGA GTG CTT CAC ACG GAG GCT TCA GGC CG-3') and release strand (R: 5'-CGG CCT GAA GCC TCC GTG TGA AGC ACT CTT CTC CTC TCT GGG CGT GCG AT-3') from biomers.net, Ulm, Germany. Stock solutions of strand A and B were prepared separately at 3 mM DNA concentration. The stock solution contained: 10% 10x TE buffer, 200 mM NaCl, 4% acrylamide, 3 mM DNA strand A or B and deionized water. Directly after mixing, nitrogen was bubbled through this solution for 5 min. Initiator mixture (0.05 g $(\text{NH}_4)_2\text{S}_2\text{O}_8$ and 25 μl TEMED (Sigma, Germany) in 0.5 ml H_2O) was added to a final concentration of 1.4% followed by bubbling nitrogen for an additional 5 min. The stock solutions were mixed 1:1 and 20 μl droplets containing 10 nM QDs were placed in coverslip chambers (Nunc, Wiesbaden, Germany) for FCS measurements. For video microscopy, the gel contained 100 pM QDs and was placed into a silicon grease ring of ~ 5 mm diameter on a glass coverslip. To crosslink the polyacrylamide solution, linker strands L were added to a final concentration of 0.5 mM, corresponding to a crosslink density of 33%. Dissolution of the gel was achieved by adding a twofold excess of release strand R.

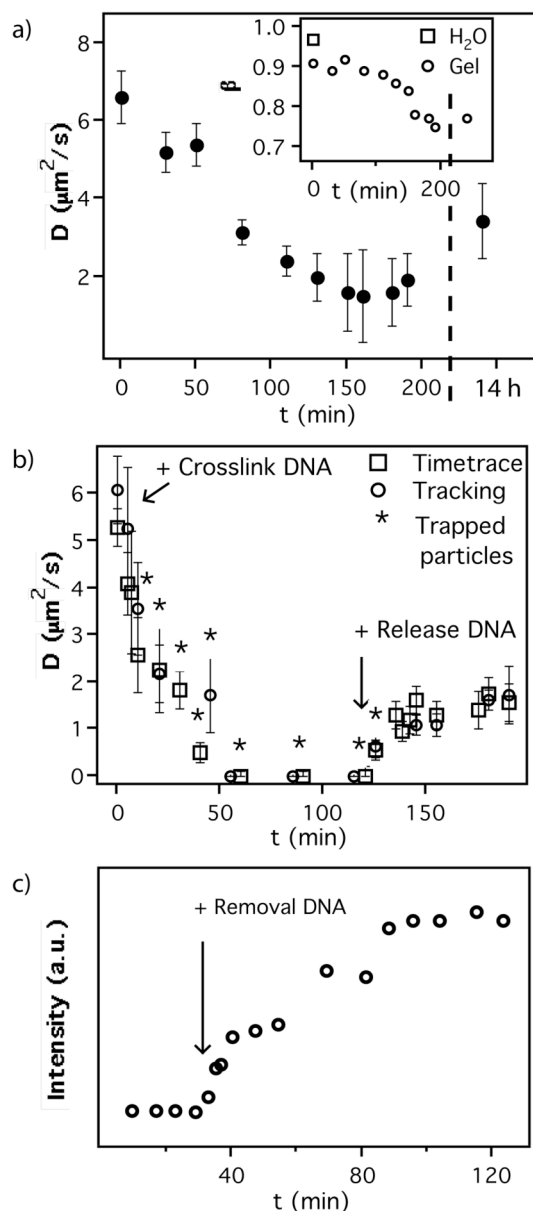


Figure 4. a) Diffusion constants of the QDs during the crosslinking and release process measured with FCS and fitted with Eq. 1. Error bars represent the standard deviation obtained from 5-10 single measurements. Inset: β -values obtained from fits with Eq. 1, indicating an increasing contribution of anomalous diffusion for increasing crosslinking density. b) Diffusion constants of the QDs during the crosslinking and release process determined from the time traces recorded by video microscopy (cf. Figs. 2 & 3). c) A crosslinked gel with captured fluorescent nanoparticles disintegrates upon addition of the release-DNA and dispenses the particles into the buffer solution. The increasing fluorescence was monitored with a fluorescence spectrometer at constant wavelength mode.

FCS measurements: FCS measurements were performed on a commercial FCS setup (microscope Axiovert 200 with 40 x C-Apochromat water immersion objective (NA 1.2) and ConfoCor2 module, Carl Zeiss, Jena, Germany). For excitation, the 488 nm line of an argon ion laser was used. Only 1% of the maximum illumination intensity of 2.91 mW was used to minimize saturation effects [25]. The emitted light was sent through a 50/50 beamsplitter and fed into two identical independent detection channels with 505 nm long pass filters and pinholes with 70 μm diameter. The signals of the avalanche photodiode detectors were cross-correlated to remove artifacts like detector afterpulsing. A detailed description of FCS theory and techniques can be found in [26]. FCS measurements of fluorescent

nanocrystals^[10,27] differ from those on organic fluorophores, as QDs exhibit no triplet behavior, but show blinking on all time-scales from nanoseconds to seconds. The distribution of blinking times follows a power law [14]. As for organic fluorophores the fluorescence decay time of QDs of a few nanoseconds is too fast to be detected in an FCS measurement. Since until now no analytical expression to fit FCS-data obtained from fluorophores exhibiting power-law-dependent blinking behavior could be derived, we fitted the curves with a simple FCS model that only takes diffusion into account. For calibration of the sample volume (i.e. to determine the parameters r_0 and z_0 , the radius and the longitudinal extension of the focal volume) the dye Alexa 488 ($D = 316 \mu\text{m}^2\text{s}^{-1}$, Molecular Probes) was used. The triplet behavior of Alexa 488 was taken into account during calibration. For all measurements r_0 was found to be between 180 and 190 nm. The ratio z_0/r_0 was always between 6 and 7. The auto-correlation functions obtained from QD-measurements were fitted with an expression for freely diffusing particles without the term describing the triplet behavior [16,26]:

$$G(\tau) = \frac{1}{N} \cdot \frac{1}{1 + \left(\frac{\tau}{\tau_D}\right)^\beta} \cdot \frac{1}{\sqrt{1 + \frac{r_0^2}{z_0^2} \left(\frac{\tau}{\tau_D}\right)^\beta}} \quad (1)$$

The two free parameters are the mean number of particles N in the focal volume and the diffusion time τ_D . To test the data for signatures of anomalous diffusion, the exponent β was introduced as a third free parameter. Each FCS data point was generated from at least 5 x 30 s measurement time.

Single Molecule Fluorescence Microscopy: We used a home-built single molecule, objective type TIR fluorescence microscope in epi-fluorescence mode to image single fluorescent quantum dots. Core elements are a sensitive EM-CCD Camera (Andor iXON Du-879) and a high numerical aperture objective (Carl Zeiss, Alpha Plan Fluor, 100x NA 1.45). For excitation we used cw laser light at 473 nm with sample plane intensity of approximately 10 kWcm^{-2} . Fluorescence emission was collected at 508 $\text{nm} \pm 10 \text{ nm}$. Kinetic image series were collected with 25 ms exposure time and treated with Image J in order to calculate collapsed fluorescence image time traces.

Fluorescence Spectroscopy: Approximately 5 μl of the crosslinked gel, loaded with 20 nM QDs, were placed on the bottom of a glass cuvette containing 300 μl TE buffer (200 mM NaCl). The cuvette was mounted in a fluorescence spectrometer (Jobin Yvon Fluorolog-322). In order to collect fluorescence only from released particles, the excitation light (480 nm) was precluded from the gel itself. Fluorescence was collected at 525 nm. After 30 min 10 μl of release DNA (3 mM) were added. To overcome slow diffusion of the particles in the comparably large cuvette-volume, the cuvette was shaken gently between the measurements.

Videos of gel triggered gel dissolution available as supplementary information.

Keywords:

DNA structures • Sol-gel processes • nanoparticles • fluorescence • diffusion

- [1] N. C. Seeman, *Nature* **2003**, 421, 427; F. C. Simmel, W. U. Dittmer, *Small* **2005**, 1, 284; J. Bath, A. J. Turberfield, *Nat Nano* **2007**, 2, 275.

- [2] B. Yurke, A. J. Turberfield, A. P. Mills, F. C. Simmel, J. L. Neumann, *Nature* **2000**, 406, 605.
- [3] D. C. Lin, B. Yurke, N. A. Langrana, *J. Biomech. Eng. - Trans. ASME* **2004**, 126, 104.
- [4] W. D. Novaes, A. Berg, *Aesthetic Plast. Surg.* **2003**, 27, 376; V. Breiting, A. Aasted, A. Jorgensen, P. Opitz, A. Rosetzky, *Aesthetic Plast. Surg.* **2004**, 28, 45; E. A. Smith, F. W. Oehme, *Rev. Environ. Health* **1991**, 9, 215.
- [5] C. Gelfi, P. G. Righetti, *Electrophoresis* **1981**, 2, 213.
- [6] M. Kenney, S. Ray, T. C. Boles, *BioTechniques* **1998**, 25, 516.
- [7] T. Pellegrino, S. Kudera, T. Liedl, A. M. Javier, L. Manna, W. J. Parak, *Small* **2005**, 1, 48.
- [8] D. L. Holmes, N. C. Stellwagen, *Electrophoresis* **1991**, 12, 612.
- [9] T. Pellegrino, L. Manna, S. Kudera, T. Liedl, D. Koktysh, A. L. Rogach, S. Keller, J. Radler, G. Natile, W. J. Parak, *Nano Lett.* **2004**, 4, 703.
- [10] T. Liedl, S. Keller, F. C. Simmel, J. O. Radler, W. J. Parak, *Small* **2005**, 1, 997.
- [11] D. Magde, E. L. Elson, W. W. Webb, *Biopolymers* **1974**, 13, 29.
- [12] X. Ye, P. Tong, L. J. Fetters, *Macromolecules* **1998**, 31, 5785.
- [13] M. Nirmal, B. O. Dabbousi, M. G. Bawendi, J. J. Macklin, J. K. Trautman, T. D. Harris, L. E. Brus, *Nature* **1996**, 383, 802.
- [14] M. Kuno, D. P. Fromm, H. F. Hamann, A. Gallagher, D. J. Nesbitt, *J. Chem. Phys.* **2000**, 112, 3117.
- [15] M. J. Saxton, *Biophys. J.* **1996**, 70, 1250.
- [16] M. Wachsmuth, W. Waldeck, J. Langowski, *J. Mol. Biol.* **2000**, 298, 677.
- [17] A. Pluen, P. A. Netti, R. K. Jain, D. A. Berk, *Biophys. J.* **1999**, 77, 542.
- [18] Y. Qiu, K. Park, *Adv. Drug Deliv. Rev.* **2001**, 53, 321.
- [19] R. Pelton, *Adv. Colloid Interface Sci.* **2000**, 85, 1; X. H. Xia, Z. B. Hu, M. Marquez, *J. Controlled Release* **2005**, 103, 21.
- [20] T. Miyata, N. Asami, T. Uragami, *Nature* **1999**, 399, 766.
- [21] D. Sidransky, *Nature Reviews Cancer* **2002**, 2, 210; P. Anker, J. Lyautey, C. Lederrey, M. Stroun, *Clin. Chim. Acta* **2001**, 313, 143.
- [22] J. S. Bois, S. Venkataraman, H. M. Choi, A. J. Spakowitz, Z. G. Wang, N. A. Pierce, *Nucleic Acids Res.* **2005**, 33, 4090; G. Seelig, B. Yurke, E. Winfree, *J. Am. Chem. Soc.* **2006**, 128, 12211.
- [23] S. Seetharaman, M. Zivarts, N. Sudarsan, R. R. Breaker, *Nat. Biotech.* **2001**, 19, 336.
- [24] S. H. Um, J. B. Lee, N. Park, S. Y. Kwon, C. C. Umbach, D. Luo, *Nature Materials* **2006**, 5, 797.
- [25] J. Enderlein, I. Gregor, D. Patra, J. Fitter, *Curr. Pharm. Biotech.* **2004**, 5, 155; I. Gregor, D. Patra, J. Enderlein, *Chemphyschem* **2005**, 6, 164.
- [26] P. Schwille, J. Bieschke, F. Oehlenschlager, *Biophys. Chem.* **1997**, 66, 211; O. Krichevsky, G. Bonnet, *Rep. Prog. Phys.* **2002**, 65, 251.
- [27] D. R. Larson, W. R. Zipfel, R. M. Williams, S. W. Clark, M. P. Bruchez, F. W. Wise, W. W. Webb, *Science* **2003**, 300, 1434; S. Doose, J. M. Tsay, F. Pinaud, S. Weiss, *Anal. Chem.* **2005**, 77, 2235.

Received: ((will be filled in by the editorial staff))
Published online on ((will be filled in by the editorial staff))

Bibliography

- [1] T. Liedl, T. L. Sobey, and F. C. Simmel. DNA-based nanodevices. *Nanotoday*, 2(2):36–41, 2007.
- [2] T. Liedl and F. C. Simmel. Determination of DNA melting temperatures in diffusion-generated chemical gradients. *Analytical Chemistry*, *accepted*, 2007.
- [3] T. Liedl and F. C. Simmel. Switching the conformation of a DNA molecule with a chemical oscillator. *Nano Letters*, 5(10):1894–1898, 2005.
- [4] T. Liedl, M. Olapinski, and F. C. Simmel. A surface-bound DNA switch driven by a chemical oscillator. *Angewandte Chemie-International Edition*, 45(30):5007–5010, 2006.
- [5] T. Liedl, S. Keller, F. C. Simmel, J. O. Radler, and W. J. Parak. Fluorescent nanocrystals as colloidal probes in complex fluids measured by fluorescence correlation spectroscopy. *Small*, 1(10):997–1003, 2005.
- [6] T. Liedl, H. Dietz, B. Yurke, and F. C. Simmel. Controlled trapping and release of quantum dots in a DNA-linked hydrogel. *submitted*, 2007.
- [7] N. C. Seeman. DNA in a material world. *Nature*, 421(6921):427–431, 2003.
- [8] J. H. Chen and N. C. Seeman. Synthesis from DNA of a molecule with the connectivity of a cube. *Nature*, 350(6319):631–633, 1991. 0028-0836.
- [9] W. M. Shih, J. D. Quispe, and G. F. Joyce. A 1.7-kilobase single-stranded DNA that folds into a nanoscale octahedron. *Nature*, 427(6975):618–621, 2004.
- [10] R. P. Goodman, I. A. T. Schaap, C. F. Tardin, C. M. Erben, R. M. Berry, C. F. Schmidt, and A. J. Turberfield. Rapid chiral assembly of rigid DNA building blocks for molecular nanofabrication. *Science*, 310(5754):1661–1665, 2005.
- [11] P. W. K. Rothemund. Folding DNA to create nanoscale shapes and patterns. *Nature*, 440(7082):297–302, 2006.
- [12] B. Yurke, A. J. Turberfield, A. P. Mills, F. C. Simmel, and J. L. Neumann. A DNA-fuelled molecular machine made of DNA. *Nature*, 406(6796):605–608, 2000.

- [13] J. S. Shin and N. A. Pierce. A synthetic DNA walker for molecular transport. *Journal of the American Chemical Society*, 126(35):10834–10835, 2004.
- [14] C. S. Lee, R. W. Davis, and N. Davidson. A physical study by electron microscopy of terminally repetitious, circularly permuted dna from coliphage particles of escherichia-coli 15. *Journal Of Molecular Biology*, 48(1):1, 1970. 0022-2836.
- [15] C. Green and C. Tibbetts. Reassociation rate limited displacement of dna-strands by branch migration. *Nucleic Acids Research*, 9(8):1905–1918, 1981. 0305-1048.
- [16] Y. Chen, M. S. Wang, and C. D. Mao. An autonomous DNA nanomotor powered by a DNA enzyme. *Angewandte Chemie-International Edition*, 43(27):3554–3557, 2004.
- [17] J. Bath, S. J. Green, and A. J. Turberfield. A free-running DNA motor powered by a nicking enzyme. *Angewandte Chemie-International Edition*, 44(28):4358–4361, 2005.
- [18] R. Pei, S. K. Taylor, D. Stefanovic, S. Rudchenko, T. E. Mitchell, and M. N. Stojanovic. Behavior of polycatalytic assemblies in a substrate-displaying matrix. *Journal Of The American Chemical Society*, 128(39):12693–12699, 2006.
- [19] W. U. Dittmer, S. Kempter, J. O. Radler, and F. C. Simmel. Using gene regulation to program DNA-based molecular devices. *Small*, 1(7):709–712, 2005.
- [20] J. Kim, J. J. Hopfield, and E. Winfree. Neural network computation by in vitro transcriptional circuits. *Advances in Neural Information Processing Systems*, 17:681–688, 2004.
- [21] J. Kim, K. S. White, and E. Winfree. Construction of an in vitro bistable circuit from synthetic transcriptional switches. *Molecular Systems Biology*, 2, 2006.
- [22] F. C. Simmel and W. U. Dittmer. Dna nanodevices. *Small*, 1(3):284–299, 2005. 1613-6810.
- [23] F. C. Simmel. DNA nanodevices: Prototypes and applications. *Nanodevices for the Life Sciences*, 89, 2006.
- [24] D. L. Nelson and M. M. Cox. Lehninger principles of biochemistry. www.worthpublishers.com/lehninger/.
- [25] V. A. Bloomfield, D. M. Crothers, and J. R. Tinoco. *Nucleic acids*. University Science Books, 2000.
- [26] B. Tinland, A. Pluen, J. Sturm, and G. Weill. Persistence length of single-stranded DNA. *Macromolecules*, 30(19):5763–5765, 1997. 0024-9297.
- [27] P. J. Flory. *Statistical Mechanics of Chain Molecules*. Wiley, 1988.

- [28] A. Panjkovich and F. Melo. Comparison of different melting temperature calculation methods for short DNA sequences. *Bioinformatics*, 21(6):711–722, 2005.
- [29] S. V. Suggs, T. Hirose, T. Miyake, E. H. Kawashima, M. J. Johnson, K. Itakura, and R. B. Wallace. Use of synthetic oligodeoxyribonucleotides for the isolation of specific cloned DNA sequences. *Development biology using purified genes*, pages 683–693, 1981.
- [30] J. Marmur and P. Doty. Heterogeneity in deoxyribonucleic acids.1. dependence on composition of the configurational stability of deoxyribonucleic acids. *Nature*, 183(4673):1427–1429, 1959. 0028-0836.
- [31] J. Marmur and P. Doty. Determination of base composition of deoxyribonucleic acid from its thermal denaturation temperature. *Journal Of Molecular Biology*, 5(1):109, 1962.
- [32] P. M. Howley, M. A. Israel, M. F. Law, and M. A. Martin. Rapid method for detecting and mapping homology between heterologous DNAs - evaluation of polyomavirus genomes. *Journal Of Biological Chemistry*, 254(11):4876–4883, 1979.
- [33] J. G. Wetmur. DNA probes - applications of the principles of nucleic-acid hybridization. *Critical Reviews In Biochemistry And Molecular Biology*, 26(3-4):227–259, 1991. 1040-9238.
- [34] K. J. Breslauer, R. Frank, H. Blocker, and L. A. Marky. Predicting DNA duplex stability from the base sequence. *Proceedings Of The National Academy Of Sciences Of The United States Of America*, 83(11):3746–3750, 1986.
- [35] J. SantaLucia and D. Hicks. The thermodynamics of DNA structural motifs. *Annual Review Of Biophysics And Biomolecular Structure*, 33:415–440, 2004.
- [36] M. Petersheim and D. H. Turner. Base-stacking and base-pairing contributions to helix stability - thermodynamics of double-helix formation with ccgg, ccgcp, ccggap, accgcp, ccggup, and accggup. *Biochemistry*, 22(2):256–263, 1983.
- [37] B. Ding and N. C. Seeman. Operation of a DNA robot arm inserted into a 2d DNA crystalline substrate. *Science*, 314(5805):1583–1585, 2006. 0036-8075.
- [38] M. Rief, H. Clausen-Schaumann, and H. E. Gaub. Sequence-dependent mechanics of single DNA molecules. *Nature Structural Biology*, 6(4):346–349, 1999. 1072-8368.
- [39] H. Clausen-Schaumann, M. Rief, C. Tolksdorf, and H. E. Gaub. Mechanical stability of single DNA molecules. *Biophysical Journal*, 78(4):1997–2007, 2000. 0006-3495.
- [40] W. M. Shu, D. S. Liu, M. Watari, C. K. Riener, T. Strunz, M. E. Welland, S. Balasubramanian, and R. A. McKendry. DNA molecular motor driven micromechanical cantilever arrays. *Journal Of The American Chemical Society*, 127(48):17054–17060, 2005.

- [41] T. Forster. Zwischenmolekulare Energiewanderung und Fluoreszenz. *Annalen Der Physik*, 2(1-2):55–75, 1948.
- [42] J. R. Lakowicz. *Principles of Fluorescence Spectroscopy*. Kluwer Academic / Plenum Publisher, 2 edition, 1999.
- [43] K. H. Drexhage. Interaction of light with monomolecular dye layers. *Progress in optics*, 12, 1974.
- [44] D. H. Waldeck, A. P. Alivisatos, and C. B. Harris. Nonradiative damping of molecular electronic excited-states by metal-surfaces. *Surface Science*, 158(1-3):103–125, 1985. 0039-6028.
- [45] R. R. Chance, A. Prock, and R. Silbey. Molecular fluorescence and energy transfer near interfaces. *Advances in Chemical Physics*, 37:1–65, 1978.
- [46] Z. Gueroui and A. Libchaber. Single-molecule measurements of gold-quenched quantum dots. *Physical Review Letters*, 93(16), 2004. 0031-9007 166108.
- [47] C. S. Yun, A. Javier, T. Jennings, M. Fisher, S. Hira, S. Peterson, B. Hopkins, N. O. Reich, and G. F. Strouse. Nanometal surface energy transfer in optical rulers, breaking the fret barrier. *Journal Of The American Chemical Society*, 127(9):3115–3119, 2005. 0002-7863.
- [48] J. R. Lakowicz, Y. B. Shen, S. D’Auria, J. Malicka, J. Y. Fang, Z. Gryczynski, and I. Gryczynski. Radiative decay engineering 2. effects of silver island films on fluorescence intensity, lifetimes, and resonance energy transfer. *Analytical Biochemistry*, 301(2):261–277, 2002. 0003-2697.
- [49] K. T. Shimizu, W. K. Woo, B. R. Fisher, H. J. Eisler, and M. G. Bawendi. Surface-enhanced emission from single semiconductor nanocrystals. *Physical Review Letters*, 89(11), 2002. 0031-9007 117401.
- [50] C. Sadhu, S. Dutta, and K. P. Gopinathan. Influence of formamide on the thermal-stability of DNA. *Journal Of Biosciences*, 6(6):817–821, 1984.
- [51] B. L. McConaughy, C. D. Laird, and B. J. McCarthy. Nucleic acid reassociation in formamide. *Biochemistry*, 8(8):3289, 1969.
- [52] J. Casey and N. Davidson. Rates of formation and thermal stabilities of rna-DNA and DNA-DNA duplexes at high-concentrations of formamide. *Nucleic Acids Research*, 4(5):1539–1552, 1977.
- [53] R. D. Blake and S. G. Delcourt. Thermodynamic effects of formamide on DNA stability. *Nucleic Acids Research*, 24(11):2095–2103, 1996.

- [54] M. A. Unger, H. P. Chou, T. Thorsen, A. Scherer, and S. R. Quake. Monolithic micro-fabricated valves and pumps by multilayer soft lithography. *Science*, 288(5463):113–116, 2000.
- [55] C. L. Hansen, E. Skordalakes, J. M. Berger, and S. R. Quake. A robust and scalable microfluidic metering method that allows protein crystal growth by free interface diffusion. *Proceedings Of The National Academy Of Sciences Of The United States Of America*, 99(26):16531–16536, 2002.
- [56] F. C. Simmel and B. Yurke. Using DNA to construct and power a nanoactuator. *Physical Review E*, 6304(4), 2001. Part 1 041913.
- [57] D. S. Liu and S. Balasubramanian. A proton-fuelled DNA nanomachine. *Angewandte Chemie-International Edition*, 42(46):5734–5736, 2003.
- [58] Y. Chen, S. H. Lee, and C. Mao. A DNA nanomachine based on a duplex-triplex transition. *Angewandte Chemie-International Edition*, 43(40):5335–5338, 2004.
- [59] D. S. Liu, A. Bruckbauer, C. Abell, S. Balasubramanian, D. J. Kang, D. Klenerman, and D. J. Zhou. A reversible ph-driven DNA nanoswitch array. *Journal Of The American Chemical Society*, 128(6):2067–2071, 2006.
- [60] G. Nicolis and I. Prigogine. *Self organization in non-equilibrium systems*. Wiley, 1977.
- [61] M. Meinhard. *The algorithmic beauty of sea shells*. Springer, 1995.
- [62] A. J. Koch and H. Meinhardt. Biological pattern-formation - from basic mechanisms to complex structures. *Reviews Of Modern Physics*, 66(4):1481–1507, 1994.
- [63] W. Driever and C. Nüsslein-Volhard. The bicoid protein determines position in the drosophila embryo in a concentration-dependent manner. *Cell*, 54(1):95–104, 1988.
- [64] P. W. Ingham. The molecular-genetics of embryonic pattern-formation in drosophila. *Nature*, 335(6185):25–34, 1988.
- [65] M. C. Cross and P. C. Hohenberg. Pattern-formation outside of equilibrium. *Reviews Of Modern Physics*, 65(3):851–1112, 1993. 0034-6861 Part 2.
- [66] A. M. Turing. The chemical basis of morphogenesis. *Philosophical Transactions Of The Royal Society Of London Series B-Biological Sciences*, 237(641):37–72, 1952.
- [67] I. Prigogine and R. Lefever. Symmetry breaking instabilities in dissipative systems.2. *Journal Of Chemical Physics*, 48(4):1695–1700, 1968.
- [68] C. J. Campbell, M. Fialkowski, R. Klajn, I. T. Bensemann, and B. A. Grzybowski. Color micro- and nanopatterning with counter-propagating reaction-diffusion fronts. *Advanced Materials*, 16(21):1912–1917, 2004.

- [69] R. Klajn, M. Fialkowski, I. T. Bensemann, A. Bitner, C. J. Campbell, K. Bishop, S. Smoukov, and B. A. Grzybowski. Multicolour micropatterning of thin films of dry gels. *Nature Materials*, 3(10):729–735, 2004.
- [70] A. J. Lotka. Analytical note on certain rhythmic relations in organic systems. *Proceedings Of The National Academy Of Sciences Of The United States Of America*, 6:410–415, 1920.
- [71] J. D. Murray. *Mathematical biology I*. Springer, 3 edition, 1989.
- [72] A. T. Winfree. Biological rhythms and behavior of populations of coupled oscillators. *Journal Of Theoretical Biology*, 16(1):15, 1967. 0022-5193.
- [73] F. Halberg. Chronobiology. *Annual Review Of Physiology*, 31:675, 1969.
- [74] R. E. Dolmetsch, K. L. Xu, and R. S. Lewis. Calcium oscillations increase the efficiency and specificity of gene expression. *Nature*, 392(6679):933–936, 1998.
- [75] S. Dano, P. G. Sorensen, and F. Hynne. Sustained oscillations in living cells. *Nature*, 402(6759):320–322, 1999.
- [76] G. S. Pitt, N. Milona, J. Borleis, K. C. Lin, R. R. Reed, and P. N. Devreotes. Structurally distinct and stage-specific adenylyl cyclase genes play different roles in dictyostelium development. *Cell*, 69(2):305–315, 1992.
- [77] D. M. F. Cooper, N. Mons, and J. W. Karpen. Adenylyl cyclases and the interaction between calcium and camp signaling. *Nature*, 374(6521):421–424, 1995.
- [78] M. B. Elowitz and S. Leibler. A synthetic oscillatory network of transcriptional regulators. *Nature*, 403(6767):335–338, 2000. 0028-0836.
- [79] A. N. Zaikin and Zhabotinsky. A. M. Concentration wave propagation in 2-dimensional liquid-phase self-oscillating system. *Nature*, 225(5232):535, 1970.
- [80] R. J. Field, R. M. Noyes, and E. Koros. Oscillations in chemical systems.2. thorough analysis of temporal oscillation in bromate-cerium-malonic acid system. *Journal Of The American Chemical Society*, 94(25):8649, 1972. 0002-7863.
- [81] G. Rabai, M. Orban, and I. R. Epstein. Systematic design of chemical oscillators.64. design of ph-regulated oscillators. *Accounts Of Chemical Research*, 23(8):258–263, 1990.
- [82] K. Kurin-Csorgei, I. R. Epstein, and M. Orban. Systematic design of chemical oscillators using complexation and precipitation equilibria. *Nature*, 433(7022):139–142, 2005.
- [83] K. Gehring, J. L. Leroy, and M. Gueron. A tetrameric DNA-structure with protonated cytosine-cytosine base-pairs. *Nature*, 363(6429):561–565, 1993.

- [84] G. E. Plum. Thermodynamics of oligonucleotide triple helices. *Biopolymers*, 44(3):241–256, 1997.
- [85] A. Rich. DNA comes in many forms. *Gene*, 135(1-2):99–109, 1993.
- [86] E. C. Edblom, M. Orban, and I. R. Epstein. A new iodate oscillator - the landolt reaction with ferrocyanide in a cstr. *Journal Of The American Chemical Society*, 108(11):2826–2830, 1986.
- [87] G. Rabai and M. T. Beck. High-amplitude hydrogen-ion concentration oscillation in the iodate-thiosulfate-sulfite system under closed conditions. *Journal Of Physical Chemistry*, 92(17):4831–4835, 1988.
- [88] G. Rabai and I. R. Epstein. Systematic design of chemical oscillators.80. ph oscillations in a semibatch reactor. *Journal Of The American Chemical Society*, 114(4):1529–1530, 1992.
- [89] B. Dubertret, M. Calame, and A. J. Libchaber. Single-mismatch detection using gold-quenched fluorescent oligonucleotides. *Nature Biotechnology*, 19(4):365–370, 2001. 1087-0156.
- [90] H. Du, M. D. Disney, B. L. Miller, and T. D. Krauss. Hybridization-based unquenching of DNA hairpins on au surfaces: Prototypical "molecular beacon" biosensors. *Journal Of The American Chemical Society*, 125(14):4012–4013, 2003. 0002-7863.
- [91] M. Brucale, G. Zuccheri, and B. Samori. The dynamic properties of an intramolecular transition from DNA duplex to cytosine-thymine motif triplex. *Organic and Biomolecular Chemistry*, 3(4):575–577, 2005. 1477-0520.
- [92] J. D. Badjic, V. Balzani, A. Credi, S. Silvi, and J. F. Stoddart. A molecular elevator. *Science*, 303(5665):1845–1849, 2004. 0036-8075.
- [93] J. D. Badjic, C. M. Ronconi, J. F. Stoddart, V. Balzani, S. Silvi, and A. Credi. Operating molecular elevators. *Journal Of The American Chemical Society*, 128(5):1489–1499, 2006. 0002-7863.
- [94] Y. Qiu and K. Park. Environment-sensitive hydrogels for drug delivery. *Advanced Drug Delivery Reviews*, 53(3):321–339, 2001.
- [95] J. Kopecek. Smart and genetically engineered biomaterials and drug delivery systems. *European Journal Of Pharmaceutical Sciences*, 20(1):1–16, 2003.
- [96] N. A. Peppas. Hydrogels and drug delivery. *Current Opinion In Colloid and Interface Science*, 2(5):531–537, 1997.
- [97] T. Tanaka, D. Fillmore, S. T. Sun, I. Nishio, G. Swislow, and A. Shah. Phase-transitions in ionic gels. *Physical Review Letters*, 45(20):1636–1639, 1980.

- [98] R. Pelton. Temperature-sensitive aqueous microgels. *Advances In Colloid And Interface Science*, 85(1):1–33, 2000.
- [99] B. Jeong, S. W. Kim, and Y. H. Bae. Thermosensitive sol-gel reversible hydrogels. *Advanced Drug Delivery Reviews*, 54(1):37–51, 2002.
- [100] R. Yoshida, K. Uchida, Y. Kaneko, K. Sakai, A. Kikuchi, Y. Sakurai, and T. Okano. Comb-type grafted hydrogels with rapid de-swelling response to temperature-changes. *Nature*, 374(6519):240–242, 1995.
- [101] A. A. Obaidat and K. Park. Characterization of glucose dependent gel-sol phase transition of the polymeric glucose-concanavalin a hydrogel system. *Pharmaceutical Research*, 13(7):989–995, 1996. 0724-8741.
- [102] S. J. Lee and K. Park. Synthesis and characterization of sol-gel phase-reversible hydrogels sensitive to glucose. *Journal Of Molecular Recognition*, 9(5-6):549–557, 1996. 0952-3499.
- [103] A. A. Obaidat and K. Park. Characterization of protein release through glucose-sensitive hydrogel membranes. *Biomaterials*, 18(11):801–806, 1997. 0142-9612.
- [104] T. P. Hsu and C. Cohen. Observations on the structure of a polyacrylamide-gel from electron-micrographs. *Polymer*, 25(10):1419–1423, 1984. 0032-3861.
- [105] D. L. Holmes and N. C. Stellwagen. Estimation of polyacrylamide-gel pore-size from ferguson plots of normal and anomalously migrating DNA fragments.1. gels containing 3-percent n,n'-methylenebisacrylamide. *Electrophoresis*, 12(4):253–263, 1991. 0173-0835.
- [106] D. L. Holmes and N. C. Stellwagen. Estimation of polyacrylamide-gel pore-size from ferguson plots of linear DNA fragments.2. comparison of gels with different cross-linker concentrations, added agarose and added linear polyacrylamide. *Electrophoresis*, 12(9):612–619, 1991. 0173-0835.
- [107] A. Pluen, B. Tinland, J. Sturm, and G. Weill. Migration of single-stranded DNA in polyacrylamide gels during electrophoresis. *Electrophoresis*, 19(10):1548–1559, 1998. 0173-0835.
- [108] C. Gelfi and P. G. Righetti. Polymerization kinetics of polyacrylamide gels.1. effect of different cross-linkers. *Electrophoresis*, 2(4):213–219, 1981.
- [109] T. Miyata, N. Asami, and T. Uragami. A reversibly antigen-responsive hydrogel. *Nature*, 399(6738):766–769, 1999.
- [110] D. C. Lin, B. Yurke, and N. A. Langrana. Mechanical properties of a reversible, DNA-crosslinked polyacrylamide hydrogel. *Journal Of Biomechanical Engineering-Transactions Of The Asme*, 126(1):104–110, 2004.

- [111] F. Caruso. Nanoengineering of particle surfaces. *Advanced Materials*, 13(1):11–+, 2001. 0935-9648.
- [112] M. E. Akerman, W. C. W. Chan, P. Laakkonen, S. N. Bhatia, and E. Ruoslahti. Nanocrystal targeting in vivo. *Proceedings Of The National Academy Of Sciences Of The United States Of America*, 99(20):12617–12621, 2002. 0027-8424.
- [113] X. H. Gao, Y. Y. Cui, R. M. Levenson, L. W. K. Chung, and S. M. Nie. In vivo cancer targeting and imaging with semiconductor quantum dots. *Nature Biotechnology*, 22(8):969–976, 2004. 1087-0156.
- [114] A. Jordan, R. Scholz, P. Wust, H. Fahling, and R. Felix. Magnetic fluid hyperthermia (mfh): Cancer treatment with ac magnetic field induced excitation of biocompatible superparamagnetic nanoparticles. *Journal Of Magnetism And Magnetic Materials*, 201:413–419, 1999. 0304-8853.
- [115] Q. A. Pankhurst, J. Connolly, S. K. Jones, and J. Dobson. Applications of magnetic nanoparticles in biomedicine. *Journal Of Physics D-Applied Physics*, 36(13):R167–R181, 2003.
- [116] M. Bruchez, M. Moronne, P. Gin, S. Weiss, and A. P. Alivisatos. Semiconductor nanocrystals as fluorescent biological labels. *Science*, 281(5385):2013–2016, 1998. 0036-8075.
- [117] T. Pellegrino, S. Kudera, T. Liedl, A. M. Javier, L. Manna, and W. J. Parak. On the development of colloidal nanoparticles towards multifunctional structures and their possible use for biological applications. *Small*, 1(1):48–63, 2005.
- [118] C. Kirchner, T. Liedl, S. Kudera, T. Pellegrino, A. M. Javier, H. E. Gaub, S. Stolzle, N. Fertig, and W. J. Parak. Cytotoxicity of colloidal cdse and cdse/zns nanoparticles. *Nano Letters*, 5(2):331–338, 2005.
- [119] P. Schwille, J. Bieschke, and F. Oehlenschlager. Kinetic investigations by fluorescence correlation spectroscopy: The analytical and diagnostic potential of diffusion studies. *Biophysical Chemistry*, 66(2-3):211–228, 1997.
- [120] O. Krichevsky and G. Bonnet. Fluorescence correlation spectroscopy: the technique and its applications. *Reports On Progress In Physics*, 65(2):251–297, 2002.
- [121] S. Mangenot, S. Keller, and J. Radler. Transport of nucleosome core particles in semidilute DNA solutions. *Biophysical Journal*, 85(3):1817–1825, 2003. 0006-3495.
- [122] C. F. Schmidt, M. Barmann, G. Isenberg, and E. Sackmann. Chain dynamics, mesh size, and diffusive transport in networks of polymerized actin - a quasielastic light-scattering and microfluorescence study. *Macromolecules*, 22(9):3638–3649, 1989. 0024-9297.

-
- [123] A. J. Turberfield, J. C. Mitchell, B. Yurke, A. P. Mills, M. I. Blakey, and F. C. Simmel. DNA fuel for free-running nanomachines. *Physical Review Letters*, 90(11), 2003. 0031-9007 118102.
- [124] G. Seelig, B. Yurke, and E. Winfree. Catalyzed relaxation of a metastable DNA fuel. *Journal Of The American Chemical Society*, 128(37):12211–12220, 2006.
- [125] S. Seetharaman, M. Zivarts, N. Sudarsan, and R. R. Breaker. Immobilized rna switches for the analysis of complex chemical and biological mixtures. *Nature Biotechnology*, 19(4):336–341, 2001.
- [126] M. N. Stojanovic, P. de Prada, and D. W. Landry. Catalytic molecular beacons. *Chembiochem*, 2(6):411–415, 2001.
- [127] M. N. Stojanovic and D. M. Kolpashchikov. Modular aptameric sensors. *Journal Of The American Chemical Society*, 126(30):9266–9270, 2004.

Vielen Dank...

... an alle Mitarbeiter des LS Kottahus und alle Mitarbeiter anderer Institute, die ich immer um Rat fragen konnte, insbesondere die Mitarbeiter des LS Rädler und des LS Gaub. Mein besonderer Dank gilt:

Fritz Simmel, für Deine unermüdliche Unterstützung, die ausgezeichneten Ideen, den idealen Freiraum für die Forschung in deiner Gruppe und die gleichzeitig hervorragende Betreuung, die interessanten Gespräche die unabhängig vom Thema immer aufschlussreich waren und schließlich für die gute Zeit und den Spaß den ich in Deiner Gruppe hatte.

Jörg Kotthaus, für die Möglichkeit, an Deinem Lehrstuhl in einer perfekten Atmosphäre und unter perfekten Bedingungen arbeiten zu können sowie die wertvollen Ratschläge die ich von Dir erhalten habe.

Joachim Rädler, für die ununterbrochene Unterstützung meiner Arbeit, die zahlreichen interessanten Diskussionen sowie die Möglichkeit Deine Labors zu nutzen.

Wolfgang Parak, für die ausgezeichnete Zusammenarbeit, die Diskussionen und die hilfreichen Tipps.

Hendrik Dietz, ohne Deinen 1A-Spitzenaufbau wäre das 5. Kapitel nie in dieser Form entstanden.

Den aktuellen und ehemaligen Mitarbeiteren der Gruppe für Geduld, Hilfe und Spaß: Miachel Olapinski (Danke für die Nutzung Deines Fluorolog-Mods), Eike Friedrichs, Andreas Reuter, Stefan Beyer, Patrick Nickels, Ralf Jungmann, Tom Sobey, Stefan Renner, Philipp Schneider, Bernd Heindl, Andreas Fischer.

Den unglaublich wichtigen und überhaupt nie zuviel gelobten Personen, die den Laden am Laufen halten und immer wertvolle und essentielle Tipps geben: Stefan Schöffberger, Alexander Paul, Stephan Manus, Bert Lorenz, Wolfgang Kurpazs und Pit Kiermaier.

Martina Jüttner, Eva Natzer, Marie-Christine Blüm und Evelyn Morgenroth für Hilfe und Beistand bei organisatorischen und finanziellen Fragen.

Dem IDK-NBT, der DFG und NIM Dank für die Finanzierung meiner Arbeit und meiner Forschungsreisen.

Dagmar und Stefan Beyer, Hendrik Dietz und Richard Neher, für unermüdliches Korrekturlesen der Arbeit und die konstruktive Kritik.

Erik Winfree, Jongmin Kim, and Rizal Hariadi from Caltech for the support, the experience and the fun I had in your group.

Ned Seeman and Ruojie Sha from NYU for the insight in rational DNA design, the inspiring discussions and the great time I had in your lab.

Bernie Yurke for the helpful and interesting discussions.

Danke auch an Personen, die zwar nicht immer messbar aber ganz wesentlich zum Gelingen der Arbeit beigetragen haben, wie zum Beispiel Daniel König, Daniel Schröer, Susi Kempfer und alle anderen die für die gute und freundschaftliche Atmosphäre an den Lehrstühlen mitverantwortlich sind.

Herzlichen Dank auch an diejenigen, die mich ausserhalb der Arbeit ertragen und aufgebaut haben: Danke Familie, nochmal Danke Dagmar, Danke Richard.

Danke.

Lebenslauf von Tim Liedl
Thuisbrunner Str. 18
81243 München

4.3.1976 in München geboren

1982 – 1986:
Besuch der Grundschule an der Limesstraße in München

1986 – 1995:
Besuch des Max Born Gymnasium in Germering bei München

1995 – 1997:
Zivildienst im Kreiskrankenhaus Pasing in München

Sommersemester 1997:
Studium der Musikwissenschaften an der LMU München

1997 - 2003:
Studium Diplom - Physik an der LMU München

Juni 1999:
Erhalt des Physikvordiploms

Wintersemester 1999 und Sommersemester 2000:
Erasmusstipendium für Physikstudium an der
Universidad de Sevilla, Spanien

Februar 2004:
Erhalt des Diploms in Physik.
Thema der Diplomarbeit die unter Anleitung von Prof. Dr. Wolfgang J.
Parak erstellt wurde: „Biologische Anwendungen von Nanokristallen“

März 2004 bis Mai 2007:
Wiss. Mitarbeiter in der Gruppe von PD Dr. Friedrich C Simmel.